Publication Year	2015
Acceptance in OA@INAF	2020-03-19T16:58:33Z
Title	Star and jet multiplicity in the high-mass star forming region IRAS 05137+3919
Authors	CESARONI, Riccardo; MASSI, Fabrizio; ARCIDIACONO, CARMELO; BELTRAN SOROLLA, MARIA TERESA; Persi, P.; et al.
DOI	10.1051/0004-6361/201526199
Handle	http://hdl.handle.net/20.500.12386/23412
Journal	ASTRONOMY & ASTROPHYSICS
Number	581

A&A 581, A124 (2015)
DOI: 10.1051/0004-6361/201526199
© ESO 2015

Astronomy & Astrophysics

Star and jet multiplicity in the high-mass star forming region IRAS 05137+3919⋆,⋆⋆

R. Cesaroni[1], F. Massi[1], C. Arcidiacono[1,2], M. T. Beltrán[1], P. Persi[3], M. Tapia[4], S. Molinari[3], L. Testi[5,1], L. Busoni[1], A. Riccardi[1], K. Boutsia[6], S. Bisogni[7,1], D. McCarthy[8], and C. Kulesa[8]

[1] INAF, Osservatorio Astrofisico di Arcetri, Largo E. Fermi 5, 50125 Firenze, Italy
e-mail: [cesa;fmassi;mbeltran;riccardi;lbusoni]@arcetri.astro.it
[2] INAF, Osservatorio Astronomico di Bologna, via Ranzani 1, 40127 Bologna, Italy
e-mail: carmelo.arcidiacono@oabo.inaf.it
[3] INAF, Istituto di Astrofisica e Planetologia Spaziale, Via Fosso del Cavaliere 100, 00133 Roma, Italy
e-mail: [paolo.persi;sergio.molinari]@iaps.inaf.it
[4] Instituto de Astronomía, Universidad Nacional Autónoma de México, Apdo. Postal 877, Ensenada, B. C., CP 22830, Mexico
e-mail: mt@astrosen.unam.mx
[5] European Southern Observatory, Karl-Schwarzschild-Str. 2, 85748 Garching, Germany
e-mail: ltesti@eso.org
[6] INAF, Osservatorio Astronomico di Roma, via di Frascati 33, 00040 Monte Porzio Catone, Italy
e-mail: konstantina.boutsia@oa-roma.inaf.it
[7] Università degli Studi di Firenze, via Sansone 1, 50019 Sesto Fiorentino, Italy
e-mail: susanna@arcetri.inaf.it
[8] Steward Observatory, The University of Arizona, 933 N. Cherry Ave., Tucson, TX 85721, USA
e-mail: dwmccarthy@gmail.com, ckulesa@as.arizona.edu

Received 27 March 2015 / Accepted 16 July 2015

ABSTRACT

Context. We present a study of the complex high-mass star forming region IRAS 05137+3919 (also known as Mol8), where multiple jets and a rich stellar cluster have been described in previous works.
Aims. Our goal is to determine the number of jets and shed light on their origin, and thus determine the nature of the young stars powering these jets. We also wish to analyse the stellar clusters by resolving the brightest group of stars.
Methods. The star forming region was observed in various tracers and the results were complemented with ancillary archival data. The new data represent a substantial improvement over previous studies both in resolution and frequency coverage. In particular, adaptive optics provides us with an angular resolution of 80 mas in the near IR, while new mid- and far-IR data allow us to sample the peak of the spectral energy distribution and thus reliably estimate the bolometric luminosity.
Results. Thanks to the near-IR continuum and millimetre line data we can determine the structure and velocity field of the bipolar jets and outflows in this star forming region. We also find that the stars are grouped into three clusters and the jets originate in the richest of these, whose luminosity is $\sim 2.4 \times 10^4\ L_\odot$. Interestingly, our high-resolution near-IR images allow us to resolve one of the two brightest stars (A and B) of the cluster into a double source (A1+A2).
Conclusions. We confirm that there are two jets and establish that they are powered by B-type stars belonging to cluster C1. On this basis and on morphological and kinematical arguments, we conclude that the less extended jet is almost perpendicular to the line of sight and that it originates in the brightest star of the cluster, while the more extended one appears to be associated with the more extincted, double source A1+A2. We propose that this is not a binary system, but a small bipolar reflection nebula at the root of the large-scale jet, outlining a still undetected circumstellar disk. The gas kinematics on a scale of ~0.2 pc seems to support our hypothesis, because it appears to trace rotation about the axis of the associated jet.

Key words. stars: early-type – stars: formation – ISM: jets and outflows

1. Introduction

Observationally, the study of high-mass star formation is severely hindered by the difficulty of identifying the object of interest in a crowded region. This is basically the result of the large distances of OB-type stars (typically, several kpc) and the presence of numerous, lower mass stars in the same field. As a matter of fact, OB-type stars form in rich clusters, which makes it difficult to distinguish the phenomena associated with the high-mass star(s) of interest from those associated with other cluster

⋆ Based on observations carried out with the Large Binocular Telescope. The LBT is an international collaboration among institutions in the United States, Italy and Germany. LBT Corporation partners are: The University of Arizona on behalf of the Arizona university system; Istituto Nazionale di Astrofisica, Italy; LBT Beteiligungsgesellschaft, Germany, representing the Max-Planck Society, the Astrophysical Institute Potsdam, and Heidelberg University; The Ohio State University, and The Research Corporation, on behalf of The University of Notre Dame, University of Minnesota, and University of Virginia.
⋆⋆ Appendix A is available in electronic form at http://www.aanda.org

members. High angular resolution is thus crucial for this type of investigation, since the (projected) separation inside these rich stellar cluster may be $\ll 1''$. Resolutions that high can be attained by IR and radio interferometers as well as by 8-m class telescopes operating at IR wavelengths, which are made possible through adaptive optics techniques.

With this in mind, we have focused our attention on a massive star forming region, where evidence of multiple, young stellar objects (YSOs) was found. The corresponding counterpart in the IRAS PSC is IRAS 05137+3919, also known as Mol 8 from the catalogue of Molinari et al. (1996). These authors quote a kinematic distance of 10.8 kpc and a corresponding luminosity (estimated from the IRAS fluxes) of $5.6 \times 10^4\ L_\odot$. Recently, Honma et al. (2011) have measured the parallax of the water masers in this object, resulting in a distance of $11.6^{+5.3}_{-2.8}$ kpc. The same authors also establish a lower limit of 8.3 kpc. This is consistent with a more recent parallax measurement by Reid et al. (2014), who derive a distance of $7.7^{+3.4}_{-1.8}$ kpc, implying an uncertainty of a factor ∼2 in luminosity. In the following, we adopt the minimum distance of 8.3 kpc estimated by Honma et al. (2011), with the caveat that higher values are possible.

IRAS 05137+3919 does not satisfy the colour constraints established by Wood & Churchwell (1989) to identify (UC) HII regions in the IRAS PSC, because the colour index [60–12] = 1.29 lies – although marginally – below the limit of 1.3. Indeed, despite the luminosity above $10^4\ L_\odot$, the source was not detected at 6 cm and 2 cm by Molinari et al. (1998), while only weak, compact continuum emission (0.33 mJy; Molinari et al. 2002) was measured at 3.6 cm. Whether this originates in an HII region or in a thermal jet still needs to be understood, but it appears likely that the 3.6 cm continuum emission is associated with one of the members of the embedded stellar cluster detected in the near IR by various authors (Ishii et al. 1998, 2002; Varricat et al. 2010) and studied by Faustini et al. (2009), Kumar et al. (2006), and Nikoghosyan & Azatyan (2014, 2015). The most likely candidates for ionising the radio source are two bright stars located at the centre of the cluster and already identified by Varricat et al. (2010).

Interstingly, that cluster lies also close to the geometrical center of a bipolar outflow mapped in the ^{12}CO(1–0) line by Zhang et al. (2001, 2005). Varricat et al. (2010) imaged two bipolar jets in the H_2 v = 1–0 S(1) line, also centred on the stellar cluster and directed approximately NE–SW and NW–SE. Hereafter, we refer to these, respectively, as Jet 1 and Jet 2, following Varricat et al. (2010). The former is roughly oriented like the ^{12}CO outflow by Zhang et al. (2001, 2005) and the HCO^+(1–0) outflow mapped by Molinari et al. (2002) with the OVRO interferometer. The presence of shocked H_2 emission is confirmed by the near-IR spectra obtained by Ishii et al. (2001), which refer to the NW–SE jet.

Based on these previous findings, we decided to perform a multi-wavelength study of IRAS 05137+3919 with the main goal to relate the properties of the stellar cluster to those of the outflows/jets and hence identify the sources powering the flows and establish their nature. For these purposes, we obtained outflow maps a factor ∼4 better in angular resolution than those by Zhang et al. (2005) and imaged the stellar cluster with an 8-m class telescope employing adaptive optics to attain ∼0.″08. We also used the continuum far-IR images of the *Herschel*/Hi-GAL survey (Molinari et al. 2010) to accurately estimate the cluster luminosity. After describing the observational details in Sect. 2, we illustrate the results in Sect. 3, while the analysis and discussion of our findings is presented in Sect. 4. Finally, the conclusions are drawn in Sect. 5.

2. Observations and data reduction

2.1. Large binocular telescope

2.1.1. Near-IR images with LUCI

Near-IR images were taken in the night of December 12, 2009 with LUCI (Seifert et al. 2003) at the Large Binocular Telescope (Mount Graham, Arizona), through the standard broad-band filters H (λ_c = 1.653 μm) and K_s (λ_c = 2.163 μm), and the narrow-band filters FeII (λ_c = 1.646 μm, including the [FeII] 1.64-μm line) and H_2 (λ_c = 2.122 μm, including the H_2 v = 1–0 $S(1)$ line at 2.12 μm). We used the N3.75 camera with a pixel scale of ∼0.″12 and a field of view of 4′ × 4′. We took ten dithered images both at H and at K_s, each composed of 17 coadds of 2 s exposures (H) and 15 coadds of 2 s exposures (K_s). A set of 14 dithered images, each resulting from coadding five exposures of 20 s, were taken at H_2, whereas eight dithered images were taken at FeII, each of them a coadd of nine exposures of 20 s. Total exposure times were then 300 s (K_s), 340 s (H), 1400 s (H_2), and 1440 s (FeII), respectively. The dithering pattern consisted in alternatively imaging the target in the central part, the eastern part, and the western part of the detector field (i.e., with a throw of ∼1′ in right ascension), with a random jitter of a few arcsec when the target was in the same area of the detector. These allowed us to obtain sky images from the on-source images themselves, by median filtering together 4 frames selected so that the target area did not overlap in the stack, which would have been a problem due to the extended emission feature in the field centre. All the images were flat-fielded, bad-pixel corrected, sky-subtracted, registered, and combined by using standard IRAF[1] routines. We note that, given the dithering strategy adopted, all final combined images attain their maximum signal-to-noise ratio in a central area ∼2′ wide in right ascension. The full width at half maximum (FWHM) of the point-spread function (PSF) was between ∼0.″5 and ∼0.″6.

We scaled the K_s and H_2 final mosaics appropriately (by assuming a constant stellar continuum flux, which is correct only as a zero-order approximation) and then subtracted one from the other, to obtain a continuum-free map of pure H_2 line emission. In practice, we solved the two equations that give the intensities measured in the H_2 and K_s filters

$$I_{H_2} = \left(\int S_\nu^{H_2}\, d\nu + S_\nu^c \Delta\nu_{H_2} \right) t_{H_2}\, \eta_{H_2} \quad (1)$$

$$I_{K_s} = \left(\int S_\nu^{H_2}\, d\nu + S_\nu^c \Delta\nu_{K_s} \right) t_{K_s}\, \eta_{K_s} \quad (2)$$

with respect to $\int S_\nu^{H_2}\, d\nu$ and S_ν^c, where $S_\nu^{H_2}$ and S_ν^c are the H_2 line and continuum flux densities, $\Delta\nu_{H_2}$ and $\Delta\nu_{K_s}$ the widths of the H_2 and K_s filters, t_{H_2} and t_{K_s} the corresponding integration times, and η_{H_2} and η_{K_s} the transparencies of the two filters. We followed the same procedure with the H and FeII final mosaics, but no [FeII] emission could be detected in the subtracted image, so we do not discuss the [FeII] data further.

We performed PSF-fit photometry on the K_s and H final averaged (mosaiced) images by using the DAOPHOT routines in IRAF. In total, we found 1303 sources with detection at both K_s and H, 143 sources with detection at K_s and 60 sources with detection at H (see Table A.1). Unfortunately, the standard

[1] IRAF is distributed by the National Optical Astronomy Observatory, which is operated by the Associated Universities for Research in Astronomy, Inc., under cooperative agreement with the National Science Foundation.

star observed for calibration during the night was saturated in all frames. Thus, we calibrated our photometry on 2MASS, by matching our sources to 2MASS PSC entries. For both bands, the colour range spanned by the common stars is too narrow to clearly show any colour effects between our instrumental magnitudes and 2MASS magnitudes, so we neglected colour terms. We obtained K_s(2MASS) − K_s(instrumental) = 23.81 ± 0.06 and H(2MASS) − H(instrumental) = 24.52 ± 0.05. The limiting magnitudes (at 3σ) are $K_s \simeq 20$ and $H \simeq 20.5$. A simple method of estimating the photometric completeness limits relies on histograms of magnitudes. Typically, the number of sources retrieved increases with increasing magnitudes up to a maximum value. Beyond this value, the source statistics is dominated by the decreasing efficiency in retrieving faint sources. Thus, the histogram maximum yields a rough estimate of the completeness limit. We conservatively assumed it to be 1 magnitude brighter than the histogram maximum. In fact, we found two nearby peaks at H, but the brighter one disappears when counting only sources in the 2′ innermost part of the image. So the brighter peak is probably due to including sources from parts of the image with lower signal-to-noise ratio. The completeness limits we estimated are Ks(compl) ∼ 17.75 and H(compl) ≃ 18.25.

Finally, we calibrated the line emission fluxes on the final averaged (mosaiced) H_2 image by repeating our photometry on the H_2 image and matching it to the K_s calibrated photometry, correcting the stellar fluxes to the λ_c of the narrow-band filter. Photometry of the H_2 knots was then performed on the continuum-subtracted H_2 images by means of task POLYPHOT in IRAF, enclosing each knot with polygons following the emission contour at 3σ of the background counts as closely as possible. The identified knots and corresponding fluxes are given in Tables A.2 to A.4, where we have classified the knots on the basis of their association with Jet 1, Jet 2, and Jet 3 (defined in Sect. 3.3). For the H_2 images the 3σ sensitivity level is equal to 4×10^{-16} erg s^{-1} cm^{-1} arcsec^{-2}.

2.1.2. Near-IR images with FLAO and the PISCES camera

The data were collected on October 9 and 12, 2013, using the PISCES Near Infrared Camera (McCarthy et al. 2001) installed at the focal plane of the First Light Adaptive Optics system (Esposito et al. 2010, 2011) of the Large Binocular Telescope. The detector has a pixel scale of ∼0.″02, with a field of view of 21″ × 21″. The observations were carried out through the H_2, H, and K_s filters. We used a star 10″ west from our field center with R, I mag ∼12.0 as the reference for the AO loop, closed using 153 modes. The average Strehl Ratio on the centre of the field was 40% being measured on the H_2 images. The electronic cross-talk between the quadrants in the PISCES Hawaii-I detector was corrected for each frame using `Corquad`, an IRAF procedure developed by Roelof de Jong[2].

We obtained one image per band by registering and combining together, after sky subtraction: 119 exposures of 5 s at K_s (total integration time 595 s); 62 exposures of 25 s at H_2 (total integration time 1550 s); and 3 exposures of 10 s at H (30 s). Due to the deteriorating weather conditions, only the latter small set of H frames is available. Each single frame was first drizzled, bad-pixel corrected, and flat fielded using standard IRAF routines. The PSF-FWHMs we measured are ∼0.″08 in all final images.

[2] See http://66.194.178.32/~rfinn/pisces.html

We performed aperture photometry on the PISCES final images by using the DAOPHOT routines in IRAF. We found 66 sources with detection both at K_s and H, 83 sources with detection at K_s, and 24 sources with detection at H (see Table A.5). We used aperture radii of ∼1 PSF-FWHM and annuli with inner and outer radii of ∼2–4 PSF-FWHM to derive the sky level, with the median as an estimator. We calibrated K_s and H by comparing the instrumental magnitudes to those obtained with LUCI (which in turn are calibrated on 2MASS) for the matching stars. Again, the colour range spanned by the data points is too narrow to show any clear colour effects, so we neglected colour terms. We obtained K_s(LUCI, 2MASS) − K_s(PISCES, instrumental) = 23.46 ± 0.10 and H(LUCI, 2MASS) − H(PISCES, instrumental) = 24.68 ± 0.11. We note that a few points depart by up to 0.4 mag from these relations. The most extreme differences are clearly due to unresolved objects in the LUCI images. Nevertheless, part of the scatter is probably due to PSF variations over the PISCES field (anisoplanatism), which is typical of AO-assisted images (e.g., Esslinger & Edmunds 1998). So, we can actually expect intrinsic errors of up to 0.1–0.2 mag in our PISCES photometry. The limiting magnitudes (at 3σ) are $K_s \simeq 22.5$ and $H \simeq 21$. We estimated the completeness limits as explained in Sect. 2.1.1. The distribution of K_s displays two nearby peaks (see Sect. 4.1), but the brightest one is likely to be intrinsic to the local stellar population. Thus, we derived K_s(completeness) ≃19.25 and H(completeness) ≃ 18.75. Finally, from the K_s and H_2 images we obtained a continuum-free, pure H_2 line emission map following the method described in Sect. 2.1.1.

2.2. Ground based mid-IR observations

Ground-based diffraction-limited mid-infrared images at 8.9, 9.9, 12.7, and 18.7 μm of IRAS 05137+3919 were taken on the night of November 9, 2006 with the mid-infrared camera CID (Salas et al. 2006) mounted on the 2.1 m telescope of the Observatorio Astronómico Nacional at San Pedro Mártir, Baja California, Mexico. This camera is equipped with a Rockwell 128 × 128 square pixel Si:As BIB detector array that delivers an effective scale of 0.″55/pixel covering a fully-sampled area of 62″ × 62″. The images were taken with the standard chop-nodding mode to remove the sky and telescope emission background. The standard stars α Lyr, β And, α Aur, α Her, and γ Aqu were observed before and after the programme sources at similar air masses for flux calibration, following Salas et al. (2006), in order to measure the PSF at each wavelength. These values (FWHM) ranged from ∼1.7″ at the shortest wavelength, to ∼2.″1 at 18.7 μm. Individual images were obtained at ten nodding positions, 20″ apart, while we chopped at 3 Hz with a throw of 22″. After all cycles, the total on-source integration time in each filter was 1440 s.

The astrometry of the images was determined by alignment with WISE and *Spitzer*/IRAC images. For this purpose, we smoothed the 8.9 and 9.8 μm images to 2″ resolution and overlaid them by eye on the 4.5 μm IRAC image. The same procedure was adopted for the 12.7 and 18.7 μm images, which were compared to the 12 μm WISE image after smoothing them to 6.″5 resolution. Albeit not very accurate, this method results in an astrometrical error $\lesssim$1″, which will suffice for our purposes.

A single mid-IR source was detected at all wavelengths. At $\lambda < 13$ μm, the source may be slightly resolved, with diameters $\gtrsim$2″. The measured photometry on the CID calibrated images with a 4″ aperture yields the following fluxes: 1.2 Jy

at 8.9 μm, 1.5 Jy at 9.9 μm, 3.8 Jy at 12.7 μm, and 10.7 Jy at 18.7 μm. These values have 10% errors, dominated by uncertainties in the flux calibrations on standard stars as discussed by Salas et al. (2006).

2.3. IRAM 30-m telescope

The observations were performed with the IRAM 30-m antenna on Pico Veleta (Spain) on July 13 and 14, 2003. The source was mapped with HERA, a multi-beam heterodyne dual polarization receiver, consisting of two arrays of 3×3 pixels with 24″ spacing (Schuster et al. 2004). Areas of ∼4′ × 4′ and ∼3′ × 3′ centred around the position α(J2000) = $05^h17^m13\overset{s}{.}8$, δ(J2000) = 39°22′20″ were covered, respectively, in the ^{12}CO and C^{18}O $J = 2 \rightarrow 1$ rotational transitions. The maps were made in on-the-fly mode, scanning along the right ascension direction. The receiver was suitably rotated to allow for a sampling with 4″ intervals in declination, perpendicular to the scanning direction, while the data were acquired along the scanning direction every 4″. This results in excellent sampling of the 12″ half-power beam width (HPBW) of the telescope. Position switch and frequency switch were used, respectively, for the ^{12}CO(2–1) and C^{18}O(2–1) line observations. The VESPA autocorrelator was chosen as a backend, with a spectral resolution of 0.1 km s^{-1} and 0.053 km s^{-1}, respectively, for the ^{12}CO and C^{18}O(2–1) lines. The pointing accuracy was regularly checked (typically every hour) on strong, pointlike continuum sources. The data presented in this paper are expressed in main beam brightness temperature, $T_{\rm MB}$, assuming a forward efficiency of 0.90 and a beam efficiency of 0.52 for ^{12}CO(2–1) and 0.55 for C^{18}O(2–1). The conversion to flux density, S_ν, is given by the expression S_ν(Jy) = 4.7 $T_{\rm MB}$(K). The data were reduced and analysed by means of the GILDAS software[3]. The spectra were smoothed to 0.5 km s^{-1} before creating channel maps of the line emission.

3. Results

The observational findings of our study are illustrated in the following, where we concentrate on four main issues: the large-scale structure, extending over ∼100″, or ∼4 pc, around the nominal position of IRAS 05137+3919 – α(J2000) = $05^h17^m13\overset{s}{.}3$, δ(J2000) = 39°22′14″; the small-scale structure, namely the region of ≲20″, or ≲0.8 pc, imaged with the PISCES camera; the jets and corresponding outflows (hereafter "jets/outflows") mapped both in the near-IR and at 3.4 mm; and the stellar clusters, spread over ∼2′.

3.1. The large-scale structure

As already noted by various authors, two molecular clumps are detected in the IRAS 05137+3919 region, offset by ∼30″ along the N–S direction. In this study we focus on the northern one, but it is worth mentioning that the two clumps are likely physically close in space and not only in projection onto the plane of the sky, because their LSR velocities differ by only ∼1 km s^{-1} (see Brand et al. 2001). Each of them hosts a stellar cluster, as pointed out by Faustini et al. (2009).

In Fig. 1 we show a number of maps of the continuum emission of IRAS 05137+3919, ranging from the near-IR to the sub-mm. We have chosen the images with the best angular resolution available in each wavelength regime. Besides confirming the previous findings, the IR images clearly indicate the existence of a third stellar cluster, located ∼15″ to the east of the southern clump and considerably fainter than the other two clusters, which are dominating the emission at all wavelengths.

For the sake of simplicity, in the following we refer to the northern clump and associated cluster (hereafter "clump/cluster") as C1, to the southern clump/cluster as C2, and to the south-eastern cluster as C3 (see the top, right panel of Fig. 1). C1, which is the target of our investigation, is by far the most luminous at all frequencies and is the only one where free-free emission has been detected by Molinari et al. (2002), as one can see from the contour map in Fig. 1. The richness of C1 is illustrated also in the left panel of Fig. 2, where a 3-colour image of the whole region obtained from the LUCI data is shown. Here, the presence of the three clusters C1, C2, and C3 stands out clear (white colour), as well as the existence of multiple H_2 jets (red colour), which we will discuss in the following.

Thanks to the Hi-GAL images, it is now possible to obtain an accurate estimate of the far-IR flux densities and hence of the luminosities of C1 and C2. We reconstructed the corresponding spectral energy distributions (SEDs) using data from the 2MASS (Skrutskie et al. 2006), *Spitzer*/IRAC (Werner et al. 2004; Fazio et al. 2004), IRAS, MSX (Price et al. 1999), WISE (Wright et al. 2010) archives, the *Herschel*/Hi-GAL survey, the SCUBA Legacy Surveys (Di Francesco et al. 2008), and the studies of Molinari et al. (2008) and Ishii et al. (1998). When possible, the flux densities were taken from the available source catalogues. In the other cases, for each clump we integrated the continuum flux inside a suitable polygon enshrouding all the emitting region, and then subtracted the background estimated through 1D cuts across the clump centre. The flux densities computed in this way, as well as the solid angles encompassed by the polygons used for the integration are given in Table A.6, while the corresponding SEDs are shown in Fig. 3. The bolometric luminosity was estimated by integrating the SED over the whole wavelength range, after linear interpolation in the Logν–LogS_ν plot.

For the fiducial distance of 8.3 kpc we obtain 2.4×10^4 $L_\odot$ for C1 and 6.7×10^3 $L_\odot$ for C2. These numbers agree within a factor 2 with the estimates obtained from the cluster simulations of Faustini et al. (2009) and Kumar et al. (2006), once the different distance assumed in their calculations (11.5 kpc) is taken into account.

3.2. The small-scale structure

As explained in Sect. 2, with the LBT/PISCES imaging we have attained a resolution of 80 mas or 664 au over ∼20″. This allows us to investigate in detail the innermost region of C1, which is the target of the present study. Our findings are best illustrated by the 3-colour image in the right panel of Fig. 2, where several features are worth of mention.

The "white" star to the west of the image, is very likely a foreground object, not physically related to the cluster of interest for us. The two "yellow" stars at the centre are well separated, with the one to the NE (hereafter A, after Varricatt et al. 2010) appearing slightly "redder" and hence more extincted than the other (hereafter B). While the presence of this pair was already known, in our image A splits into two sources, one, brighter, to the SW (which we call A1) and another, fainter, to the NE (A2). This is more evident in Fig. 4, where we compare the LUCI to the PISCES images. Clearly, the dramatic improvement in

[3] The GILDAS software has been developed at IRAM and Observatoire de Grenoble – see http://www.iram.fr/IRAMFR/GILDAS

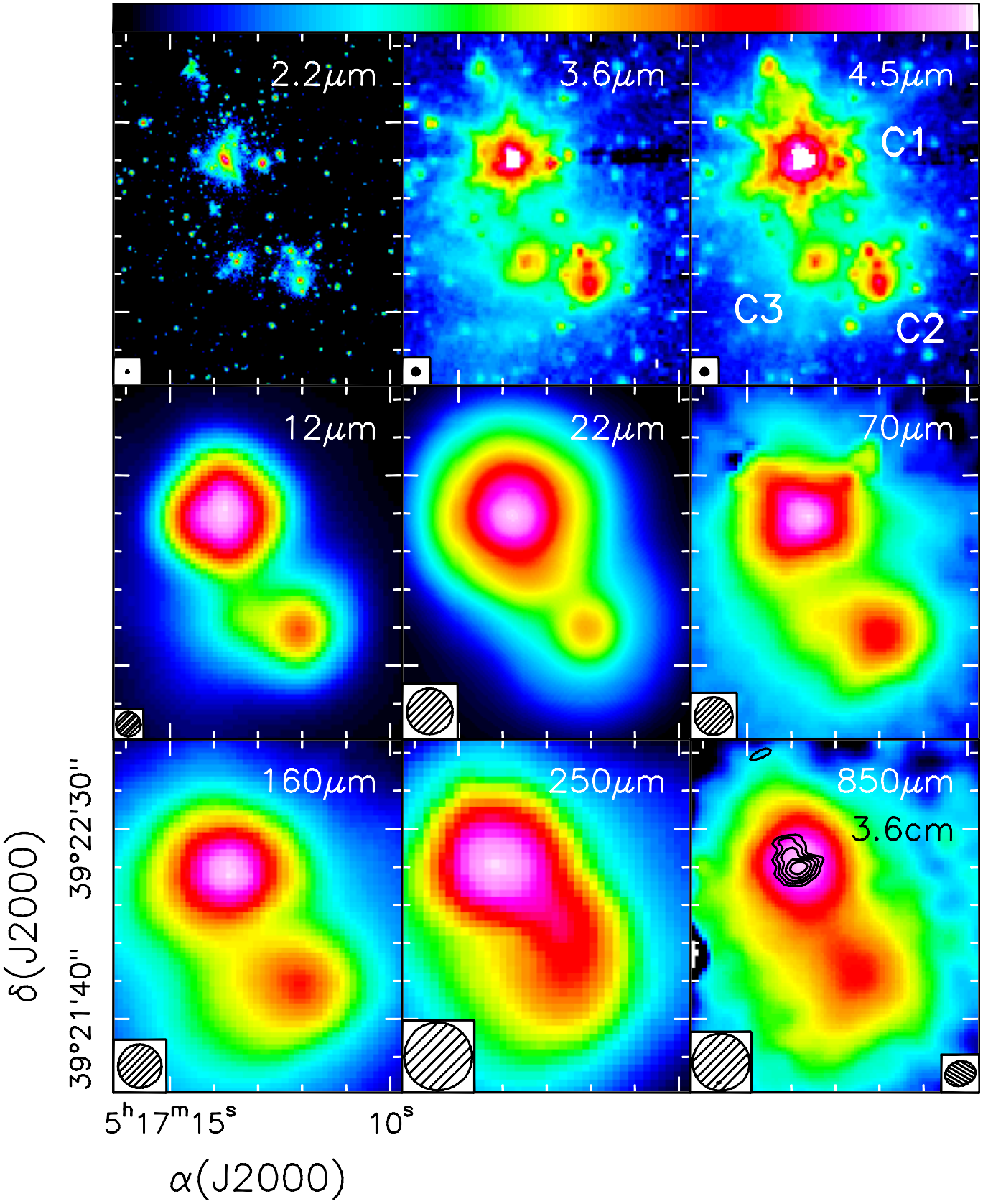

Fig. 1. Maps of the continuum emission towards IRAS 05137+3919 at different wavelengths (given in the top right of each panel). The labels in the top, right panel indicate the three clumps/clusters that we refer to in the text. The images have been taken from our LUCI data (2.2 μm), the IRAC database (at 3.4 and 4.6 μm), the WISE archive (12 and 22 μm), the *Herschel*/Hi-GAL survey (70–250 μm), and Molinari et al. (2008) (850 μm). The contours in the bottom right panel are the map of the 3.6 cm continuum emission observed by Molinari et al. (2002), while the ellipse in the bottom right denotes the corresponding angular resolution. The circle in the bottom left of each panel represents the HPBW of the corresponding image.

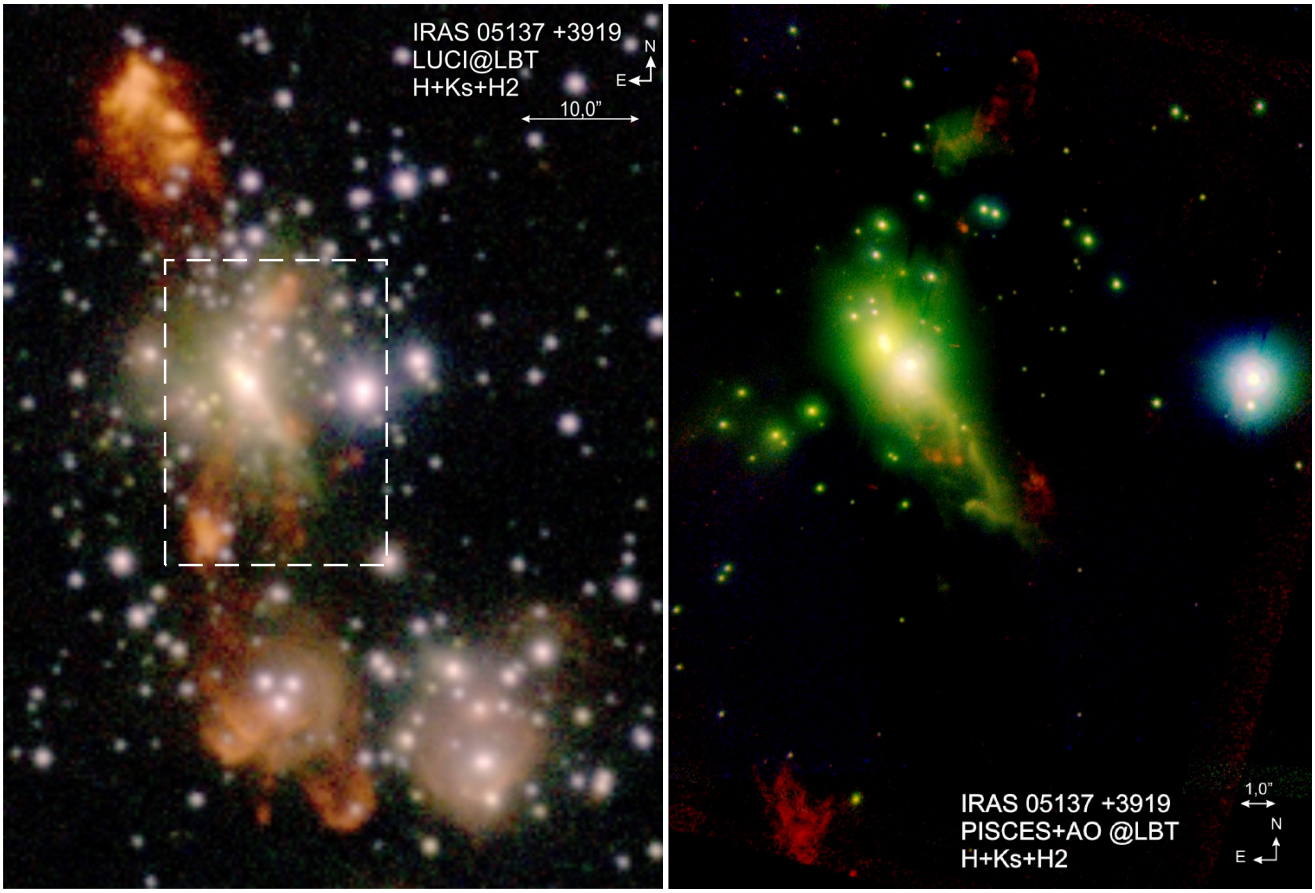

Fig. 2. Composite colour images obtained by combining the emission in the H_2 (red), K_s (green), and H (blue) filters from the LUCI (*left panel*) and PISCES (*right panel*) data. The dashed box in the left panel indicates the region shown in the right panel. The LUCI and PISCES images cover regions, respectively, of about 0.′8 × 1.′1 and 0.′3 × 0.′4.

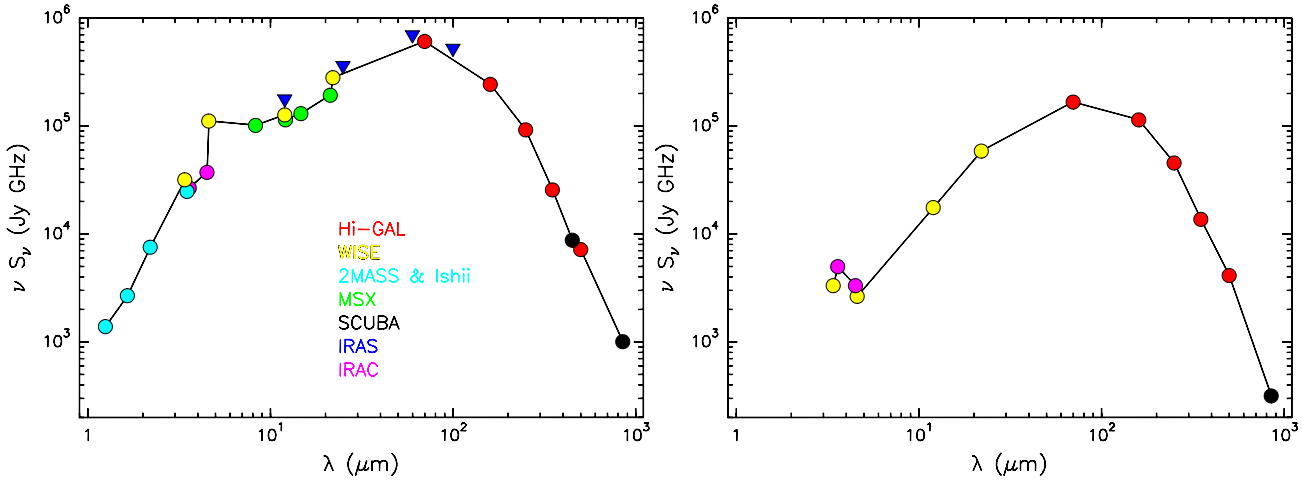

Fig. 3. Spectral energy distributions of clumps/clusters C1 (*left panel*) and C2 (*right panel*). The colour coding of the symbols is explained in the left panel. The triangles indicate upper limits.

angular resolution obtained with AO is crucial to resolve A1 from A2, whose apparent separation is ∼0.′′18 (i.e. ∼1500 au).

All three sources, A1+A2+B, are likely responsible for the mid-IR emission measured by us with the San Pedro Mártir telescope, as demonstrated by Fig. 5, where we overlay the LUCI K_s image on the four images at wavelengths ranging from 8.9 to 18.7 μm. Despite the limited astrometrical accuracy (∼1′′), it is clear that the bulk of the mid-IR emission arise from the same region where the near-IR emission peaks. In turn, this implies that the three sources are responsible for most of the luminosity estimated for C1 (2.4×10^4 $L_\odot$), because their mid-IR emission at 12.7 and 18.7 μm corresponds to ∼80% of the flux densities measured within much greater HPBWs with MSX and WISE (see Table A.6).

An interesting feature seen in Fig. 2 is the "green" arc of continuum emission extending to the SW from B. This almost

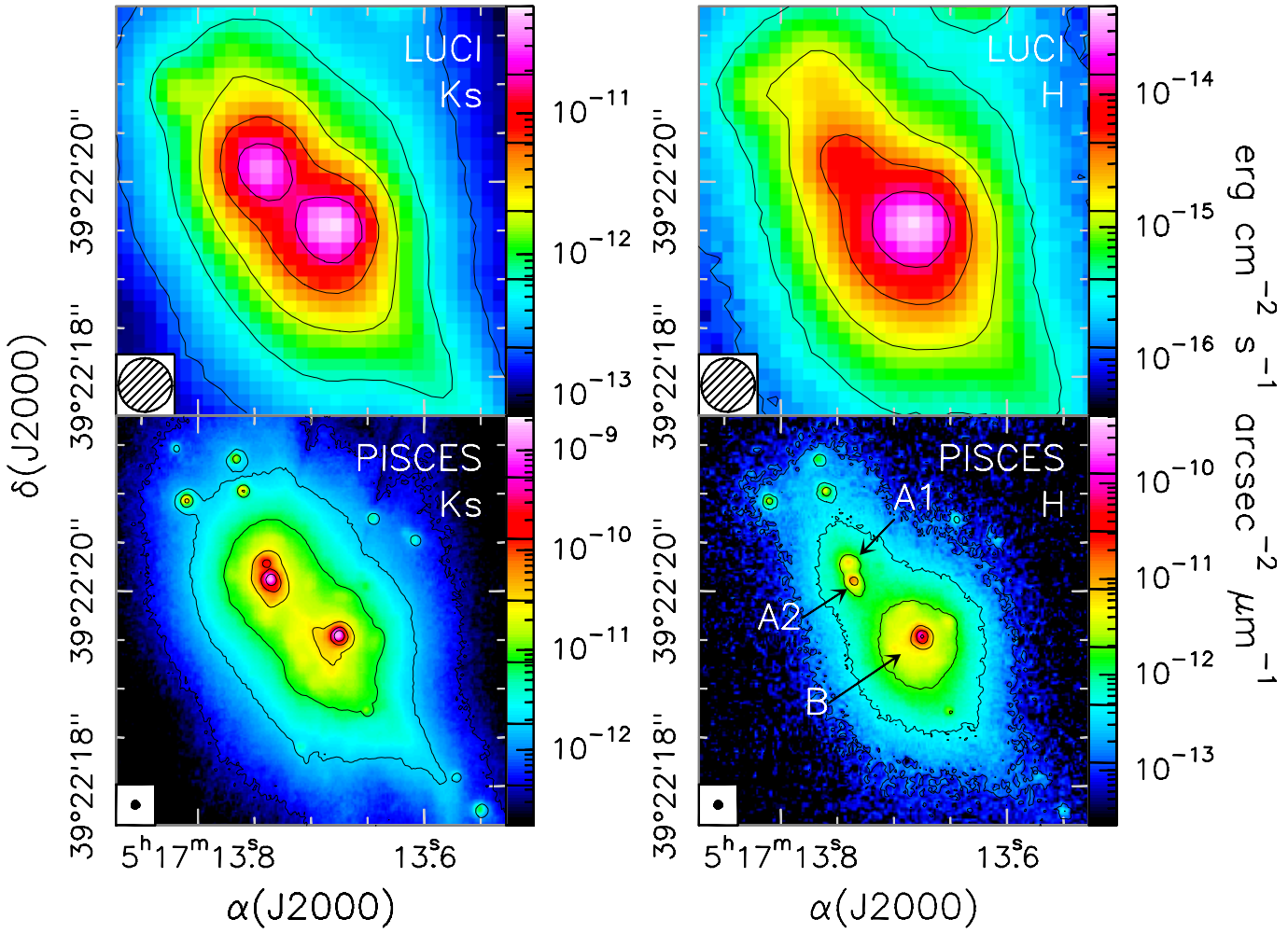

Fig. 4. Images of the central region of clump/cluster C1, where a pair of bright stars (A and B) had been detected in previous studies. The *left and right panels* refer, respectively, to K_s and H band images, while the *upper and lower panels* show, respectively, images obtained with the LUCI and PISCES+AO cameras. The values of the contour levels are indicated by marks in the corresponding colour scales. Note how employing AO allows us to resolve star A into the two sources A1 and A2.

coincides with three H_2 knots, which can be recognised from their red colour in the image. Whether the arc and the knots are physically related is difficult to establish, but it is possible that both are manifestations of the same phenomenon, perhaps a bow shock due to Jet 1. In any case, the knots are in all likelihood due to the interaction between the jet and the dense gas associated with C1. As explained in Sect. 1, Jet 1 was first observed by Varricat et al. (2010) and is confirmed by our images (see below).

Finally, at the top and bottom of the right panel of Fig. 2, one sees two other "red" regions of H_2 line emission, shaped like bow shocks. These correspond to (part of) Jet 2, also identified by Varricat et al. (2010).

3.3. The bipolar jets/outflows

Evidence for the existence of multiple jets/outflows in the IRAS 05137+3919 region has been provided by various studies, as described in Sect. 1. Our high-resolution images shed new light on this issue, thanks to their superior sensitivity and angular resolution. Moreover, the velocity information conveyed by the ^{12}CO maps makes it possible to discriminate between the blue- and red-shifted lobes. In Fig. 6, maps of the outflow lobes are shown, obtained by integrating the ^{12}CO(2–1) emission over the line wings, in various velocity intervals. These maps are compared to the H_2 images obtained with LUCI, which fully confirm the existence of two bipolar jets associated with C1.

The left panel of Fig. 6 displays the high-velocity (HV) emission, which nicely coincides with Jet 2 and indicates that this jet likely lies close to the plane of the sky, because the red and blue lobes overlap significantly. The low-velocity (LV) maps shown in the right panel of the same figure look more complicate. In this case, the ^{12}CO emission appears to be consistent with Jet 1, but significant blue-shifted emission is seen towards the red lobe, whereas no red-shifted emission is detected over the blue lobe. The complex pattern observed may be due to confusion between the LV gas and that moving at the systemic velocity (whereas such a confusion obviously cannot occur for the gas that expands at high speed in Jet 2). Also, one has to take into account that the blue-shifted emission to the SW might be partly contaminated by the bulk emission from C2 (see Sect. 3.1), whose systemic velocity differs by –1 km s^{-1} from that of C1. Incidentally, we note that the C1 and C2 clumps are also traced by the C^{18}O(2–1) line map – shown in the middle panel of Fig. 6.

Despite the previous caveats, we conclude that in all likelihood the LV ^{12}CO outflow is related to Jet 1, while the HV ^{12}CO outflow is associated with Jet 2.

A new feature that can be seen in our image is the presence of elongated H_2 line emission originating approximately from

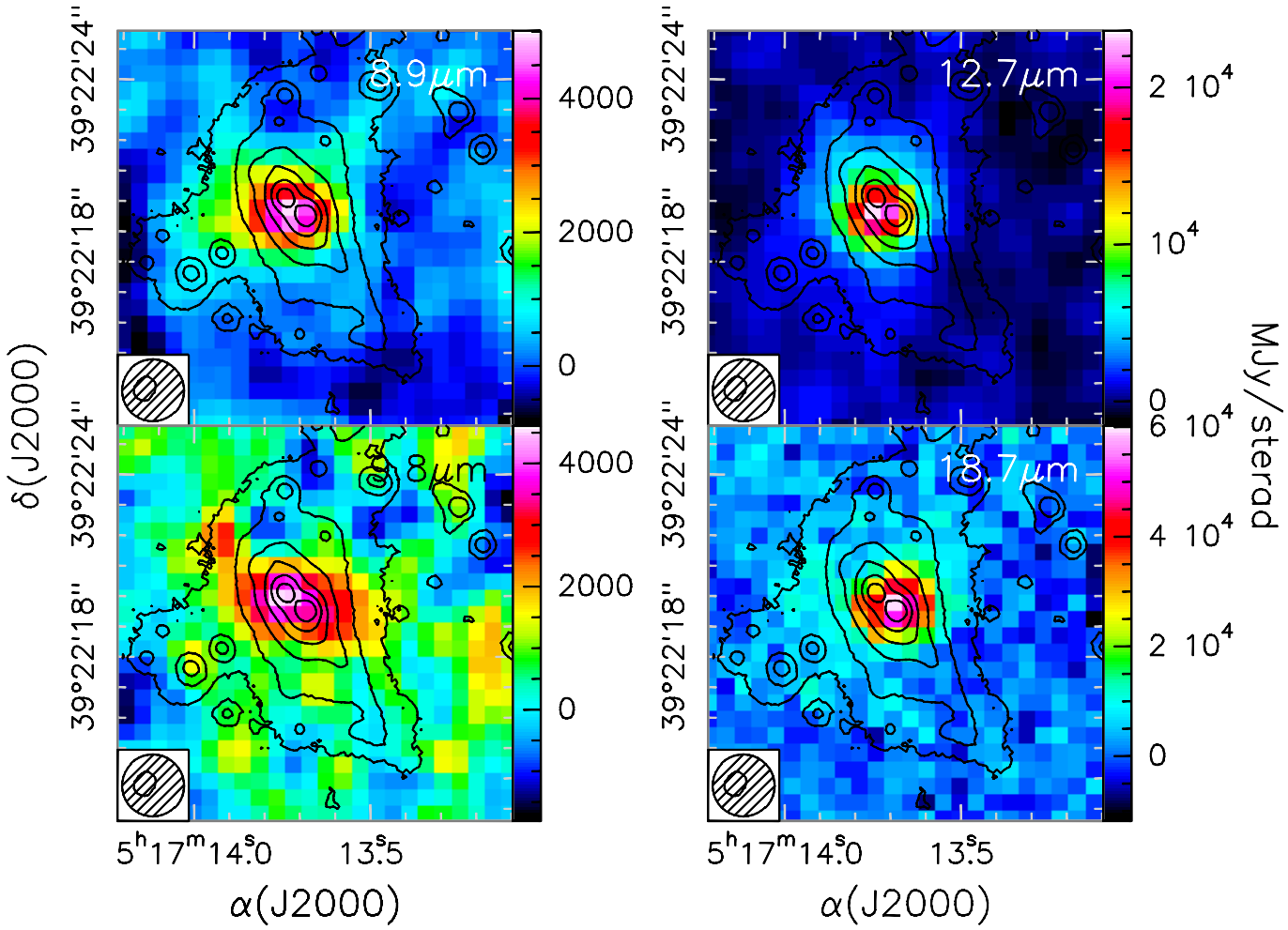

Fig. 5. Map of the LUCI K_s image (contours) overlaid on the mid-IR images acquired with the San Pedro Mártir 2.1 m telescope. stars (A and B) had been detected in previous studies. The wavelength of each image is indicated in the *top right of the panels*, while the FWHM of the PSF is drawn in the bottom left. Note that all mid-IR images have been smoothed to the resolution of the 18.7 μm image.

the peak of the $C^{18}O$ map (see Fig. 6) and extending towards W-SW over ~4″. Clearly, this feature cannot be related to Jet 2, as the two are roughly perpendicular to each other. As for Jet 1, its SW lobe spans position angles (PA) between –179° and –145° (see the bow-shock shaped H_2 knots spread over a region of 30″), quite different from that of the new H_2 feature (PA ≃ −118°). We conclude that such a feature might be a third, small-scale jet previously unobserved and in the following we refer to this as Jet 3. The nature of Jet 3 will be better discussed in Sect. 4.3.

3.4. The stellar clusters

Some properties of the stellar population associated with cluster C1 can be derived from the colour-magnitude diagram of Fig. 7, where the LUCI and PISCES photometry are overlaid. The much smaller field imaged with PISCES is less contaminated by foreground field stars and allows us to characterise the colour spread of the cluster members. While the LUCI data points are distributed along a stripe close to the zero-age main sequence (ZAMS), with a number of very extincted sources (up to $A_V \simeq 40$), the PISCES data points spread redwards of the stripe. The typical reddening of the cluster members can then be derived by reddening the ZAMS up to the nearest envelope of the PISCES data-point distribution, yielding $A_V = 5$. Thus, the LUCI sources close to the ZAMS are essentially foreground field stars, whereas the cluster members are distributed with $A_V > 5$ from the ZAMS ($H - K_s \gtrsim 0.4$).

In principle, the colour spread of the cluster members could be produced by extinction varying in the range $A_V \simeq 5$–40. However, the colour–colour diagram (J–H vs. H–K_s) of Nikoghosyan & Azatyan (2014) displays a large fraction of stellar sources with near-IR colour excess. This excess is usually caused by the presence of disks around young stars. By incorporating theoretical accreting disk models, their effect on the K_s versus H–K_s diagram has been demonstrated for disks around T Tauri stars to be accurately represented by vectors of approximately constant slope (López Chico & Salas 2007), towards brighter K_s and redder H–K_s values. More massive YSOs are usually much more embedded than T Tauri stars, and the correction proposed by López Chico & Salas (2007) is unlikely to apply to such objects. However, the presence of a spherical envelope around the disk should cause a greater decrease of H–K_s for the same variation of K_s, than in the case of a "naked" disk. Therefore, one can use the López Chico & Salas (2007) correction to obtain a lower limit to the spectral type. Assuming reddening along the arrow in the bottom of Fig. 7, after de-reddening the three objects for a minimum interstellar extinction of $A_V = 5$, one obtains spectral types of B7 for A1 and A2, and B1 for B. Vice versa, assuming that only

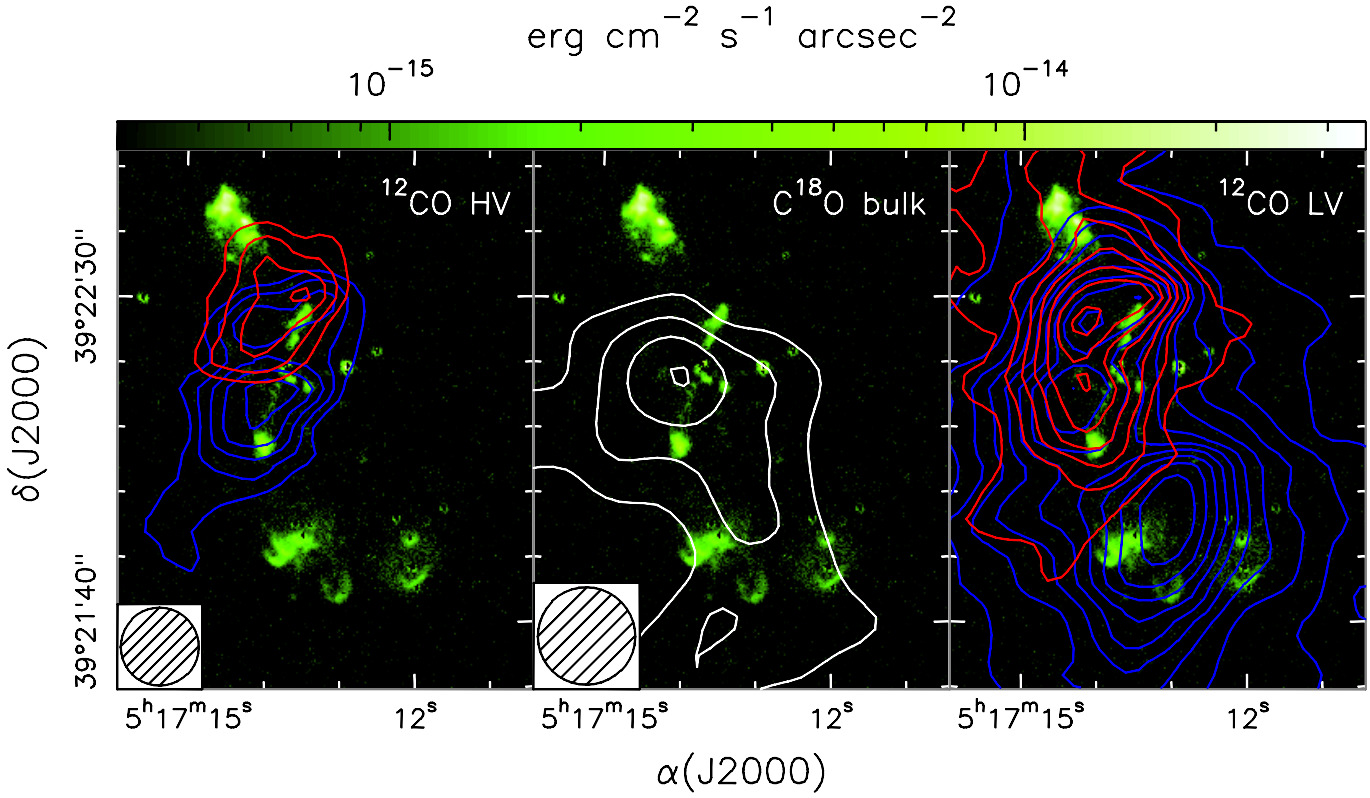

Fig. 6. *Left*: IRAM 30-m maps obtained by averaging the ^{12}CO(2–1) over the HV line wings, overlaid on the H_2 line (i.e. continuum subtracted) emission image obtained with LUCI. The integration has been performed over the LSR velocity intervals –35.65, –32.65 km s^{-1} (blue contours) and –17.65, –14.65 km s^{-1} (red contours). Contour levels range from 0.8 to 4.16 in steps of 0.48 K. The circle in the bottom left denotes the HPBW of the 30-m telescope. *Right*: same as *left panel*, for the ^{12}CO(2–1) LV wing emission. The integration was performed over the intervals –29.65, –27.65 km s^{-1} (blue contours) and –22.65, –20.65 km s^{-1} (red contours). Contour levels range from 1.2 to 15.6 in steps of 1.44 K. *Middle*: map of the C^{18}O(2–1) line emission averaged over the line, from –27.65 to –24.15 km s^{-1}. Contour levels range from 0.54 to 1.62 in steps of 0.36 K.

interstellar extinction is responsible for the reddening, along the arrow drawn in the top of Fig. 7, one estimates spectral types earlier than O8 for all three sources. The constraints set by this method on the stellar type are quite loose, but consistent with the three objects being intermediate- to high-mass stars.

Incidentally, this also proves that A1, A2, and B are part of the same system and none of them is likely to be spurious. A contaminant field star could only be a background (due to its extinction), more distant, giant or supergiant star (due to its unreddened brightness), but the probability of such a luminous object lying in the same projected area of our system is very low.

Using the extinction estimated from the colour-magnitude diagram, we can convert our K_s completeness limits into stellar mass limits. Assuming $A_V = 5$, a cluster age of 1 Myr, a distance of 8.3 kpc, and adopting the pre-main sequence tracks of Palla & Stahler (1999), we obtain a mass completeness limit of ~0.5 $M_\odot$ with the LUCI photometry and 0.1 $M_\odot$ with the PISCES photometry. For more extincted stars the completeness mass increases; e.g. $A_V = 20$ yields ~2.0 $M_\odot$ with the LUCI photometry and 0.7 $M_\odot$ with the PISCES photometry. However, we note that these values refer to "naked" stars. On the other hand, stars exhibiting a near-IR excess shine brighter at K_s, as already said, and the effective mass completeness limit decreases. The assumed age is consistent with that derived by Faustini et al. (2009), and the extinction values at the cluster peaks (derived from the sub-mm emission) listed by those authors towards C1 ($A_V = 18$) and C2 ($A_V = 8$) lie inside our adopted range. We also note that our K_s completeness limits are ~1 mag (LUCI) and ~2.5 mag (PISCES) less than achieved by Faustini et al. (2009), allowing us to improve on their results. A detailed analysis of the cluster stellar population will be presented in Sect. 4.1.

4. Analysis and discussion

The purpose of the following sections is to tie the large to the small scale structures in IRAS 05137+3919, and thus identify the sources powering the jets/outflows and establish their nature.

4.1. Characterization of the stellar population

A problem with young stellar clusters, especially those as distant as IRAS 05137+3919, is that their central areas are dominated by diffuse emission, source crowding, and the wings of the PSF of the brightest stars, which lead to a local worsening of the photometric completeness limit. In turn, this biases the derived properties (e.g., cluster density profile, number of members, etc.). We can assess this effect towards IRAS 05137+3919, by comparing the histograms of K_s PISCES sources and LUCI sources inside the field imaged by PISCES. These are shown in Fig. 8. We adopted a bin width of 0.5 mag, larger than the maximum uncertainty on the PISCES photometry. Clearly, the LUCI histogram peak is brighter than the LUCI completeness limit estimated all over the LUCI field of view. In addition, the number of K_s sources brighter than the completeness limit and retrieved with LUCI is less than those detected with PISCES. An

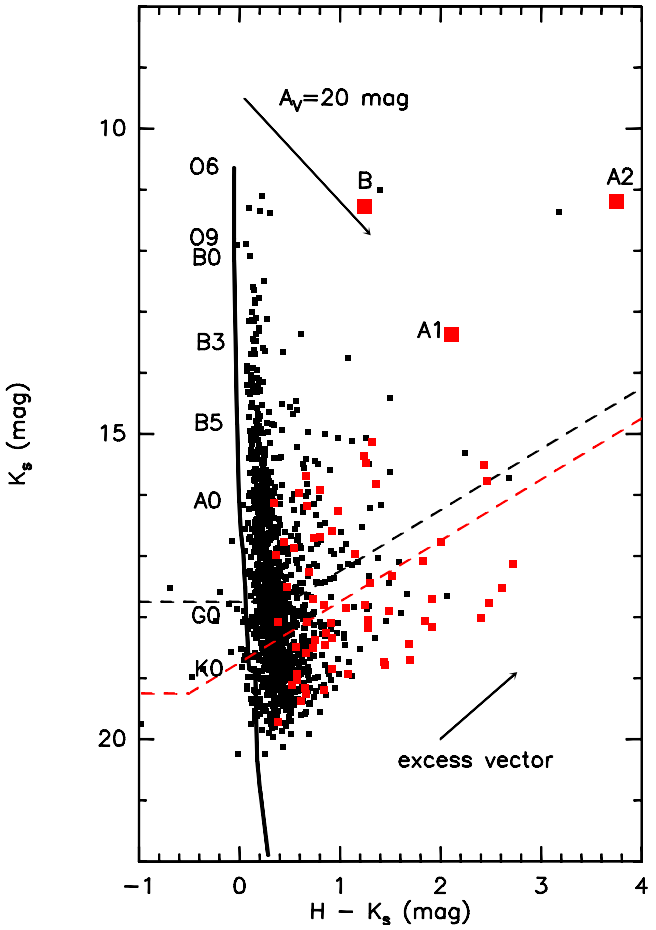

Fig. 7. K_s vs. H–K_s diagram of the sources retrieved in the LUCI field (black squares) and in the PISCES field (red squares). The dashed lines shows the completeness limit of the LUCI photometry (black) and the PISCES photometry (red). The black solid line is the ZAMS at a distance of 8.3 kpc (derived using the colours of Koornneef 1983 and the absolute magnitudes of Allen 1976 and Panagia 1973). The position of a few spectral types is labelled. The arrow in the top shows the effects of an extinction of $A_V = 20$ (according to Rieke & Lebofsky 1985). The arrow in the bottom corresponds to the median disk excess vector of López-Chico & Salas (2007) for the accretion disk models of D'Alessio et al. (2005). The three brightest members of the cluster C1 are labelled, as well.

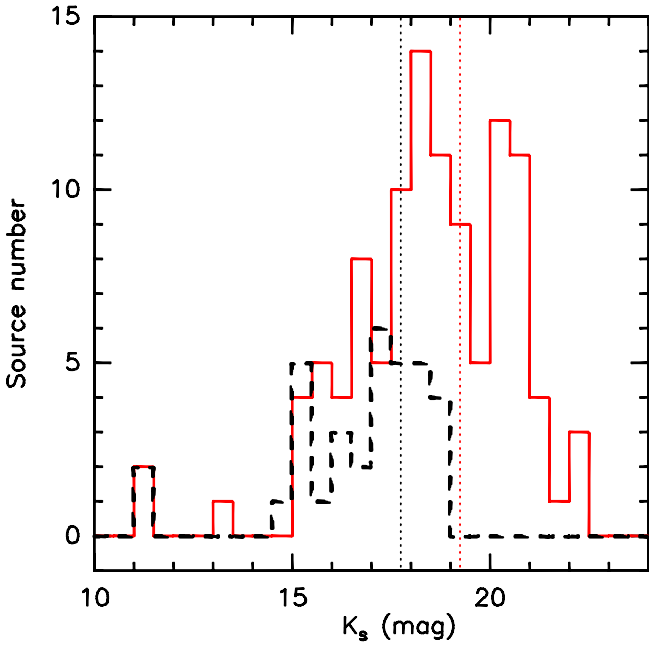

Fig. 8. Histograms of the distribution of K_s source magnitudes inside the field of view of PISCES. The red solid line indicates PISCES sources, the black dashed one LUCI sources. The vertical black and red dotted lines show, respectively, the completeness limit of the LUCI and PISCES K_s photometries, estimated from the whole corresponding field (see text).

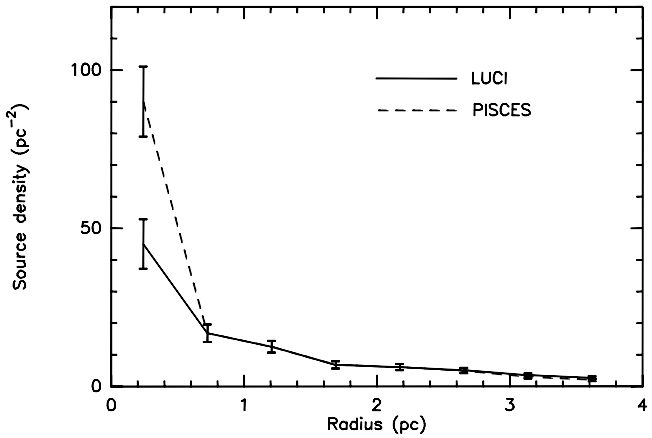

Fig. 9. Surface radial density of K_s sources derived in concentric annuli centred at the position of B, the brightest cluster member. The solid line indicates the density as computed from the LUCI photometry. The dashed line indicates the density computed by replacing the LUCI photometry with the PISCES photometry inside the area corresponding to the field of view of PISCES. The sources are counted up to the LUCI completeness limit (i.e. $K_s \simeq 17.75$). The errorbars show the Poissonian count fluctuations.

interesting characteristic of the PISCES histogram is its double peak. While the fainter peak is due to increasing incompleteness in sampling the stellar background population, the brighter peak is very likely an intrinsic feature of the C1 cluster population, as it lies well above the completeness limit of PISCES (red dotted line in Fig. 8).

How much the degraded completeness limit in the innermost, densest part of C1 affects the observed cluster properties can be assessed by plotting the surface radial density of K_s sources as derived in concentric annuli centered at the brightest cluster member (i.e. B). As shown in Fig. 9, when the LUCI sources are replaced by the PISCES ones inside the field of view of PISCES (and only counting sources with $K_s \leq 17.75$, the LUCI completeness limit), the surface density doubles at the centre. The outermost annuli give an approximate measure of the field star density, which may be subtracted from the central peak to derive the real stellar density of cluster C1. Note that the density *plateau* between 1 pc and 2 pc is due to the small clusters C2 and C3, rather than to a halo of members around C1.

The number of cluster members can be derived from the radial surface density distribution in Fig. 9 like the "richness indicator" I_c (see e.g. Testi et al. 1998). This implies integrating on the inner annuli and using the outermost annuli to estimate the background correction. We have integrated up to a radius of 0.97 pc and 1.93 pc to obtain, respectively, the total richness indicators for C1 ($I_c = 87 \pm 2$ stars) and C1+C2+C3 ($I_c = 120 \pm 4$ stars). For this purpose, we used the radial surface density corrected with the PISCES photometry (dashed line in figure). We

note that I_c is much larger than obtained by Faustini et al. (2009), due both to our crowdness correction and more sensitive completeness limit. Our estimate of 87 stars pc^{-2} seems comparable to the values derived by Testi et al. (1999) for their sample of Herbig Be stars. However, one must take into account that their sensitivity is better than ours by a couple of magnitudes at K_s, after suitable scaling for the smaller distance of their targets (less than ∼1 kpc). Therefore, we may reasonably conclude that C1 is significantly richer than the clusters around Herbig Be stars. Once more, we speculate that this might be related to the age of the cluster, as ours is younger than those of Testi et al., being associated with molecular gas and powerful outflow activity.

Finally, I_c can be converted into a *total* number of cluster members provided a suitable initial mass function (IMF) is assumed. However, such a conversion is hindered by the uncertainty on the mass completeness limit. The latter depends on the real distribution of the extinction, which we cannot derive from our data, and stellar age. We have quoted a mass completeness limit (corresponding to $K_s = 17.75$) between 0.5 and 2 $M_\odot$, but this should be further decreased if the cluster is younger than the adopted value of 1 Myr. In addition, in clusters that young, a high fraction of low-mass stars are still associated with a circumstellar disk and do exhibit a near-IR excess (see Sect. 3.4), which makes their detection easier. If we roughly assume that the I_c value is representative of >1 $M_\odot$ stars, by considering a standard IMF (e.g. Scalo 1998), then the total number of C1+C2+C3 members (down to 0.1 $M_\odot$) would be ∼700. In this case, the IMF would predict 2 members with $M \gtrsim 15\ M_\odot$. We conclude that our cluster analysis supports the existence of 2–3 early B-type stars, consistent with our estimates of the luminosities of sources A1, A2, and B.

4.2. Characterization of the jets/outflows

As illustrated in Sect. 3.3, evidence for the existence of up to 3 H_2 jets is seen in the IRAS 05137+3919 region. Here we focus our analysis on the most prominent of these, namely Jet 1 and Jet 2, and postpone the discussion of Jet 3 to Sect. 4.3.1.

4.2.1. Jet 1

While the existence of Jet 2 is out of question, due to its nice bipolar and well collimated morphology, the structure of Jet 1 is more complex and casts some doubts on the unicity of this jet. A priori, one might consider the possibility that the complex pattern of this jet might be due to precession. Although such a hypothesis cannot be ruled out, we prefer not to discuss it any further, because a precessing jet should describe an S-shaped pattern on the plane of the sky (see e.g. Fig. 18 of Cesaroni et al. 2005), while no convincing evidence of such a pattern is seen in our case. We thus attempt to explain the observed features with the simplest possible model, without invoking additional mechanisms besides expansion.

Is it possible that Jet 1 is in fact the result of the combination of multiple, distinct jets? To investigate this issue and establish the origin of the jets, in Fig. 10 we compare our near-IR images with other IR and molecular line maps. In the left panel we show an overlay of the 4.5 μm *Spitzer*/IRAC map on the LUCI image of the H_2 line emission. One sees that basically all of the H_2 knots belonging to Jet 1 coincide with peaks of the 4.5 μm emission. This is consistent with the presence of unresolved H_2 lines in the bandwidth covered by the *Spitzer*/IRAC 4.5 μm filter. The middle and right panels clearly illustrate the presence of three stellar clusters, already discussed in Sect. 3.1, traced by the low-resolution 3.4 μm WISE image and resolved in our 1.6 and 2.2 μm LUCI images. We also compare the near-IR emission to the HCO^+(1–0) interferometric map of Molinari et al. (2002), to show that the brightest cluster is associated with a dense molecular core in C1, and lies close to the geometrical centre of jets 1 and 2. We thus believe it is very reasonable to assume that the YSOs powering these jets/outflows lie inside C1, and we will base all our reasoning on such an assumption.

The left panel of Fig. 10 shows that the SW lobe of Jet 1 consists of a number of bow-shock-like features spread over a broad region, unlike the NE lobe, which appears well collimated. One may hence wonder whether Jet 1 is not a single jet, but the result of multiple jets overlapping in the plane of the sky. A priori, the H_2 knots falling in the regions corresponding to clusters C2 and C3 might belong to small jets powered by stars of those two clusters. However, careful inspection of the H_2 image reveals that all of the knots to the SW have bow-shock shapes pointing to the S-SW, which is inconsistent with the driving source to be located in C2 or C3. We thus believe that in all likelihood these knots belong to Jet 1, whose origin lies in cluster C1. If this is the case, why does the SW lobe appear so much less collimated than the NE lobe? A possibility is that the two lobes are intrinsically similar, but the SW one looks wider because it is impinging against C2 and C3, where one sees H_2 shocked emission. The NE lobe, in contrast, is expanding through lower density medium, which could confine the H_2 emission to internal shocks along the jet axis (see e.g. Stone et al. 1997).

4.2.2. Jet 2

Jet 2 looks much better defined than Jet 1 and is clearly centred on the peak of the molecular clump C1, as shown by the comparison with the HCO^+ line emission (middle panel of Fig. 10). As already noted, the ^{12}CO(2–1) outflow appears to mirror the pattern of the H_2 jet, thus allowing a kinematical analysis of the jet/outflow structure. For this purpose, we assume that the YSO powering this outflow coincides with one among A1, A2, and B. Evidence in favour of this hypothesis will be provided in Sect. 4.3. In Fig. 11 we show the position–velocity (PV) plot along the Jet 2 axis, namely for PA = −17°. While the LV emission (between −30 km s^{-1} and −22 km s^{-1}) is confused by the extended ^{12}CO bulk emission close to the systemic velocity of ∼−25 km s^{-1} (Brand et al. 2001), beyond this interval one sees both red- and blue-shifted emission, both at positive (∼10″) and negative (∼−10″) offsets. However, the mean velocity of the emission is slightly skewed to the red at positive offsets and to the blue at negative ones. We will demonstrate that such a difference can be explained by a (small) inclination of the outflow with respect to the plane of the sky.

To prove our hypothesis and obtain an estimate of the inclination angle (important for a correct estimate of the outflow parameters), we have applied the conical outflow model of Cesaroni et al. (1999) to our case. This is a simple-minded model that assumes that the outflowing material is confined inside a cone with aperture angle θ, inclination angle ϕ with respect to the plane of the sky, length of each lobe R_0, and expansion velocity $V = V_0 (R/R_0)$. The model computes the pattern inside which emission is expected in the PV plot. Reasonable guesses for the input parameters θ, ϕ, and V_0 can be obtained by solving Eqs. (A.6)–(A.8) of Cesaroni et al. (1999). For this purpose,

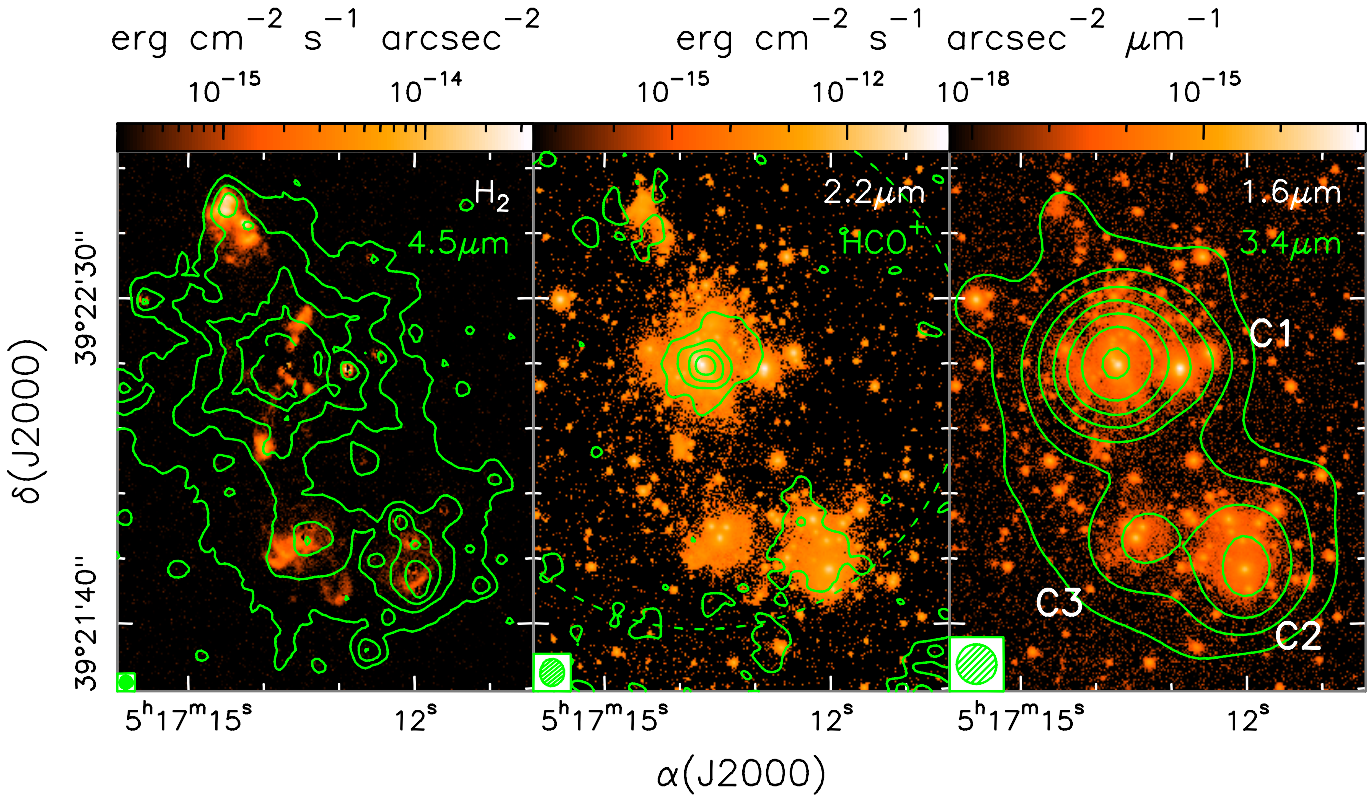

Fig. 10. *Left*: overlay of the 4.5 μm *Spitzer*/IRAC image (contours) on the LBT/LUCI image of the H_2 line emission (continuum subtracted). Contours are drawn in 5 logarithmic steps from 1 to 60 MJy/sterad. The angular resolution of the contour maps is indicated by the circle in the bottom left. *Middle*: same as left panel, for the overlay of the HCO^+(1–0) line OVRO map by Molinari et al. (2002), corrected for primary beam attenuation, on our LBT/LUCI K_s-filter image. The HCO^+ map has been obtained by averaging the emission between –28.76 and –20.78 km s^{-1}. Contour levels range from 57 to 342 in steps of 95 mJy/beam. The dashed circle denotes the primary beam of the OVRO interferometer. *Right*: same as left panel, for the overlay of the WISE 3.4 μm map on the LBT/LUCI H-filter image. Contours are drawn in 6 logarithmic steps from 1 to 76 MJy/sterad. Labels C1, C2, and C3 have the same meaning as in Fig 1.

we need an estimate of the projection of θ on the plane of the sky, θ', and the maximum and minimum velocities along the line of sight (relative to the systemic velocity of –25 km s^{-1}) observed in each lobe, $V^{(1)}_{z,max}$ and $V^{(2)}_{z,min}$ (in the notation of Cesaroni et al. 1999). The latter are obtained from Fig. 11 and are, respectively, 8.8 km s^{-1} and 7 km s^{-1}, while θ' can be estimated from the jet/outflow maps in Fig. 6 and is about 15°–30°. The solution of the three equations is $\phi \simeq 0°$, $\theta' \simeq \theta \simeq 15°$–$30°$, and $V_0 \simeq$ 16–31 km s^{-1}. Since the outflow axis lies very close to the plane of the sky, R_0 can be obtained directly from the outflow maps and is ∼14″.

The best fit was obtained by slightly varying the input values around these guesses. and is represented by the solid pattern in Fig. 11 (computed from Eqs. (A.2) and (A.3) of Cesaroni et al. 1999), which corresponds to $R_0 = 14''$, $V_0 = 30$ km s^{-1}, $\theta = 15°$, and $\phi = 2°$. The model mimics the shape of the ^{12}CO emission quite well and proves that the outflow axis is indeed almost perpendicular to the line of sight. It is instructive to check how much the pattern would change for a slightly different inclination angle, e.g. $\phi = 10°$. This is shown by the white, dashed lines in Fig. 11, which are significantly offset from the best fit. We thus conclude that the uncertainty on the inclination is very small.

It is also useful to derive the main outflow parameters. These have been computed by integrating the ^{12}CO(2–1) line emission over the lobes, in the velocity intervals –35.15, –29.65 km s^{-1} and –21.15, –16.65 km s^{-1}. In the calculation we assume LTE at a temperature of 30 K, optically thin emission, and a ^{12}CO abundance relative to H_2 of 10^{-4}. The resulting parameters have been divided by the outflow dynamical time scale $t_{dyn} = R_0/V_0 \simeq$ 0.56 pc/30 km s^{-1} $\simeq 1.8 \times 10^4$ yr, to obtain the mass loss rate, $\dot{M} = 4.2 \times 10^{-4}\ M_\odot\,\mathrm{yr}^{-1}$, and momentum rate $\dot{P} \simeq 9.2 \times 10^{-3}\ M_\odot$ km s^{-1} yr^{-1}. The latter has been corrected for the inclination of the flow with respect to the line of sight, assuming the outflow model described above. From $\dot{P}$ one can estimate the bolometric luminosity (L) of the source powering the outflow by means of the relationship between Log($\dot{P}$) and Log L derived by Wu et al. (2004). From their Fig. 7 one obtains $L \simeq 3 \times 10^4\ L_\odot$, but with a large uncertainty which allows for values ranging from $10^3\ L_\odot$ to almost $10^6\ L_\odot$. While this result does not permit us to set tight constraints on the nature of the YSO powering Jet 2, it is consistent with the bolometric luminosity estimate ($2.4 \times 10^4\ L_\odot$) obtained from the SED (see Sect. 3.1) and confirms that one is indeed dealing with a high-mass star.

4.3. Identification of the sources driving the jets

Until now, we have assumed that the YSOs powering the jets/outflows in IRAS 05137+3919 are located close to the centre of the cluster shown in Fig. 2. Here, we want to prove that the origin of the jets/outflows is to be searched among the three brightest sources: A1, A2, and B. For this purpose, in Fig. 12 we present three images of the H_2 jets, which progressively zoom

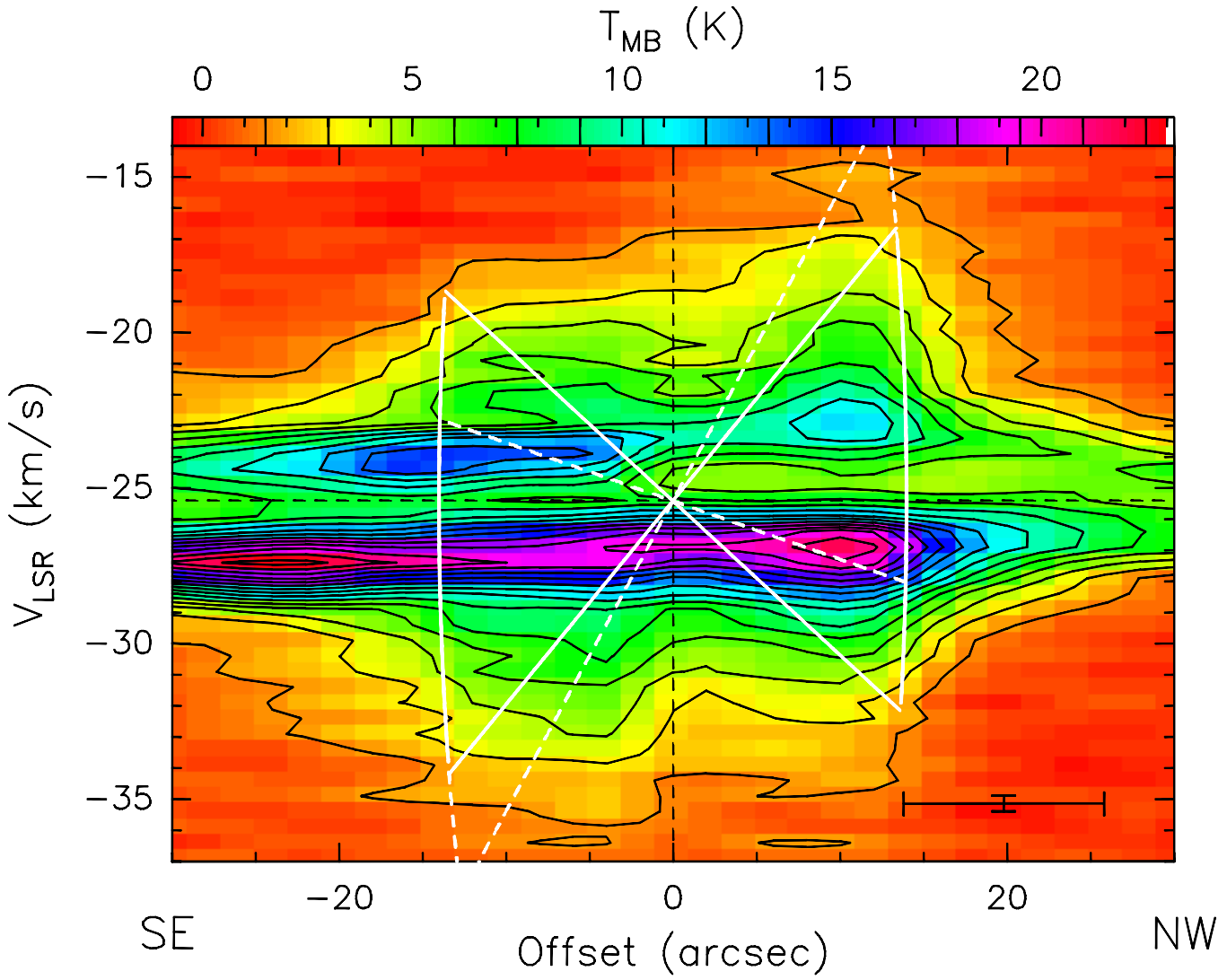

Fig. 11. Position–velocity plot of the ^{12}CO(2–1) line emission along the direction matching the axis of Jet 2, i.e. with PA = −17°. The values of the contour levels are shown in the colour scale at the top of the figure. The offset is measured from an arbitrary position. The vertical and horizontal dashed lines indicate, respectively, the position of stars A+B and the systemic velocity of the associated clump. The white solid pattern encloses the region inside which emission is expected for the conical jet model that best fits the data (see text). The dashed pattern corresponds to the same model with a slightly different inclination angle (10° instead of 2°; see text).

into the neighbourhood of the three objects. For the sake of comparison, we also draw the borders of the conical jet model described in Sect. 4.2.2 (short-dash blue lines), centred on the position of B. This looks like an obvious choice, because star B lies right along the symmetry axis of Jet 2, unlike A1 and A2. Moreover, if the origin of the flow were shifted along that axis, the model in Fig. 11 could not reproduce the blue-red symmetry of the observed PV plot. Although one cannot rule out the possibility that another deeply embedded, yet undetected star within a couple of arcsec from B is powering Jet 2, this appears quite unlikely for the following reason. A1, A2, and B lie at the very peak of the molecular line and mm continuum emission, where the column density should be highest (see Fig. 13). Despite this fact, all of them have been detected in our images, even at *H*-band, which makes it difficult to believe that any other similar (or more luminous) star *in the neighbourhood*, where the column density is lower, could be so embedded to be undetectable. We thus conclude that star B is likely to be powering Jet 2.

In Fig. 12, we also draw a tentative pattern for Jet 1 (red long-dash lines), under the working hypothesis that this originates from A1 or A2. The aperture angle of the jet is greater than for Jet 1 (∼20°), consistent with the ^{12}CO outflow map in Fig. 6. In Fig. 13 one sees that the peak of the 3.6 cm continuum emission (Molinari et al. 2002) is roughly consistent with the position of A1/A2, with a tail of emission extending to the NE, in the direction of Jet 1. This alignment suggests that at least part of the free-free emission could originate from a thermal jet tracing the root of Jet 1. The most direct evidence for a tight association between A1/A2 and Jet 1 is presented in the right panel of Fig. 12, where we plot the relative proper motions of the H_2O masers observed by Honma et al. (2011). These are clearly expanding along the Jet 1 axis, from a centre whose position is compatible (within the astrometrical uncertainty of the IR images) with that of the A1/A2 pair. Since water masers are believed to form in shocks, the observed association indicates that the maser motions are tracing the innermost part of the jet.

This result casts some doubt on the interpretation of A1 and A2 as a binary system. Since the two objects are aligned along the Jet 1 axis, one should consider the possibility that they are the lobes of a small bipolar reflection nebula. Such

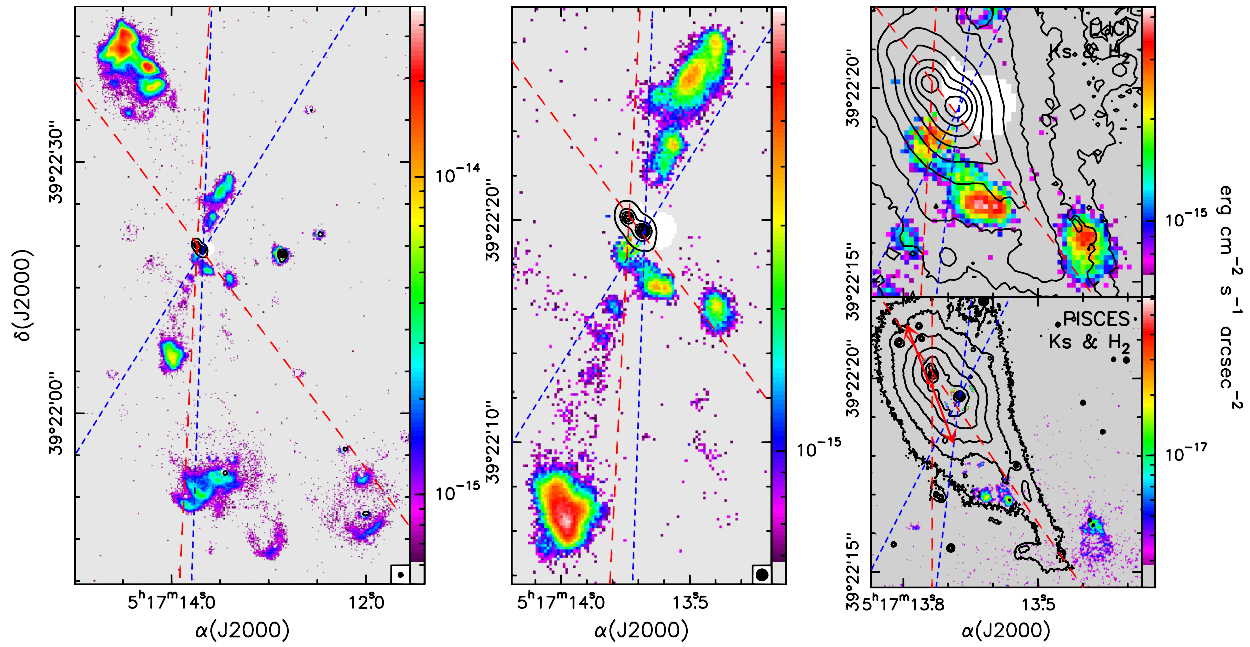

Fig. 12. *Left*: LUCI image of the H_2 line emission (continuum subtracted) tracing the jets in IRAS 05137+3919. The artefact due to continuum subtraction at the position of stars A1, A2, and B has been blanked (white area). The contours are a map of the continuum emission measured in the K_s filter. The contour levels have been chosen to show only the brightest stars in the field. The red long-dash and blue short-dash lines indicate, respectively, the borders of Jet 1 and Jet 2. *Middle*: same as left panel, for a smaller region centred on the jets' origin. *Right*: same as left panel, for a comparison between the H_2 line and K_s continuum images taken with LUCI (*top*) and PISCES (*bottom*). The red points and corresponding arrows denote the H_2O maser spots and associated relative proper motions measured by Honma et al. (2011).

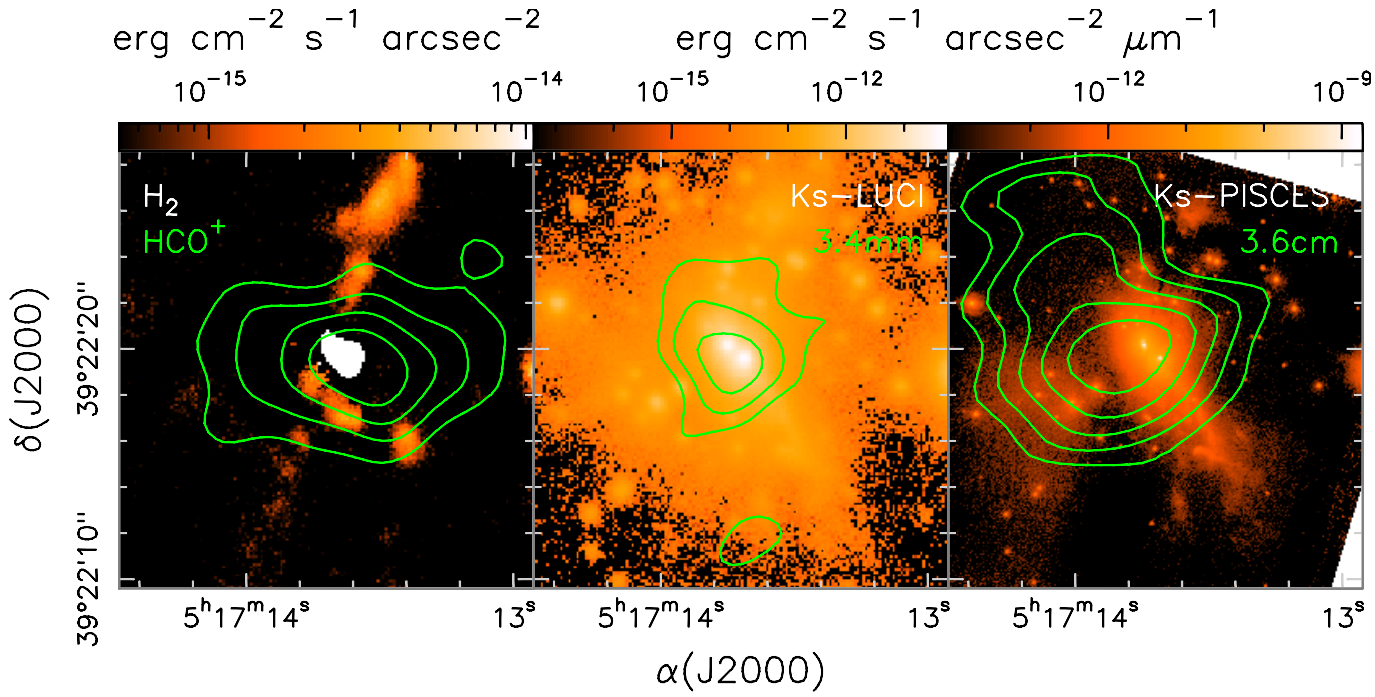

Fig. 13. *Left*: overlay of the contour map of the HCO^+(1–0) line (from Molinari et al. 2002) obtained by averaging the emission between –27.08 and –23.72 km s^{-1}, on the H_2 line (i.e. continuum subtracted) LUCI image. Contour levels range from 150 to 420 in steps of 90 mJy/beam. Like in Fig. 12, the area around stars A1, A2, and B has been blanked to mask an artefact caused by the continuum-subtraction process. *Middle*: overlay of the contour map of the 3.4 mm continuum emission (from Molinari et al. 2002) on the 2.2 μm continuum LUCI image. Contour levels range from 2.64 to 4.4 in steps of 0.88 mJy/beam. *Right*: overlay of the contour map of the 3.6 cm continuum emission (from Molinari et al. 2002) on the 2.2 μm continuum PISCES image. Contour levels range from 0.069 to 0.161 in steps of 0.023 mJy/beam.

an interpretation is supported by a comparison in the PISCES K_s image between the shapes of A1 and A2, on the one hand, and B, on the other hand. While the latter appears approximately circular, A1 and A2 are slightly elongated, respectively, in the E–W and N–S directions. Since the separations of the sources from the guide star are similar, the different shapes are unlikely to be due to anisoplanatism. We used DAOPHOT in IRAF to compare the PSFs by performing some experiments on the K_s image. We

found that when using B as the reference PSF, after PSF subtraction through a fit, both A1 and A2 are oversubtracted, consistent with them being slightly more extended. Moreover, when using A2 as the reference PSF, after subtraction A1 is still oversubtracted, whereas B is now undersubtracted, consistent with A1 being slightly more extended than A2. In summary, the PSFs of A1 and A2 differ from each other and that of A1 departs the most from a stellar PSF.

In the light of the previous results, it seems plausible that A1 and A2 are not point-like stars but the marginally resolved lobes of a bipolar reflection nebula. In this case, the dark lane between the lobes could be due to a circumstellar disk, with size on the order of the separation between A1 and A2, namely ~1500 au. This value is similar to the diameter of disks around high-mass (proto)stars (see Cesaroni et al. 2007). Note that the distance between the two maser spots is ~1120 au, slightly less than the separation A1–A2, in agreement with a scenario where the masers trace the expansion of the jet in the densest part of it, closer to the star than the IR lobes, as observed in other similar objects (e.g. the massive protostar IRAS 20126+4104; see Cesaroni et al. 2013). We note also that the brightest source, A2, lies to the SW, namely in the direction of the blue-shifted lobe of jet1, consistent with the expectation that the brighter lobe of a reflection nebula is the one pointing to the observer.

In conclusion, one should seriously consider the possibility that the pair A1/A2 is not a binary system, but a bipolar nebula associated with a disk+jet system from a massive star.

4.3.1. Jet 3

Finally, we investigate the nature of (putative) Jet 3. The right panel of Fig. 12 shows an enlargement of it, with a comparison between the LUCI and PISCES images. At lower angular resolution the H_2 emission seems to trace an elongated lobe, made out of 3 knots, with the northernmost of these lying ~1″ to the south of A1/A2. This structure suggests that one might indeed be observing a jet originating from another (lower-mass) star beside A1, A2, and B. However, in the high resolution image the first knot to the E disappears, whereas the others are still visible albeit partly resolved out. In our opinion, this indicates that the northern knot is an artefact due to residuals in the subtraction of the K_s continuum from the H_2 filter, in the LUCI images. If this is the case, the other knots could be associated with Jet 1. In conclusion, while the presence of a third jet from another (possibly low-mass) YSO in the cluster cannot be excluded, we prefer to consider the simplest possible scenario, where all H_2 knots are explained with only two jets (Jet 1 and Jet 2). Only future, more sensitive images of the jet/outflow structure could help us to establish the correct interpretation.

4.4. Nature of A1/A2 and B

The luminosity measured in Sect. 3.1 sets an upper limit of $\sim 2.4 \times 10^4\ L_\odot$ to that of the most massive member of cluster C1. There is little doubt that the luminosity must be dominated by A1/A2 and B, as these are by far the brightest sources in the field, with A2 being the brightest at K_s-band (11.2 mag) and the one with the largest colour index (H–K_s = 3.8 mag). We deduce that the corresponding star is the most massive in the cluster, no matter whether A2 is a real star or the lobe of a reflection nebula. Actually, in the latter case, one would see only part of the photons emitted by the embedded star, thus lending further support to our previous statement that this is the most massive member of cluster C1.

When discussing the luminosity of C1, is worth taking into account the inclination of the jets with respect to the line of sight. We have seen that Jet 2 lies close to the plane of the sky. A similar conclusion is likely to hold also for Jet 1, if A1 and A2 are reflection nebulae, because if the jet axis were close to the line of sight the nebulosity associated with the red-shifted lobe would not be detected. It has been shown (see Fig. 10 of Whitney et al. 2003) that beaming of photons along the jet axis, the so-called "flashlight effect", may lead to an underestimate of the source luminosity by a factor 2 – or even more (see Zhang et al. 2013). We thus caution that the luminosity of C1 might be significantly greater than our previous estimate of $\sim 2.4 \times 10^4\ L_\odot$.

We have attempted a more precise estimate of the total luminosity of A1+A2+B by fitting only the 2MASS J, H, K_s, our 8.9–18.7 μm, and the L-band measurements by Ishii et al. (1998), with the on-line model fitter[4] by Robitaille et al. (2013). The other fluxes in Fig. 3 were set as upper limits. In the calculations we have fixed the distance to 8.3 kpc and assumed an interstellar visual extinction $A_V < 5$ (see Rowles & Frobrich 2013). Despite the loose constraints, the first 50 best-fit models span a relatively small range in luminosity, $L_{mod} = (4.4–15) \times 10^3\ L_\odot$. Taken at face value, this implies that 38–82% of the luminosity of cluster C1 is due to the lower-mass members of it. A range of values for the maximum stellar mass among A1, A2, and B is obtained under the two opposite assumptions that either only one star is responsible for L_{mod}, or all three stars equally contribute to L_{mod}. Correspondingly, one obtains a range for the most massive star in the cluster of 8–15 $M_\odot$ (see e.g. Diaz-Miller et al. 1998).

Alternatively, the luminosity of the most massive star(s) can be derived from the radio continuum flux density, assuming that this originates from an optically thin HII region around an early-type star. One can compute the stellar Lyman continuum emission, and hence the luminosity, as done by Molinari et al. (2002), who obtain a Lyman continuum photon rate of $\sim 2 \times 10^{45}$ s^{-1} (after scaling from their distance of 11.5 kpc to ours of 8.3 kpc), corresponding to a luminosity of $\sim 6 \times 10^3\ L_\odot$ and a stellar mass of ~11 $M_\odot$. These numbers appear to agree quite well with our previous estimates; however one should keep in mind that the radio continuum emission could be due to a thermal jet rather than a photoionised HII region. Multi-wavelength radio maps with better angular resolution are needed to establish the nature of this emission.

Finally, we attempt an estimate of the luminosity using the H_2 line emission. Following Caratti o Garatti et al. (2006), one may relate L to the luminosity in the H_2 line, L_{H_2}, by means of the expression $\mathrm{Log}[L_{H_2}(L_\odot)] = (0.58 \pm 0.06)\,\mathrm{Log}[L(L_\odot)] - (1.4 \pm 0.06)$ which holds for jets associated with stars from 0.1 to $10^5\ L_\odot$ (see Caratti o Garatti et al. 2013). We have computed L_{H_2} following the recipe of Caratti o Garatti et al. (2006), namely integrating the emission over all H_2 knots belonging to the jet and then multiplying by 10 to correct for the energy radiated in the other non-observed H_2 transitions. A further correction for the interstellar extinction must be applied. The Robitaille model fit previously described corresponds to a range A_V = 1.2–2.9, which translates into a correction factor at the wavelength of the H_2 filter (2.12 μm) of $10^{A_{2.12\ \mu m}/2.5}$ = 1.13–1.35 (where we assume a ratio $A_{2.12\ \mu m}/A_V = 0.112$; see Rieke & Lebofsky 1985). From the LUCI H_2 image we obtain $L_{H_2} \simeq 7.4\ L_\odot$ for Jet 1 and

[4] See http://caravan.astro.wisc.edu/protostars/sedfitter.php

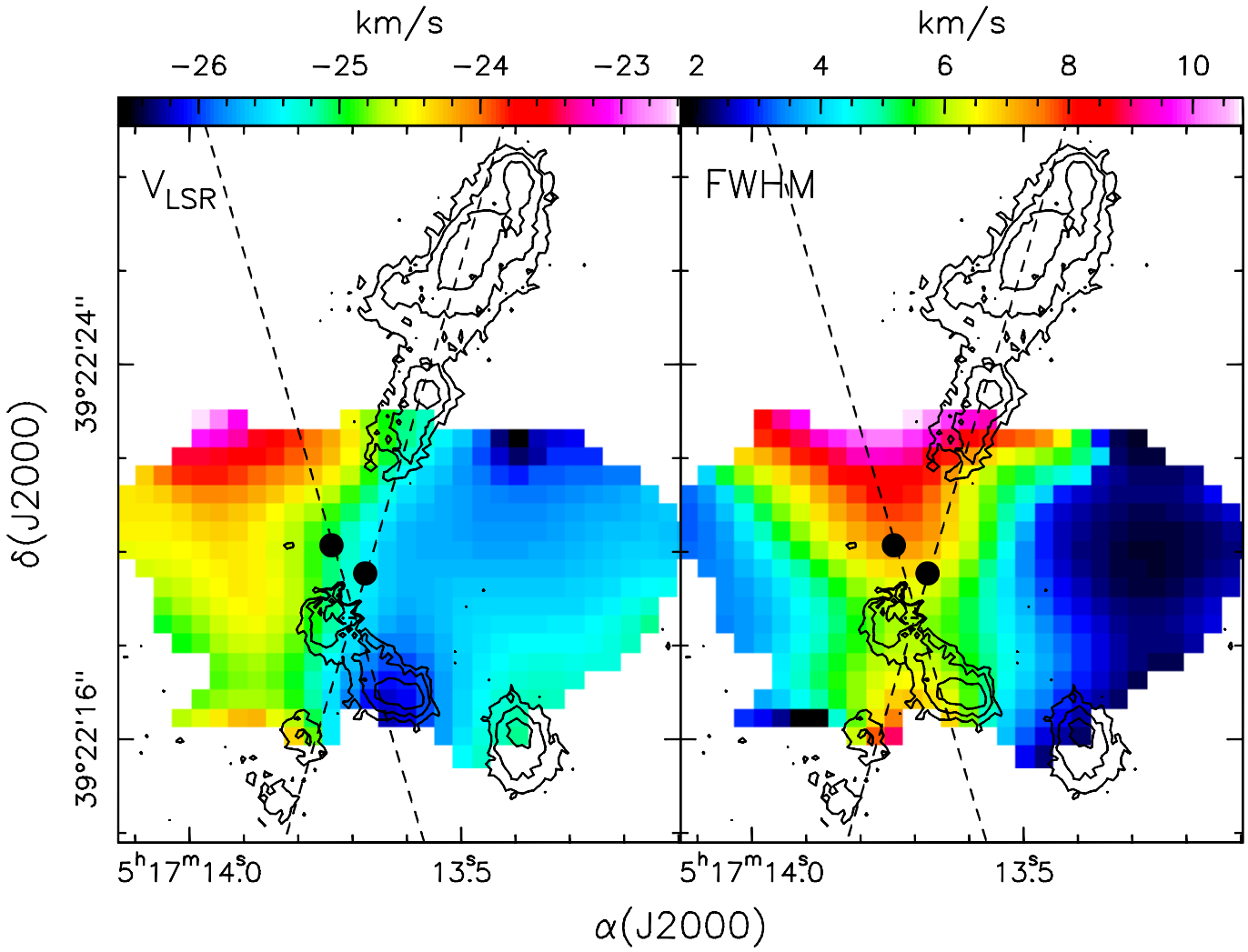

Fig. 14. *Left*: overlay of the H_2 line (i.e. continuum subtracted) LUCI image (contours) on a map of the peak LSR velocity of the HCO^+(1–0) line observed by Molinari et al. (2002). The artefacts due to continuum subtraction in the H_2 image have been blanked as already done in Fig. 12. The dashed lines represent the axes of Jet 1 and Jet 2, while the two black points indicate the positions of stars A1+A2 and B. *Right*: same as left panel, for the HCO^+(1–0) line full width at half maximum.

$L_{H_2} \simeq 1.5\ L_\odot$ for Jet 2, which imply, respectively, $L \simeq 8\times10^3\ L_\odot$ and $L \simeq 5\times10^2\ L_\odot$. These values are in good agreement with the those previously obtained from the IR fluxes and free-free radio emission, and confirm that star B could be powering Jet 2, while Jet 1 could originate from A1+A2, the most massive star(s) in cluster C1.

4.5. Structure and kinematics of the molecular core

The interferometric observations of Molinari et al. (2002) have established the presence of a compact molecular core, where stars A1+A2 and B seem to be embedded. It is interesting to investigate the structure and kinematics of this core in relationship to the observed jets and stars. In Fig. 13 we plot a map of the HCO^+(1–0) bulk emission (contours in the left panel) on the image of the H_2 line emission. Note that the HCO^+ map in this figure differs from that in the middle panel of Fig. 10 because the latter has been obtained by integrating the HCO^+ emission over the whole line profile, whereas the former considers only a small range around the systemic velocity. The shape of the core appears elongated E–W, namely roughly perpendicular to Jet 1 and Jet 2.

In Fig. 14 we analyse the velocity field of the core, through maps of the peak velocity and line full width at half maximum (FWHM). These parameters have been obtained with a Gaussian fit to the HCO^+ line profile, pixel by pixel, over the whole region where HCO^+ emission was detected above 5σ. A clear velocity gradient is present in the E–W direction, with A1, A2 and B lying at positions where the velocity equals the systemic velocity of –25 km s^{-1}. The line FWHM is minimum to the E and W of the core, and attains its maximum to the N and S, approximately where the jets emerge from the core. This suggests that the core is significantly perturbed by the material expanding along those directions. The question is how to interpret the shift observed in the peak velocity. It is possible that such a shift is due to Jet 1, whose red–blue symmetry looks consistent with the direction joining the maximum (located to the NE) and minimum (to the SW) HCO^+ peak velocities. However, maximum/minimum velocities are seen also to the SE/NW and looking at the whole velocity field one gets the impression that the mean velocity gradient is directed E–W rather than NE–SW.

With this in mind, one is tempted to interpret the velocity gradient as rotation of the core about the jets' axes. Under this hypothesis, the mass needed to guarantee rotational equilibrium

of an oblate core with angular diameter ∼8″ and rotation velocity ∼2 km s^{-1} is ∼150 $M_\odot$. This may be compared with the mass of the core computed from the 3.4 mm continuum flux of 21 mJy (see Table 3 of Molinari et al. 2002). In our calculation we adopt a dust absorption coefficient of 0.01 cm^2 g^{-1} at 1.3 mm (for a gas-to-dust mass ratio of 100 and using the estimates of Ossenkopf & Henning 1994), scaling like $\propto \lambda^{-\beta}$ with $\beta = 1$, and a dust temperature of 60 K (estimated from the ratio of the NH_3(1,1) and (2,2) inversion transitions observed in the RMS survey[5] (Lumsden et al. 2013). Under these assumptions we obtain ∼120 $M_\odot$, with a large error due to the uncertainty on the dust absorption coefficient and dust temperature. Nonetheless, the core mass is of the same order of magnitude as the dynamical mass, consistent with the hypothesis of a core in rotational equilibrium.

Based on the above, one may speculate that the stellar cluster is the result of the fragmentation of a rotating core, yielding a couple of massive stars with (remnants of) circumstellar disks, whose observable manifestations are Jet 1 and Jet 2. Further interferometric observations of the dense molecular gas are required to lend support to the proposed scenario.

5. Summary and conclusions

We performed observations at near-IR, mid-IR, and millimetre wavelengths of the star forming region IRAS 05137+3919 to investigate the complex jet structure and the associated stellar cluster(s). The dramatically improved sensitivity and resolution as well as the broad frequency coverage obtained by complementing our data with archival data, allow us to obtain a number of results:

- We identify 3 stellar clusters (C1, C2 and C3) in the region, with the two richest ones being embedded in molecular clumps.
- The luminosity of the richest cluster, C1, which contains the brightest stars, is ∼2.4 × 10^4 $L_\odot$, a value typical of early B-type stars. We indeed conclude that the most massive star in C1 has a mass of ∼8–15 $M_\odot$.
- Employing adaptive optics, we resolve the densest part of cluster C1 thus significantly increasing the number of known cluster members with respect to previous estimates based on lower resolution images. In particular, we find that of the two brightest stars, A and B, previously identified, the first is actually made of two distinct sources that we name A1 and A2.
- The stellar cluster C1 turns out to be richer and less concentrated than those observed by other authors around Herbig Be stars and we thus speculate that the difference could be due to an evolutionary effect.
- We confirm the existence of (at least) 2 bipolar jets/outflows and demonstrate that they originate from C1. Using various approaches, we come to the conclusion that both jets must be powered by early B-type stars.
- By comparing the geometry and velocity field of the jets/outflows to the properties and location of the stars, we propose that the smaller jet is powered by the more luminous and less embedded star B, whereas the largest jet originates from the pair A1+A2.
- We speculate that A1+A2 could be a small bipolar nebula along the jet axis, outlining a disk of ∼10^3 au seen in silhouette. This hypothesis is supported by the fact that the molecular gas appears to rotate (although on a much larger scale of ∼0.2 pc) about the jet axis.

Our findings demonstrate the potential of sub-arcsecond resolution in the near IR to investigate high-mass star forming regions and call for further imaging at (sub)millimetre wavelengths with comparable resolution to shed light on the circumstellar environment and its connection with the large-scale jets. To date, only the ALMA interferometer can resolve structures as small as ∼100 mas and thus allow one to study the gas kinematics and physical properties on scales ≲100 au in IRAS 05137+3919 and similar regions.

Acknowledgements. It is a pleasure to thank Francesca Bacciotti and Daniele Galli for instructive discussions on jets from YSOs. M.T. acknowledges support from UNAM/PAPIIT grant No. IN-101813. This work is based in part on observations made with the *Spitzer* Space Telescope, which is operated by the Jet Propulsion Laboratory, California Institute of Technology under a contract with NASA. This publication also makes use of data products from the Two Micron All Sky Survey, which is a joint project of the University of Massachusetts and the Infrared Processing and Analysis Center/California Institute of Technology, funded by the National Aeronautics and Space Administration and the National Science Foundation.

References

Allen, C. W. 1976, Astrophysical Quantities, 3rd edn. (London: Athlone press)
Brand, J., Cesaroni, R., Palla, F., & Molinari, S. 2001, A&A, 370, 230
Caratti o Garatti, A., Giannini, T., Nisini, B., & Lorenzetti, D. 2006, A&A, 449, 1077
Caratti o Garatti, A., Stecklum, B., Linz, H., Garcia Lopez, R., & Sanna, A. 2013, Protostars and Planets VI, Heidelberg, July 15–20, Poster #1K043 http://www.mpia-hd.mpg.de/homes/ppvi/posters/1K043.pdf
Cesaroni, R., Felli, M., Jenness, T., et al. 1999, A&A, 345, 949
Cesaroni, R., Neri, R., Olmi, L., et al. 2005, A&A, 434, 1039
Cesaroni, R., Galli, D., Lodato, G., Walmsley, C. M., & Zhang, Q. 2007, in Protostars and Planets V, eds. B. Reipurth, D. Jewitt, & K. Keil (Tucson: Univ. of Arizona Press), 197
Cesaroni, R., Massi, F., Arcidiacono, C., et al. 2013, A&A, 549, A146
D'Alessio, P., Merín, B., Calvet, N., Hartmann, L., & Montesinos, B. 2005, Rev. Mex. Astron. Astrofis., 41, 61
Diaz-Miller, R. I., Franco, J., & Shore, S. N. 1998, ApJ, 501, 192
Di Francesco, J., Johnstone, D., Kirk, H., MacKenzie, T., & Ledwosinka, E. 2008, ApJS, 175, 277
Esposito, S., Riccardi, A., Quirós-Pacheco, F., et al. 2010, Appl. Opt., 49, 174
Esposito, S., Riccardi, A., Pinna, E., et al. 2011, in Astronomical Adaptive Optics Systems and Applications IV, eds. R. K. Tyson, & M. Hart, Proc. SPIE, 8149, 814902
Esslinger, O, & Edmunds, M. G., 1998, A&AS, 129, 617
Faustini, F., Molinari, S., Testi, L., & Brand, J. 2009, A&A, 503, 801
Fazio, G. G., Hora, J. L., Allen, L. E., et al. 2004, ApJS, 154, 10
Honma, M., Hirota, T., Kan-Ya, Y., et al. 2011, PASJ, 63, 17
Ishii, M., Nagata, T., Sato, S., Watanabe, M., & Yao, Y. 1998, ApJ, 116, 868
Ishii, M., Nagata, T., Sato, S., et al. 2001, ApJ, 121, 3191
Ishii, M., Hirao, T., Nagashima, C., Nagata, T., & Sato, S. 2002, ApJ, 124, 430
Koornneef, J. 1983, A&A, 128, 84
Kumar, M. S. N., Keto, E., & Clerkin, E. 2006, A&A, 449, 1033
López-Chico, T. A., & Salas, L., 2007, Rev. Mex. Astron. Astrofis., 43, 155
Lumsden, S. L., Hoare, M. G., Urquhart, J. S., et al. 2013, ApJS, 208, 11
McCarthy, D. W., Jr., Ge, J., Hinz, J. L., Finn, R. A., & de Jong, R. S. 2001, PASP, 113, 353
Molinari, S., Brand, J., Cesaroni, R., & Palla, F. 1996, A&A, 308, 573
Molinari, S., Brand, J., Cesaroni, R., Palla, F., & Palumbo, G. G. C. 1998, ApJ, 336, 339
Molinari, S., Testi, L., Rodríguez, L. F., & Zhang, Q. 2002, ApJ, 570, 758
Molinari, S., Pezzuto, S., Cesaroni, R., et al. 2008, A&A, 481, 345
Molinari, S., Swinyard, B., Bally, J., et al. 2010, PASP, 122, 314
Nikoghosyan, E. H., & Azatyan, N. 2014, Astrophysics, 57, 330
Nikoghosyan, E. H., & Azatyan, N. 2015, Astrophysics, submitted [arXiv:1501.06717v1]
Ossenkopf, V., & Henning, Th. 1994, A&A, 291, 943
Palla, F., & Stahler, S. W. 1999, ApJ, 525, 722
Panagia, N. 1973, AJ, 78, 929

[5] See http://rms.leeds.ac.uk/cgi-bin/public/RMS_DATABASE.cgi

Price, S. D., Egan, M. P., & Shipman, R. F. 1999, Astrophysics with Infrared Surveys: A prelude to SIRTF, 177, 394
Reid, M. J., Menten, K. M., Brunthaler, X. W., et al. 2014, ApJ, 783, 130
Rieke, G. H., & Lebofsky, M. J. 1985, ApJ, 288, 618
Robitaille, T. P., Whitney, B. A., Indebetouw, R., & Wood, K. 2007, ApJS, 169, 328
Rowles, J., & Froebrich, D. 2009, MNRAS, 395, 1640
Salas, S., Cruz-González, I., & Tapia, M. 2006, Rev. Mex. Astron. Astrofis., 42, 273
Scalo, J. 1998, The IMF Revisited: A Case for Variations. In The Stellar Initial Mass Function, Proc. of the 38th Herstmonceux Conf., eds. G. Gilmore, & D. Howell, ASP Conf. Ser., 142, 201
Schuster, K.-F., Boucher, C., Brunswig, W., et al. 2004, A&A, 423, 1171
Seifert, W., Appenzeller, I., Baumeister, H., et al. 2003, Proc. SPIE, 4841, 962
Skrutskie, M. F., Cutri, R. M., Stiening, R., et al. 2006, AJ, 131, 1163
Stone, J. M., Xu, J., & Hardee, P. E. 1997, ApJ, 483, 136
Testi, L., Palla, F., & Natta, A. 1998, A&AS, 133, 81
Testi, L., Palla, F., & Natta, A. 1999, A&A, 342, 515
Varricatt, W. P., Christopher, J. D., Ramsay, S., & Todd, S. P. 2010, MNRAS, 404, 661
Werner, M., Roellig, T., Low, F., et al. 2004, ApJS, 154, 1
Whitney, B. A., Wood, K., Bjorkman, J. E., & Wolff, M. J. 2003, ApJ, 591, 1049
Wood, D. O. S., & Churchwell, E. 1989, ApJ, 340, 265
Wright, E. L., Eisenhardt, P. R. M., Mainzer, A. K., et al. 2010, AJ, 140, 1868
Wu, Y., Wei, Y., Zhao, M., et al. 2004, A&A, 426, 503
Zhang, Q., Hunter, T. R., Brand, J., et al. 2001, ApJ, 552, L167
Zhang, Q., Hunter, T. R., Brand, J., et al. 2005, ApJ, 625, 864
Zhang, Y., Tan, J. C., De Buizer, J. M., et al. 2013, ApJ, 767, 58

Pages 19 to 46 are available in the electronic edition of the journal at http://www.aanda.org

Appendix A

Table A.1. Coordinates, magnitudes, and colour of the sources identified in the LUCI field. The symbol "–" indicates a non-detection.

RA (hh mm ss)	Dec (dd mm ss)	H (mag)	K_s (mag)	H–K_s (mag)
05 17 08.27	39 20 05.7	17.696 ± 0.067	18.434 ± 0.075	0.738 ± 0.101
05 17 17.36	39 20 06.1	17.414 ± 0.052	18.193 ± 0.073	0.779 ± 0.090
05 17 04.02	39 20 15.5	17.140 ± 0.068	18.266 ± 0.058	1.126 ± 0.089
05 17 15.98	39 20 18.6	18.734 ± 0.047	19.134 ± 0.052	0.400 ± 0.070
05 16 58.23	39 20 18.6	17.635 ± 0.035	17.840 ± 0.033	0.205 ± 0.048
05 17 10.02	39 20 23.7	18.748 ± 0.051	19.199 ± 0.045	0.451 ± 0.068
05 17 02.51	39 20 25.5	16.127 ± 0.015	16.402 ± 0.013	0.275 ± 0.020
05 17 21.91	39 20 28.7	16.961 ± 0.033	17.446 ± 0.034	0.485 ± 0.047
05 17 28.64	39 20 29.9	15.775 ± 0.021	16.042 ± 0.017	0.267 ± 0.027
05 17 29.06	39 20 30.1	18.862 ± 0.080	19.173 ± 0.094	0.311 ± 0.123
05 17 16.69	39 20 37.2	17.603 ± 0.026	17.967 ± 0.025	0.364 ± 0.036
05 17 19.40	39 20 38.8	17.675 ± 0.022	18.101 ± 0.029	0.426 ± 0.036
05 17 00.70	39 20 38.6	19.008 ± 0.109	19.272 ± 0.072	0.264 ± 0.131
05 17 02.26	39 20 39.9	18.578 ± 0.064	19.035 ± 0.054	0.457 ± 0.084
05 17 06.13	39 20 40.1	18.120 ± 0.030	18.394 ± 0.027	0.274 ± 0.040
05 17 22.89	39 20 41.5	18.600 ± 0.045	19.069 ± 0.049	0.469 ± 0.067
05 16 57.39	39 20 52.6	18.697 ± 0.124	18.947 ± 0.093	0.250 ± 0.155
05 17 14.58	39 20 52.9	17.951 ± 0.029	18.495 ± 0.028	0.544 ± 0.040
05 17 09.44	39 20 52.9	19.187 ± 0.048	19.559 ± 0.069	0.372 ± 0.084
05 17 11.29	39 20 55.0	19.419 ± 0.075	19.938 ± 0.103	0.519 ± 0.127
05 17 01.21	39 20 56.3	17.546 ± 0.032	17.772 ± 0.021	0.226 ± 0.038
05 17 10.33	39 20 57.8	19.740 ± 0.103	20.059 ± 0.080	0.319 ± 0.130
05 17 07.45	39 20 58.9	14.695 ± 0.008	14.893 ± 0.009	0.198 ± 0.012
05 17 26.87	39 21 00.4	17.628 ± 0.036	17.920 ± 0.035	0.292 ± 0.050
05 17 14.82	39 21 02.1	19.465 ± 0.081	19.971 ± 0.069	0.506 ± 0.106
05 17 25.31	39 21 03.3	16.220 ± 0.021	16.442 ± 0.017	0.222 ± 0.027
05 17 11.59	39 21 03.5	18.306 ± 0.028	18.782 ± 0.030	0.476 ± 0.041
05 17 15.45	39 21 04.8	19.005 ± 0.058	19.571 ± 0.049	0.566 ± 0.076
05 17 07.36	39 21 05.0	18.724 ± 0.049	19.095 ± 0.036	0.371 ± 0.061
05 17 05.00	39 21 05.2	19.288 ± 0.065	19.715 ± 0.072	0.427 ± 0.097
05 16 57.89	39 21 07.0	17.950 ± 0.048	18.146 ± 0.041	0.196 ± 0.063
05 17 17.80	39 21 07.5	19.088 ± 0.052	19.453 ± 0.049	0.365 ± 0.071
05 17 05.88	39 21 08.0	18.190 ± 0.025	18.589 ± 0.029	0.399 ± 0.038
05 17 14.58	39 21 08.6	18.593 ± 0.029	19.175 ± 0.041	0.582 ± 0.050
05 17 08.07	39 21 08.9	17.322 ± 0.015	17.695 ± 0.016	0.373 ± 0.022
05 17 25.68	39 21 09.5	17.842 ± 0.045	18.211 ± 0.031	0.369 ± 0.055
05 17 02.07	39 21 09.5	18.198 ± 0.035	18.469 ± 0.036	0.271 ± 0.050
05 16 59.45	39 21 11.2	19.369 ± 0.119	19.712 ± 0.127	0.343 ± 0.174
05 17 12.37	39 21 13.9	15.668 ± 0.008	15.947 ± 0.007	0.279 ± 0.011
05 17 16.66	39 21 15.7	18.356 ± 0.032	18.724 ± 0.035	0.368 ± 0.047
05 17 07.99	39 21 17.0	17.103 ± 0.016	17.419 ± 0.012	0.316 ± 0.020
05 17 12.90	39 21 19.9	18.099 ± 0.021	18.521 ± 0.025	0.422 ± 0.033
05 17 14.91	39 21 20.1	17.731 ± 0.020	18.187 ± 0.016	0.456 ± 0.026
05 17 11.21	39 21 21.2	15.388 ± 0.006	15.788 ± 0.007	0.400 ± 0.009
05 17 03.03	39 21 22.4	18.257 ± 0.040	18.549 ± 0.034	0.292 ± 0.052
05 17 23.37	39 21 26.6	15.390 ± 0.013	15.734 ± 0.013	0.344 ± 0.018
05 17 12.41	39 21 27.5	16.859 ± 0.012	17.293 ± 0.009	0.434 ± 0.015
05 17 08.41	39 21 29.3	14.205 ± 0.006	14.395 ± 0.008	0.190 ± 0.010
05 17 11.52	39 21 29.6	16.553 ± 0.010	17.111 ± 0.008	0.558 ± 0.013
05 17 14.48	39 21 30.8	19.221 ± 0.060	19.560 ± 0.061	0.339 ± 0.086
05 17 10.52	39 21 31.1	19.136 ± 0.056	19.651 ± 0.074	0.515 ± 0.093
05 17 20.64	39 21 31.5	16.677 ± 0.011	17.047 ± 0.012	0.370 ± 0.016
05 17 06.36	39 21 32.3	18.935 ± 0.052	19.528 ± 0.079	0.593 ± 0.095
05 17 15.30	39 21 32.9	18.528 ± 0.029	19.117 ± 0.040	0.589 ± 0.049
05 17 18.33	39 21 33.0	19.216 ± 0.077	19.516 ± 0.062	0.300 ± 0.099
05 17 14.82	39 21 35.2	16.148 ± 0.007	16.559 ± 0.006	0.411 ± 0.009
05 16 59.51	39 21 39.1	15.035 ± 0.013	15.201 ± 0.011	0.166 ± 0.017
05 17 10.99	39 21 39.6	17.665 ± 0.020	17.928 ± 0.016	0.263 ± 0.026
05 17 17.79	39 21 39.9	18.696 ± 0.038	19.202 ± 0.046	0.506 ± 0.060
05 17 25.53	39 21 46.8	16.247 ± 0.025	16.575 ± 0.015	0.328 ± 0.029
05 17 13.82	39 21 46.7	19.105 ± 0.042	19.735 ± 0.068	0.630 ± 0.080
05 17 09.30	39 21 47.7	19.116 ± 0.053	19.553 ± 0.061	0.437 ± 0.081
05 17 21.77	39 21 48.3	19.306 ± 0.091	19.738 ± 0.078	0.432 ± 0.120

Table A.1. continued.

RA (hh mm ss)	Dec (dd mm ss)	H (mag)	K_s (mag)	H–K_s (mag)
05 17 12.83	39 21 48.2	16.519 ± 0.008	16.902 ± 0.008	0.383 ± 0.011
05 17 15.15	39 21 48.4	15.979 ± 0.013	16.523 ± 0.009	0.544 ± 0.016
05 17 12.54	39 21 49.8	15.056 ± 0.010	16.315 ± 0.012	1.259 ± 0.016
05 17 11.85	39 21 52.5	15.949 ± 0.011	16.635 ± 0.009	0.686 ± 0.014
05 17 13.90	39 21 55.2	18.505 ± 0.035	19.212 ± 0.048	0.707 ± 0.059
05 17 15.76	39 21 55.5	18.587 ± 0.029	19.280 ± 0.046	0.693 ± 0.054
05 17 19.74	39 21 56.6	18.184 ± 0.035	18.555 ± 0.030	0.371 ± 0.046
05 17 11.56	39 21 57.1	14.454 ± 0.005	15.020 ± 0.004	0.566 ± 0.006
05 17 14.59	39 21 57.7	19.024 ± 0.054	19.936 ± 0.090	0.912 ± 0.105
05 17 13.62	39 21 57.9	18.334 ± 0.025	19.077 ± 0.042	0.743 ± 0.049
05 17 10.06	39 22 01.8	19.436 ± 0.069	19.978 ± 0.074	0.542 ± 0.101
05 17 09.40	39 22 02.2	17.969 ± 0.020	18.584 ± 0.022	0.615 ± 0.030
05 17 16.97	39 22 02.6	18.095 ± 0.027	18.431 ± 0.027	0.336 ± 0.038
05 17 24.55	39 22 05.4	14.708 ± 0.016	14.893 ± 0.015	0.185 ± 0.022
05 17 08.17	39 22 05.3	17.625 ± 0.020	18.308 ± 0.022	0.683 ± 0.030
05 17 12.11	39 22 06.3	19.418 ± 0.086	20.127 ± 0.075	0.709 ± 0.114
05 16 58.47	39 22 08.2	18.652 ± 0.075	18.937 ± 0.061	0.285 ± 0.097
05 17 15.45	39 22 10.0	17.018 ± 0.011	17.642 ± 0.014	0.624 ± 0.018
05 17 20.86	39 22 10.7	18.142 ± 0.028	18.463 ± 0.032	0.321 ± 0.043
05 17 11.37	39 22 16.1	15.599 ± 0.006	15.828 ± 0.006	0.229 ± 0.008
05 17 16.37	39 22 16.6	17.660 ± 0.016	18.576 ± 0.025	0.916 ± 0.030
05 17 13.21	39 22 19.2	18.809 ± 0.037	19.497 ± 0.045	0.688 ± 0.058
05 17 09.23	39 22 19.7	17.548 ± 0.019	17.775 ± 0.012	0.227 ± 0.022
05 17 12.45	39 22 21.4	13.468 ± 0.005	13.634 ± 0.005	0.166 ± 0.007
05 17 07.56	39 22 21.4	17.492 ± 0.019	17.907 ± 0.012	0.415 ± 0.022
05 17 05.48	39 22 21.4	16.002 ± 0.009	16.182 ± 0.007	0.180 ± 0.011
05 17 03.45	39 22 24.3	18.611 ± 0.038	18.924 ± 0.045	0.313 ± 0.059
05 17 11.28	39 22 25.3	18.064 ± 0.025	19.522 ± 0.035	1.458 ± 0.043
05 17 13.29	39 22 25.5	18.333 ± 0.030	19.685 ± 0.069	1.352 ± 0.075
05 17 14.30	39 22 26.2	18.251 ± 0.027	18.681 ± 0.026	0.430 ± 0.037
05 17 16.57	39 22 26.2	19.855 ± 0.095	20.278 ± 0.120	0.423 ± 0.153
05 17 00.27	39 22 26.5	18.583 ± 0.053	18.840 ± 0.064	0.257 ± 0.083
05 17 15.40	39 22 27.2	17.497 ± 0.015	17.910 ± 0.016	0.413 ± 0.022
05 17 02.92	39 22 27.5	14.693 ± 0.013	14.897 ± 0.007	0.204 ± 0.015
05 17 13.94	39 22 29.0	17.521 ± 0.021	17.998 ± 0.017	0.477 ± 0.027
05 17 13.00	39 22 29.0	18.873 ± 0.036	19.759 ± 0.062	0.886 ± 0.072
05 17 07.11	39 22 29.1	17.971 ± 0.024	18.541 ± 0.029	0.570 ± 0.038
05 17 13.12	39 22 29.9	17.749 ± 0.016	18.108 ± 0.015	0.359 ± 0.022
05 17 07.28	39 22 30.0	18.891 ± 0.039	19.228 ± 0.048	0.337 ± 0.062
05 17 27.94	39 22 30.3	18.398 ± 0.064	18.762 ± 0.057	0.364 ± 0.086
05 17 13.93	39 22 30.3	18.172 ± 0.024	18.829 ± 0.035	0.657 ± 0.042
05 17 12.76	39 22 31.1	17.851 ± 0.023	18.359 ± 0.021	0.508 ± 0.031
05 17 14.79	39 22 31.3	18.727 ± 0.052	19.250 ± 0.050	0.523 ± 0.072
05 17 00.83	39 22 32.1	18.711 ± 0.071	19.000 ± 0.052	0.289 ± 0.088
05 17 06.69	39 22 33.0	17.721 ± 0.023	18.121 ± 0.019	0.400 ± 0.030
05 17 12.26	39 22 33.3	18.941 ± 0.062	19.373 ± 0.048	0.432 ± 0.078
05 17 13.49	39 22 33.4	17.989 ± 0.019	18.537 ± 0.026	0.548 ± 0.032
05 17 13.27	39 22 34.2	16.760 ± 0.013	17.545 ± 0.012	0.785 ± 0.018
05 17 05.07	39 22 34.9	17.262 ± 0.015	17.634 ± 0.015	0.372 ± 0.021
05 17 12.55	39 22 36.2	14.293 ± 0.006	14.441 ± 0.005	0.148 ± 0.008
05 17 09.07	39 22 36.1	18.930 ± 0.061	19.825 ± 0.079	0.895 ± 0.100
05 17 14.14	39 22 37.0	17.666 ± 0.017	18.095 ± 0.025	0.429 ± 0.030
05 17 27.62	39 22 37.3	18.971 ± 0.107	19.112 ± 0.090	0.141 ± 0.140
05 17 12.61	39 22 38.4	17.840 ± 0.021	18.246 ± 0.019	0.406 ± 0.028
05 17 05.99	39 22 39.9	19.187 ± 0.063	19.519 ± 0.059	0.332 ± 0.086
05 17 20.14	39 22 41.0	18.533 ± 0.038	18.863 ± 0.034	0.330 ± 0.051
05 17 13.42	39 22 43.2	16.230 ± 0.008	16.777 ± 0.007	0.547 ± 0.011
05 17 06.83	39 22 43.4	17.867 ± 0.022	18.399 ± 0.027	0.532 ± 0.035
05 17 11.32	39 22 44.5	15.470 ± 0.006	15.698 ± 0.004	0.228 ± 0.007
05 17 14.33	39 22 46.9	17.211 ± 0.014	17.524 ± 0.012	0.313 ± 0.018
05 17 14.48	39 22 48.3	16.979 ± 0.009	17.296 ± 0.011	0.317 ± 0.014
05 17 26.57	39 22 50.8	19.019 ± 0.110	19.432 ± 0.127	0.413 ± 0.168
05 17 17.19	39 22 51.4	18.431 ± 0.028	18.773 ± 0.033	0.342 ± 0.043
05 17 04.73	39 22 53.5	14.107 ± 0.006	14.307 ± 0.005	0.200 ± 0.008
05 17 25.47	39 22 57.0	19.041 ± 0.105	19.454 ± 0.157	0.413 ± 0.189

Table A.1. continued.

RA (hh mm ss)	Dec (dd mm ss)	H (mag)	K_s (mag)	H–K_s (mag)
05 17 12.18	39 22 57.6	15.998 ± 0.006	16.225 ± 0.005	0.227 ± 0.008
05 17 15.44	39 22 57.8	19.005 ± 0.047	19.304 ± 0.048	0.299 ± 0.067
05 17 25.30	39 23 03.4	18.202 ± 0.051	18.392 ± 0.044	0.190 ± 0.067
05 17 17.17	39 23 04.7	18.467 ± 0.033	18.863 ± 0.029	0.396 ± 0.044
05 17 12.47	39 23 05.2	15.480 ± 0.005	16.119 ± 0.006	0.639 ± 0.008
05 17 14.56	39 23 05.4	18.892 ± 0.044	19.306 ± 0.047	0.414 ± 0.064
05 17 29.77	39 23 06.5	20.121 ± 0.498	20.553 ± 0.450	0.432 ± 0.671
05 17 25.49	39 23 07.6	14.941 ± 0.014	15.142 ± 0.011	0.201 ± 0.018
05 17 02.18	39 23 10.4	18.558 ± 0.056	18.801 ± 0.050	0.243 ± 0.075
05 17 04.32	39 23 10.6	18.561 ± 0.031	19.020 ± 0.052	0.459 ± 0.061
05 17 04.13	39 23 13.5	16.655 ± 0.016	16.898 ± 0.013	0.243 ± 0.021
05 17 14.28	39 23 14.8	17.573 ± 0.017	17.822 ± 0.015	0.249 ± 0.023
05 17 04.70	39 23 15.6	18.305 ± 0.041	19.157 ± 0.065	0.852 ± 0.077
05 17 25.65	39 23 16.6	15.578 ± 0.016	15.842 ± 0.011	0.264 ± 0.019
05 17 03.71	39 23 20.1	13.477 ± 0.023	13.629 ± 0.010	0.152 ± 0.025
05 17 22.38	39 23 21.5	18.133 ± 0.031	18.376 ± 0.024	0.243 ± 0.039
05 16 58.10	39 23 21.7	18.025 ± 0.050	18.085 ± 0.036	0.060 ± 0.062
05 17 04.93	39 23 21.8	18.500 ± 0.034	18.786 ± 0.035	0.286 ± 0.049
05 17 25.42	39 23 22.3	16.620 ± 0.024	16.823 ± 0.018	0.203 ± 0.030
05 17 13.26	39 23 23.6	11.338 ± 0.003	11.549 ± 0.002	0.211 ± 0.004
05 17 09.31	39 23 23.9	19.094 ± 0.051	19.439 ± 0.054	0.345 ± 0.074
05 17 09.45	39 23 29.0	18.163 ± 0.031	18.533 ± 0.026	0.370 ± 0.040
05 16 58.58	39 23 31.4	18.194 ± 0.045	18.475 ± 0.044	0.281 ± 0.063
05 17 05.03	39 23 35.2	18.100 ± 0.029	18.501 ± 0.027	0.401 ± 0.040
05 17 08.54	39 23 37.2	16.092 ± 0.009	16.238 ± 0.007	0.146 ± 0.011
05 17 20.84	39 23 40.9	16.898 ± 0.023	17.109 ± 0.011	0.211 ± 0.025
05 17 14.21	39 23 42.7	11.874 ± 0.005	11.943 ± 0.003	0.069 ± 0.006
05 17 14.68	39 23 43.7	18.214 ± 0.024	18.490 ± 0.022	0.276 ± 0.033
05 17 10.84	39 23 49.6	18.289 ± 0.031	18.488 ± 0.030	0.199 ± 0.043
05 16 59.84	39 23 51.1	18.306 ± 0.057	18.652 ± 0.047	0.346 ± 0.074
05 17 18.28	39 23 57.7	18.609 ± 0.040	18.685 ± 0.041	0.076 ± 0.057
05 17 04.84	39 24 00.5	18.337 ± 0.071	18.520 ± 0.054	0.183 ± 0.089
05 17 19.16	39 24 04.6	18.522 ± 0.051	18.822 ± 0.034	0.300 ± 0.061
05 17 13.81	39 24 07.5	19.268 ± 0.077	19.551 ± 0.070	0.283 ± 0.104
05 16 58.68	39 24 09.5	18.409 ± 0.067	18.623 ± 0.064	0.214 ± 0.093
05 17 15.29	39 24 10.9	17.438 ± 0.063	18.254 ± 0.050	0.816 ± 0.080
05 17 17.21	39 24 16.5	16.710 ± 0.032	16.804 ± 0.020	0.094 ± 0.038
05 17 26.40	39 24 17.6	18.994 ± 0.189	19.232 ± 0.165	0.238 ± 0.251
05 17 28.45	39 24 18.5	19.845 ± 0.344	20.077 ± 0.375	0.232 ± 0.509
05 17 20.04	39 24 23.2	20.239 ± 0.535	20.498 ± 0.444	0.259 ± 0.695
05 17 22.07	39 24 26.7	19.721 ± 0.377	20.185 ± 0.378	0.464 ± 0.534
05 17 21.79	39 24 27.0	19.907 ± 0.458	20.603 ± 0.513	0.696 ± 0.688
05 17 12.34	39 20 03.7	18.155 ± 0.082	18.982 ± 0.117	0.827 ± 0.143
05 17 07.51	39 20 04.1	17.910 ± 0.084	18.652 ± 0.078	0.742 ± 0.115
05 17 18.40	39 20 05.2	17.658 ± 0.056	18.374 ± 0.080	0.716 ± 0.098
05 17 08.65	39 20 05.8	17.178 ± 0.053	17.869 ± 0.059	0.691 ± 0.079
05 17 13.14	39 20 10.5	18.122 ± 0.036	18.582 ± 0.049	0.460 ± 0.061
05 16 59.00	39 20 11.6	15.669 ± 0.027	15.837 ± 0.025	0.168 ± 0.037
05 17 15.13	39 20 11.9	17.085 ± 0.023	17.433 ± 0.027	0.348 ± 0.035
05 16 59.71	39 20 12.0	17.722 ± 0.063	17.934 ± 0.044	0.212 ± 0.077
05 17 20.30	39 20 12.9	18.021 ± 0.032	18.346 ± 0.034	0.325 ± 0.047
05 17 14.24	39 20 13.3	16.372 ± 0.020	16.719 ± 0.019	0.347 ± 0.028
05 17 07.20	39 20 14.2	18.915 ± 0.058	19.398 ± 0.062	0.483 ± 0.085
05 17 00.08	39 20 14.5	18.550 ± 0.067	18.799 ± 0.057	0.249 ± 0.088
05 16 59.41	39 20 14.6	18.927 ± 0.104	19.337 ± 0.106	0.410 ± 0.148
05 17 04.94	39 20 15.5	17.772 ± 0.049	17.667 ± 0.047	–0.105 ± 0.068
05 16 58.65	39 20 16.1	18.254 ± 0.056	18.634 ± 0.050	0.380 ± 0.075
05 17 15.43	39 20 16.9	18.095 ± 0.035	18.457 ± 0.037	0.362 ± 0.051
05 17 29.05	39 20 17.6	18.130 ± 0.082	18.705 ± 0.095	0.575 ± 0.125
05 17 14.48	39 20 18.1	14.981 ± 0.012	15.209 ± 0.017	0.228 ± 0.021
05 16 58.84	39 20 19.3	18.470 ± 0.074	18.787 ± 0.086	0.317 ± 0.113
05 17 19.20	39 20 19.8	18.841 ± 0.047	19.371 ± 0.062	0.530 ± 0.078
05 17 05.73	39 20 20.5	17.529 ± 0.045	17.944 ± 0.037	0.415 ± 0.058
05 17 00.09	39 20 20.5	17.365 ± 0.026	17.578 ± 0.024	0.213 ± 0.035
05 17 05.65	39 20 21.4	18.944 ± 0.072	19.354 ± 0.064	0.410 ± 0.096

Table A.1. continued.

RA (hh mm ss)	Dec (dd mm ss)	H (mag)	K_s (mag)	H–K_s (mag)
05 17 03.58	39 20 22.4	19.041 ± 0.074	19.428 ± 0.082	0.387 ± 0.110
05 17 07.06	39 20 24.1	18.940 ± 0.048	19.326 ± 0.064	0.386 ± 0.080
05 16 58.99	39 20 24.9	17.611 ± 0.030	17.970 ± 0.026	0.359 ± 0.040
05 17 10.67	39 20 26.4	17.900 ± 0.028	18.255 ± 0.034	0.355 ± 0.044
05 17 06.87	39 20 26.8	17.962 ± 0.023	18.357 ± 0.026	0.395 ± 0.035
05 17 18.53	39 20 28.5	18.591 ± 0.039	18.915 ± 0.050	0.324 ± 0.063
05 17 21.74	39 20 29.2	17.984 ± 0.040	18.330 ± 0.037	0.346 ± 0.054
05 17 18.17	39 20 29.6	18.141 ± 0.038	18.471 ± 0.033	0.330 ± 0.050
05 17 05.54	39 20 29.8	17.885 ± 0.035	18.154 ± 0.031	0.269 ± 0.047
05 17 00.32	39 20 29.7	16.095 ± 0.013	16.271 ± 0.011	0.176 ± 0.017
05 17 00.71	39 20 30.2	19.612 ± 0.180	19.773 ± 0.113	0.161 ± 0.213
05 17 02.10	39 20 30.6	16.627 ± 0.019	16.879 ± 0.016	0.252 ± 0.025
05 16 58.27	39 20 31.6	19.337 ± 0.101	19.460 ± 0.081	0.123 ± 0.129
05 17 16.57	39 20 31.9	18.138 ± 0.034	18.531 ± 0.036	0.393 ± 0.050
05 17 15.37	39 20 32.7	18.442 ± 0.037	18.872 ± 0.035	0.430 ± 0.051
05 17 02.28	39 20 32.6	16.720 ± 0.017	16.919 ± 0.016	0.199 ± 0.023
05 17 27.14	39 20 33.2	19.152 ± 0.130	19.458 ± 0.122	0.306 ± 0.178
05 17 13.62	39 20 33.8	14.285 ± 0.012	14.490 ± 0.014	0.205 ± 0.018
05 17 11.23	39 20 33.8	19.230 ± 0.058	19.744 ± 0.072	0.514 ± 0.092
05 16 57.38	39 20 33.8	18.040 ± 0.086	18.261 ± 0.071	0.221 ± 0.112
05 17 19.31	39 20 36.2	16.610 ± 0.017	16.996 ± 0.016	0.386 ± 0.023
05 17 10.02	39 20 36.2	19.702 ± 0.080	20.062 ± 0.098	0.360 ± 0.127
05 17 22.92	39 20 36.9	17.769 ± 0.046	18.213 ± 0.042	0.444 ± 0.062
05 17 29.69	39 20 37.0	18.692 ± 0.104	18.744 ± 0.085	0.052 ± 0.134
05 17 28.07	39 20 37.0	16.402 ± 0.024	16.648 ± 0.018	0.246 ± 0.030
05 17 14.45	39 20 38.2	18.960 ± 0.048	19.435 ± 0.047	0.475 ± 0.067
05 17 09.60	39 20 38.8	19.694 ± 0.091	20.027 ± 0.088	0.333 ± 0.127
05 17 19.83	39 20 39.0	19.409 ± 0.085	19.736 ± 0.075	0.327 ± 0.113
05 17 23.24	39 20 40.1	17.655 ± 0.046	18.008 ± 0.044	0.353 ± 0.064
05 16 57.59	39 20 40.2	17.017 ± 0.034	17.382 ± 0.027	0.365 ± 0.043
05 17 21.15	39 20 41.1	18.422 ± 0.037	18.786 ± 0.043	0.364 ± 0.057
05 17 09.99	39 20 42.2	18.428 ± 0.035	18.779 ± 0.038	0.351 ± 0.052
05 17 21.90	39 20 42.4	18.168 ± 0.030	18.568 ± 0.040	0.400 ± 0.050
05 17 26.72	39 20 42.9	18.873 ± 0.104	19.103 ± 0.079	0.230 ± 0.131
05 17 28.59	39 20 44.3	18.059 ± 0.049	18.512 ± 0.053	0.453 ± 0.072
05 16 58.13	39 20 46.1	14.664 ± 0.017	14.848 ± 0.016	0.184 ± 0.023
05 17 28.28	39 20 46.6	16.027 ± 0.020	16.263 ± 0.015	0.236 ± 0.025
05 17 12.97	39 20 47.0	18.047 ± 0.020	18.356 ± 0.023	0.309 ± 0.030
05 17 09.92	39 20 47.0	18.378 ± 0.027	18.816 ± 0.028	0.438 ± 0.039
05 17 16.37	39 20 47.4	18.736 ± 0.039	19.054 ± 0.043	0.318 ± 0.058
05 16 58.19	39 20 48.0	18.885 ± 0.089	19.512 ± 0.072	0.627 ± 0.114
05 17 15.63	39 20 49.5	19.016 ± 0.047	19.499 ± 0.071	0.483 ± 0.085
05 17 07.84	39 20 49.5	12.087 ± 0.009	12.195 ± 0.010	0.108 ± 0.013
05 17 15.74	39 20 50.0	17.429 ± 0.014	17.694 ± 0.016	0.265 ± 0.021
05 16 59.12	39 20 49.9	15.745 ± 0.014	15.892 ± 0.014	0.147 ± 0.020
05 17 10.49	39 20 50.1	18.189 ± 0.048	19.105 ± 0.045	0.916 ± 0.066
05 17 25.11	39 20 51.5	17.290 ± 0.028	17.658 ± 0.024	0.368 ± 0.037
05 17 00.40	39 20 51.7	17.064 ± 0.021	17.331 ± 0.024	0.267 ± 0.032
05 17 16.06	39 20 52.3	14.886 ± 0.015	15.072 ± 0.014	0.186 ± 0.021
05 17 09.65	39 20 52.2	19.051 ± 0.042	19.584 ± 0.056	0.533 ± 0.070
05 17 01.67	39 20 52.2	16.345 ± 0.018	16.594 ± 0.014	0.249 ± 0.023
05 17 04.54	39 20 52.5	17.371 ± 0.028	17.648 ± 0.021	0.277 ± 0.035
05 17 21.16	39 20 53.6	18.040 ± 0.030	18.456 ± 0.023	0.416 ± 0.038
05 16 59.35	39 20 53.3	18.227 ± 0.041	18.435 ± 0.046	0.208 ± 0.062
05 17 10.65	39 20 54.4	17.275 ± 0.015	17.526 ± 0.015	0.251 ± 0.021
05 17 02.96	39 20 54.4	18.633 ± 0.049	19.138 ± 0.059	0.505 ± 0.077
05 17 08.58	39 20 54.6	18.983 ± 0.045	19.429 ± 0.059	0.446 ± 0.074
05 17 08.08	39 20 55.3	18.909 ± 0.047	19.244 ± 0.051	0.335 ± 0.069
05 17 13.32	39 20 56.0	19.141 ± 0.060	19.664 ± 0.057	0.523 ± 0.083
05 17 03.94	39 20 55.9	18.001 ± 0.037	18.361 ± 0.030	0.360 ± 0.048
05 17 12.90	39 20 56.4	17.743 ± 0.018	18.157 ± 0.017	0.414 ± 0.025
05 17 10.76	39 20 56.4	19.208 ± 0.053	19.627 ± 0.059	0.419 ± 0.079
05 17 13.26	39 20 57.6	18.276 ± 0.028	18.674 ± 0.035	0.398 ± 0.045
05 17 19.12	39 20 59.1	18.409 ± 0.035	18.798 ± 0.033	0.389 ± 0.048
05 17 13.93	39 20 59.9	19.341 ± 0.069	19.781 ± 0.067	0.440 ± 0.096

Table A.1. continued.

RA (hh mm ss)	Dec (dd mm ss)	H (mag)	K_s (mag)	H–K_s (mag)
05 17 11.33	39 20 59.9	19.329 ± 0.085	19.878 ± 0.069	0.549 ± 0.109
05 17 05.93	39 21 00.4	19.190 ± 0.067	19.698 ± 0.060	0.508 ± 0.090
05 17 11.49	39 21 00.6	18.412 ± 0.028	18.860 ± 0.041	0.448 ± 0.050
05 17 22.68	39 21 01.1	16.106 ± 0.017	16.378 ± 0.020	0.272 ± 0.026
05 16 58.04	39 21 01.3	14.299 ± 0.014	14.392 ± 0.012	0.093 ± 0.018
05 17 22.39	39 21 01.6	19.022 ± 0.064	19.513 ± 0.064	0.491 ± 0.091
05 17 05.88	39 21 01.5	17.992 ± 0.023	18.238 ± 0.021	0.246 ± 0.031
05 17 06.69	39 21 02.0	18.653 ± 0.034	19.194 ± 0.040	0.541 ± 0.052
05 16 59.91	39 21 02.1	17.878 ± 0.039	18.190 ± 0.034	0.312 ± 0.052
05 17 06.59	39 21 02.5	15.910 ± 0.009	16.161 ± 0.010	0.251 ± 0.013
05 17 08.20	39 21 02.8	19.307 ± 0.069	19.650 ± 0.074	0.343 ± 0.101
05 17 15.18	39 21 03.0	16.659 ± 0.010	16.924 ± 0.011	0.265 ± 0.015
05 17 14.20	39 21 03.2	18.837 ± 0.034	19.153 ± 0.037	0.316 ± 0.050
05 17 08.24	39 21 03.8	18.259 ± 0.030	18.762 ± 0.032	0.503 ± 0.044
05 17 12.61	39 21 04.0	19.359 ± 0.055	19.706 ± 0.055	0.347 ± 0.078
05 17 17.78	39 21 04.1	18.402 ± 0.036	18.781 ± 0.038	0.379 ± 0.052
05 17 08.45	39 21 04.3	18.794 ± 0.039	19.229 ± 0.044	0.435 ± 0.059
05 17 11.87	39 21 04.4	18.669 ± 0.038	19.373 ± 0.040	0.704 ± 0.055
05 17 05.69	39 21 04.4	13.578 ± 0.010	13.819 ± 0.010	0.241 ± 0.014
05 17 03.72	39 21 04.4	17.388 ± 0.027	17.677 ± 0.023	0.289 ± 0.035
05 17 13.99	39 21 04.8	19.576 ± 0.077	19.784 ± 0.064	0.208 ± 0.100
05 17 11.64	39 21 04.9	17.321 ± 0.020	17.724 ± 0.017	0.403 ± 0.026
05 17 12.97	39 21 05.1	18.118 ± 0.016	18.610 ± 0.024	0.492 ± 0.029
05 17 11.56	39 21 06.0	19.796 ± 0.111	20.152 ± 0.079	0.356 ± 0.136
05 17 19.63	39 21 06.9	19.025 ± 0.055	19.717 ± 0.075	0.692 ± 0.093
05 17 12.89	39 21 06.8	18.609 ± 0.027	19.216 ± 0.042	0.607 ± 0.050
05 17 13.39	39 21 07.6	17.230 ± 0.012	17.579 ± 0.015	0.349 ± 0.019
05 17 14.90	39 21 07.9	18.885 ± 0.050	19.227 ± 0.045	0.342 ± 0.067
05 17 00.59	39 21 08.2	15.842 ± 0.014	16.021 ± 0.011	0.179 ± 0.018
05 17 04.24	39 21 08.3	16.786 ± 0.021	17.019 ± 0.013	0.233 ± 0.025
05 17 13.92	39 21 08.4	16.971 ± 0.011	17.299 ± 0.011	0.328 ± 0.016
05 17 11.72	39 21 08.8	16.037 ± 0.009	16.335 ± 0.009	0.298 ± 0.013
05 17 10.41	39 21 09.8	16.530 ± 0.013	16.762 ± 0.011	0.232 ± 0.017
05 17 14.08	39 21 10.1	13.262 ± 0.007	13.464 ± 0.008	0.202 ± 0.011
05 17 14.88	39 21 10.4	18.122 ± 0.020	18.497 ± 0.023	0.375 ± 0.030
05 17 16.62	39 21 10.5	16.173 ± 0.041	16.475 ± 0.027	0.302 ± 0.049
05 17 00.45	39 21 10.3	16.818 ± 0.019	17.048 ± 0.019	0.230 ± 0.027
05 17 07.21	39 21 10.7	18.406 ± 0.026	18.759 ± 0.041	0.353 ± 0.049
05 17 24.82	39 21 11.1	18.623 ± 0.075	18.681 ± 0.048	0.058 ± 0.089
05 17 15.93	39 21 11.2	15.285 ± 0.007	15.494 ± 0.009	0.209 ± 0.011
05 17 14.38	39 21 11.4	16.730 ± 0.011	17.311 ± 0.010	0.581 ± 0.015
05 16 57.88	39 21 11.6	17.327 ± 0.032	17.487 ± 0.027	0.160 ± 0.042
05 17 11.20	39 21 12.0	19.345 ± 0.055	19.848 ± 0.064	0.503 ± 0.084
05 17 03.25	39 21 12.0	17.751 ± 0.031	18.093 ± 0.024	0.342 ± 0.039
05 17 14.49	39 21 12.3	16.482 ± 0.009	16.885 ± 0.010	0.403 ± 0.013
05 17 14.52	39 21 13.0	18.396 ± 0.031	18.941 ± 0.048	0.545 ± 0.057
05 16 59.57	39 21 12.7	17.603 ± 0.028	17.904 ± 0.029	0.301 ± 0.040
05 17 02.98	39 21 12.9	18.172 ± 0.040	18.513 ± 0.038	0.341 ± 0.055
05 17 01.83	39 21 13.5	17.145 ± 0.023	17.328 ± 0.016	0.183 ± 0.028
05 17 04.59	39 21 13.7	16.051 ± 0.014	16.354 ± 0.012	0.303 ± 0.018
05 17 14.60	39 21 14.0	17.865 ± 0.021	18.318 ± 0.022	0.453 ± 0.030
05 17 15.57	39 21 14.0	19.187 ± 0.058	19.627 ± 0.067	0.440 ± 0.089
05 16 59.32	39 21 14.0	15.926 ± 0.015	16.245 ± 0.013	0.319 ± 0.020
05 17 22.10	39 21 14.5	17.623 ± 0.023	18.005 ± 0.024	0.382 ± 0.033
05 17 09.67	39 21 14.9	18.633 ± 0.033	18.936 ± 0.034	0.303 ± 0.047
05 17 12.64	39 21 15.1	18.228 ± 0.027	18.661 ± 0.026	0.433 ± 0.037
05 17 25.51	39 21 15.4	16.433 ± 0.022	16.672 ± 0.015	0.239 ± 0.027
05 17 22.52	39 21 16.5	17.176 ± 0.020	17.605 ± 0.019	0.429 ± 0.028
05 17 12.68	39 21 16.9	19.408 ± 0.093	19.798 ± 0.073	0.390 ± 0.118
05 17 20.15	39 21 17.0	18.589 ± 0.036	18.946 ± 0.038	0.357 ± 0.052
05 17 09.90	39 21 17.0	18.284 ± 0.028	18.677 ± 0.025	0.393 ± 0.038
05 17 16.63	39 21 17.9	17.124 ± 0.012	17.416 ± 0.011	0.292 ± 0.016
05 17 01.60	39 21 18.0	15.333 ± 0.013	15.591 ± 0.012	0.258 ± 0.018
05 17 14.27	39 21 18.4	15.470 ± 0.006	15.723 ± 0.007	0.253 ± 0.009
05 17 09.85	39 21 18.3	17.555 ± 0.016	17.988 ± 0.018	0.433 ± 0.024

Table A.1. continued.

RA (hh mm ss)	Dec (dd mm ss)	H (mag)	K_s (mag)	H–K_s (mag)
05 17 13.75	39 21 18.4	15.864 ± 0.008	16.216 ± 0.006	0.352 ± 0.010
05 17 15.29	39 21 18.8	19.337 ± 0.080	19.881 ± 0.092	0.544 ± 0.122
05 17 20.56	39 21 19.2	18.655 ± 0.039	19.281 ± 0.058	0.626 ± 0.070
05 17 12.62	39 21 20.0	19.337 ± 0.069	19.920 ± 0.072	0.583 ± 0.100
05 17 12.73	39 21 20.3	17.659 ± 0.019	18.130 ± 0.017	0.471 ± 0.025
05 17 14.81	39 21 20.5	19.534 ± 0.062	19.922 ± 0.072	0.388 ± 0.095
05 17 19.08	39 21 21.1	18.735 ± 0.049	19.170 ± 0.049	0.435 ± 0.069
05 17 24.36	39 21 21.4	18.299 ± 0.040	18.503 ± 0.040	0.204 ± 0.057
05 17 04.63	39 21 21.7	19.373 ± 0.062	19.738 ± 0.091	0.365 ± 0.110
05 17 04.65	39 21 22.6	17.093 ± 0.017	17.403 ± 0.014	0.310 ± 0.022
05 17 14.08	39 21 22.3	16.628 ± 0.011	16.918 ± 0.020	0.290 ± 0.023
05 17 12.35	39 21 22.3	17.940 ± 0.019	18.399 ± 0.024	0.459 ± 0.031
05 17 14.45	39 21 22.4	17.351 ± 0.013	18.297 ± 0.019	0.946 ± 0.023
05 17 23.37	39 21 22.7	18.537 ± 0.036	18.972 ± 0.046	0.435 ± 0.058
05 16 58.00	39 21 22.4	17.888 ± 0.043	18.085 ± 0.036	0.197 ± 0.056
05 17 06.40	39 21 23.1	18.387 ± 0.029	18.669 ± 0.033	0.282 ± 0.044
05 17 01.42	39 21 23.9	17.179 ± 0.021	17.490 ± 0.022	0.311 ± 0.030
05 17 10.33	39 21 24.1	18.115 ± 0.022	18.646 ± 0.027	0.531 ± 0.035
05 17 13.66	39 21 24.3	16.316 ± 0.008	16.611 ± 0.008	0.295 ± 0.011
05 17 04.41	39 21 24.6	16.694 ± 0.014	17.007 ± 0.011	0.313 ± 0.018
05 17 09.13	39 21 24.7	18.032 ± 0.021	18.484 ± 0.022	0.452 ± 0.030
05 17 13.45	39 21 25.3	17.071 ± 0.013	17.560 ± 0.010	0.489 ± 0.016
05 17 15.98	39 21 25.4	18.937 ± 0.048	19.416 ± 0.052	0.479 ± 0.071
05 17 09.55	39 21 25.4	18.936 ± 0.040	19.311 ± 0.045	0.375 ± 0.060
05 17 17.43	39 21 25.7	18.857 ± 0.039	19.344 ± 0.047	0.487 ± 0.061
05 17 00.18	39 21 26.0	16.004 ± 0.013	16.215 ± 0.012	0.211 ± 0.018
05 17 29.24	39 21 26.6	18.156 ± 0.054	18.412 ± 0.052	0.256 ± 0.075
05 17 01.15	39 21 28.0	16.392 ± 0.021	16.572 ± 0.014	0.180 ± 0.025
05 17 02.34	39 21 28.1	18.713 ± 0.063	19.237 ± 0.082	0.524 ± 0.103
05 17 10.86	39 21 28.6	15.806 ± 0.008	16.479 ± 0.006	0.673 ± 0.010
05 17 28.17	39 21 28.8	16.649 ± 0.026	16.944 ± 0.020	0.295 ± 0.033
05 17 15.30	39 21 28.8	18.797 ± 0.047	19.235 ± 0.042	0.438 ± 0.063
05 17 09.73	39 21 28.8	18.394 ± 0.031	18.852 ± 0.028	0.458 ± 0.042
05 17 14.00	39 21 29.3	18.291 ± 0.032	18.672 ± 0.030	0.381 ± 0.044
05 17 13.87	39 21 31.0	19.176 ± 0.053	19.461 ± 0.050	0.285 ± 0.073
05 17 07.68	39 21 31.1	16.857 ± 0.012	17.243 ± 0.011	0.386 ± 0.016
05 17 18.23	39 21 31.2	18.618 ± 0.043	18.924 ± 0.032	0.306 ± 0.054
05 17 04.62	39 21 31.8	17.105 ± 0.018	17.374 ± 0.014	0.269 ± 0.023
05 17 22.14	39 21 32.1	18.110 ± 0.023	18.448 ± 0.032	0.338 ± 0.039
05 17 17.32	39 21 32.3	16.976 ± 0.013	17.349 ± 0.009	0.373 ± 0.016
05 17 14.42	39 21 32.7	19.257 ± 0.068	19.695 ± 0.064	0.438 ± 0.093
05 17 04.92	39 21 32.9	14.964 ± 0.008	15.146 ± 0.008	0.182 ± 0.011
05 17 19.48	39 21 33.6	17.650 ± 0.019	18.047 ± 0.021	0.397 ± 0.028
05 17 15.05	39 21 33.6	18.388 ± 0.031	19.070 ± 0.034	0.682 ± 0.046
05 17 25.21	39 21 33.9	17.685 ± 0.042	17.887 ± 0.031	0.202 ± 0.052
05 17 10.99	39 21 33.9	17.465 ± 0.013	17.904 ± 0.014	0.439 ± 0.019
05 17 05.58	39 21 34.0	19.139 ± 0.047	19.517 ± 0.065	0.378 ± 0.080
05 17 10.04	39 21 34.4	19.273 ± 0.053	19.616 ± 0.057	0.343 ± 0.078
05 17 14.72	39 21 34.6	19.415 ± 0.080	19.808 ± 0.084	0.393 ± 0.116
05 17 11.70	39 21 34.8	18.301 ± 0.032	19.042 ± 0.039	0.741 ± 0.050
05 17 09.67	39 21 35.5	18.472 ± 0.022	18.986 ± 0.027	0.514 ± 0.035
05 17 09.12	39 21 35.6	17.586 ± 0.018	18.149 ± 0.018	0.563 ± 0.025
05 17 12.62	39 21 35.8	15.612 ± 0.033	17.117 ± 0.032	1.505 ± 0.046
05 17 01.37	39 21 36.0	18.360 ± 0.050	18.674 ± 0.048	0.314 ± 0.069
05 17 08.79	39 21 36.5	15.861 ± 0.008	16.112 ± 0.006	0.251 ± 0.010
05 17 11.49	39 21 36.8	17.581 ± 0.015	18.061 ± 0.015	0.480 ± 0.021
05 17 12.14	39 21 37.0	19.223 ± 0.062	19.508 ± 0.044	0.285 ± 0.076
05 16 59.24	39 21 37.1	17.519 ± 0.032	17.701 ± 0.027	0.182 ± 0.042
05 17 15.66	39 21 37.2	17.555 ± 0.015	18.038 ± 0.018	0.483 ± 0.023
05 17 00.20	39 21 37.2	18.376 ± 0.054	18.844 ± 0.060	0.468 ± 0.081
05 17 23.78	39 21 38.0	17.723 ± 0.026	17.895 ± 0.022	0.172 ± 0.034
05 17 09.12	39 21 38.3	19.413 ± 0.075	19.736 ± 0.065	0.323 ± 0.099
05 17 22.23	39 21 38.8	15.419 ± 0.007	15.643 ± 0.010	0.224 ± 0.012
05 17 10.07	39 21 38.9	16.463 ± 0.014	17.036 ± 0.010	0.573 ± 0.017
05 17 24.40	39 21 39.4	17.158 ± 0.025	17.357 ± 0.018	0.199 ± 0.031

Table A.1. continued.

RA (hh mm ss)	Dec (dd mm ss)	H (mag)	K_s (mag)	H–K_s (mag)
05 17 08.68	39 21 39.4	18.163 ± 0.032	18.501 ± 0.025	0.338 ± 0.041
05 17 09.80	39 21 39.7	17.579 ± 0.018	18.110 ± 0.014	0.531 ± 0.023
05 17 10.75	39 21 40.6	16.486 ± 0.008	17.293 ± 0.008	0.807 ± 0.011
05 17 06.66	39 21 40.7	18.067 ± 0.029	18.875 ± 0.042	0.808 ± 0.051
05 17 09.60	39 21 40.8	17.432 ± 0.015	18.065 ± 0.016	0.633 ± 0.022
05 17 19.75	39 21 40.9	18.234 ± 0.036	18.724 ± 0.034	0.490 ± 0.050
05 17 12.74	39 21 41.0	19.142 ± 0.053	19.466 ± 0.059	0.324 ± 0.079
05 17 22.72	39 21 41.2	17.161 ± 0.016	17.466 ± 0.016	0.305 ± 0.023
05 17 20.31	39 21 42.7	15.931 ± 0.007	16.192 ± 0.008	0.261 ± 0.011
05 17 21.03	39 21 42.9	17.980 ± 0.030	18.295 ± 0.028	0.315 ± 0.041
05 17 17.31	39 21 42.9	19.361 ± 0.067	19.740 ± 0.072	0.379 ± 0.098
05 17 17.52	39 21 43.4	19.195 ± 0.056	19.737 ± 0.060	0.542 ± 0.082
05 16 59.61	39 21 43.5	17.213 ± 0.023	17.498 ± 0.022	0.285 ± 0.032
05 17 11.58	39 21 43.8	17.323 ± 0.014	18.615 ± 0.026	1.292 ± 0.030
05 17 14.05	39 21 44.8	16.822 ± 0.011	17.425 ± 0.011	0.603 ± 0.016
05 17 16.99	39 21 45.0	14.823 ± 0.006	15.150 ± 0.007	0.327 ± 0.009
05 17 12.46	39 21 45.1	17.617 ± 0.020	19.283 ± 0.040	1.666 ± 0.045
05 17 06.40	39 21 45.2	18.560 ± 0.039	18.945 ± 0.031	0.385 ± 0.050
05 17 22.66	39 21 45.4	18.755 ± 0.050	19.170 ± 0.046	0.415 ± 0.068
05 17 11.64	39 21 45.6	17.384 ± 0.017	17.730 ± 0.015	0.346 ± 0.023
05 17 11.13	39 21 45.9	15.589 ± 0.006	16.497 ± 0.006	0.908 ± 0.008
05 17 11.12	39 21 46.6	16.144 ± 0.007	16.886 ± 0.008	0.742 ± 0.011
05 17 11.31	39 21 46.3	17.029 ± 0.008	17.280 ± 0.011	0.251 ± 0.014
05 17 16.05	39 21 47.4	17.459 ± 0.016	17.882 ± 0.015	0.423 ± 0.022
05 17 02.43	39 21 47.3	18.409 ± 0.046	18.747 ± 0.047	0.338 ± 0.066
05 17 11.98	39 21 47.9	13.360 ± 0.053	13.979 ± 0.032	0.619 ± 0.062
05 17 07.92	39 21 47.9	16.809 ± 0.017	17.005 ± 0.008	0.196 ± 0.019
05 17 06.37	39 21 48.1	19.546 ± 0.084	20.350 ± 0.109	0.804 ± 0.138
05 17 18.63	39 21 48.6	18.892 ± 0.047	19.326 ± 0.058	0.434 ± 0.075
05 17 15.34	39 21 48.8	18.416 ± 0.032	19.037 ± 0.037	0.621 ± 0.049
05 17 17.98	39 21 49.0	15.261 ± 0.011	15.448 ± 0.013	0.187 ± 0.017
05 17 14.59	39 21 49.4	18.118 ± 0.020	18.867 ± 0.027	0.749 ± 0.034
05 17 12.19	39 21 49.4	17.581 ± 0.014	17.775 ± 0.019	0.194 ± 0.024
05 17 01.99	39 21 49.5	17.417 ± 0.032	17.606 ± 0.024	0.189 ± 0.040
05 17 26.68	39 21 49.9	19.083 ± 0.115	19.322 ± 0.133	0.239 ± 0.176
05 17 21.52	39 21 49.9	16.951 ± 0.012	17.277 ± 0.013	0.326 ± 0.018
05 17 10.84	39 21 49.8	16.275 ± 0.009	16.461 ± 0.011	0.186 ± 0.014
05 17 13.23	39 21 49.9	18.701 ± 0.044	19.110 ± 0.044	0.409 ± 0.062
05 17 09.36	39 21 50.0	18.255 ± 0.028	19.003 ± 0.036	0.748 ± 0.046
05 17 24.77	39 21 50.7	17.846 ± 0.043	18.067 ± 0.030	0.221 ± 0.052
05 17 17.48	39 21 50.7	16.000 ± 0.009	16.277 ± 0.010	0.277 ± 0.013
05 17 16.01	39 21 50.7	16.182 ± 0.007	16.815 ± 0.007	0.633 ± 0.010
05 16 58.62	39 21 50.5	18.981 ± 0.082	19.477 ± 0.082	0.496 ± 0.116
05 17 05.29	39 21 50.8	19.637 ± 0.102	20.016 ± 0.096	0.379 ± 0.140
05 17 09.60	39 21 51.0	17.905 ± 0.019	18.387 ± 0.020	0.482 ± 0.028
05 17 15.19	39 21 51.1	19.363 ± 0.064	19.998 ± 0.086	0.635 ± 0.107
05 17 15.73	39 21 51.2	19.208 ± 0.062	19.792 ± 0.073	0.584 ± 0.096
05 17 19.48	39 21 51.4	18.100 ± 0.031	18.440 ± 0.027	0.340 ± 0.041
05 17 07.27	39 21 51.3	18.516 ± 0.059	19.717 ± 0.071	1.201 ± 0.092
05 17 11.60	39 21 51.4	17.125 ± 0.013	18.207 ± 0.019	1.082 ± 0.023
05 17 12.46	39 21 51.5	16.793 ± 0.011	17.856 ± 0.013	1.063 ± 0.017
05 17 02.02	39 21 51.4	16.435 ± 0.018	16.639 ± 0.011	0.204 ± 0.021
05 17 11.28	39 21 51.7	16.514 ± 0.010	17.734 ± 0.012	1.220 ± 0.016
05 17 12.81	39 21 51.8	19.469 ± 0.079	19.668 ± 0.068	0.199 ± 0.104
05 16 58.48	39 21 51.6	18.223 ± 0.043	18.649 ± 0.041	0.426 ± 0.059
05 17 10.80	39 21 52.2	18.479 ± 0.032	19.053 ± 0.028	0.574 ± 0.043
05 17 07.71	39 21 52.4	17.508 ± 0.039	17.730 ± 0.026	0.222 ± 0.047
05 17 13.90	39 21 52.4	19.642 ± 0.097	19.986 ± 0.066	0.344 ± 0.117
05 17 09.68	39 21 52.5	19.485 ± 0.077	19.971 ± 0.066	0.486 ± 0.101
05 17 13.44	39 21 52.8	13.651 ± 0.005	14.092 ± 0.006	0.441 ± 0.008
05 17 11.07	39 21 53.2	18.889 ± 0.043	19.342 ± 0.046	0.453 ± 0.063
05 17 15.19	39 21 53.7	17.515 ± 0.016	18.069 ± 0.016	0.554 ± 0.023
05 17 12.16	39 21 53.7	16.249 ± 0.007	16.564 ± 0.007	0.315 ± 0.010
05 17 14.41	39 21 53.9	17.801 ± 0.018	18.455 ± 0.025	0.654 ± 0.031
05 17 14.11	39 21 54.0	17.336 ± 0.023	17.790 ± 0.021	0.454 ± 0.031

Table A.1. continued.

RA (hh mm ss)	Dec (dd mm ss)	H (mag)	K_s (mag)	H–K_s (mag)
05 17 12.35	39 21 54.1	17.429 ± 0.019	18.919 ± 0.039	1.490 ± 0.043
05 17 13.35	39 21 54.4	14.509 ± 0.006	14.935 ± 0.005	0.426 ± 0.008
05 17 13.55	39 21 54.6	14.548 ± 0.006	15.053 ± 0.006	0.505 ± 0.008
05 17 11.80	39 21 55.0	14.964 ± 0.005	15.654 ± 0.004	0.690 ± 0.006
05 17 17.67	39 21 55.1	17.544 ± 0.018	17.791 ± 0.016	0.247 ± 0.024
05 17 22.56	39 21 55.2	18.974 ± 0.057	19.337 ± 0.056	0.363 ± 0.080
05 17 09.90	39 21 55.4	15.625 ± 0.006	15.828 ± 0.004	0.203 ± 0.007
05 17 12.68	39 21 55.5	15.487 ± 0.006	16.273 ± 0.006	0.786 ± 0.008
05 17 14.68	39 21 56.1	19.555 ± 0.080	20.218 ± 0.099	0.663 ± 0.127
05 17 15.88	39 21 56.4	16.882 ± 0.010	17.598 ± 0.011	0.716 ± 0.015
05 17 14.39	39 21 56.5	19.265 ± 0.091	20.126 ± 0.113	0.861 ± 0.145
05 17 15.00	39 21 57.0	19.480 ± 0.070	19.836 ± 0.096	0.356 ± 0.119
05 16 57.77	39 21 57.0	15.100 ± 0.018	15.218 ± 0.010	0.118 ± 0.021
05 17 14.18	39 21 57.3	16.447 ± 0.009	17.301 ± 0.011	0.854 ± 0.014
05 17 10.86	39 21 57.3	19.520 ± 0.055	20.002 ± 0.078	0.482 ± 0.095
05 17 12.99	39 21 57.6	18.299 ± 0.025	18.948 ± 0.033	0.649 ± 0.041
05 17 09.82	39 21 57.7	19.409 ± 0.068	19.722 ± 0.065	0.313 ± 0.094
05 17 17.06	39 21 58.0	17.990 ± 0.018	18.327 ± 0.021	0.337 ± 0.028
05 17 14.28	39 21 58.1	17.117 ± 0.027	17.862 ± 0.019	0.745 ± 0.033
05 17 16.38	39 21 58.2	15.764 ± 0.007	16.057 ± 0.007	0.293 ± 0.010
05 17 20.18	39 21 58.9	17.673 ± 0.020	18.003 ± 0.024	0.330 ± 0.031
05 17 12.45	39 21 59.2	16.486 ± 0.010	16.712 ± 0.007	0.226 ± 0.012
05 16 59.48	39 21 59.1	15.827 ± 0.013	16.059 ± 0.012	0.232 ± 0.018
05 17 17.63	39 21 59.3	17.900 ± 0.024	18.464 ± 0.024	0.564 ± 0.034
05 17 12.90	39 21 59.4	17.962 ± 0.019	18.604 ± 0.022	0.642 ± 0.029
05 17 12.29	39 21 59.7	17.773 ± 0.019	18.265 ± 0.020	0.492 ± 0.028
05 17 09.80	39 21 59.8	19.396 ± 0.068	20.097 ± 0.091	0.701 ± 0.114
05 17 17.73	39 21 59.9	18.303 ± 0.025	18.774 ± 0.030	0.471 ± 0.039
05 17 14.46	39 22 00.1	15.215 ± 0.005	15.789 ± 0.005	0.574 ± 0.007
05 17 14.77	39 22 00.1	18.153 ± 0.020	18.997 ± 0.032	0.844 ± 0.038
05 17 11.58	39 22 00.4	17.781 ± 0.019	18.249 ± 0.018	0.468 ± 0.026
05 17 13.90	39 22 00.7	18.996 ± 0.051	19.750 ± 0.063	0.754 ± 0.081
05 17 19.76	39 22 00.8	17.551 ± 0.019	17.931 ± 0.019	0.380 ± 0.027
05 17 10.74	39 22 00.9	18.145 ± 0.024	18.550 ± 0.025	0.405 ± 0.035
05 17 03.29	39 22 01.0	18.574 ± 0.045	19.064 ± 0.043	0.490 ± 0.062
05 17 03.17	39 22 01.2	17.821 ± 0.027	18.186 ± 0.025	0.365 ± 0.037
05 17 02.82	39 22 01.2	14.845 ± 0.014	15.190 ± 0.009	0.345 ± 0.017
05 17 13.42	39 22 01.8	18.286 ± 0.031	18.532 ± 0.036	0.246 ± 0.048
05 17 13.46	39 22 02.0	16.320 ± 0.009	17.081 ± 0.008	0.761 ± 0.012
05 17 21.34	39 22 02.5	17.637 ± 0.021	18.016 ± 0.024	0.379 ± 0.032
05 17 10.96	39 22 02.4	14.922 ± 0.005	15.353 ± 0.004	0.431 ± 0.006
05 17 11.22	39 22 02.4	17.693 ± 0.018	18.053 ± 0.016	0.360 ± 0.024
05 17 14.91	39 22 03.2	16.826 ± 0.012	17.245 ± 0.008	0.419 ± 0.014
05 17 09.45	39 22 03.3	17.426 ± 0.014	18.279 ± 0.022	0.853 ± 0.026
05 17 02.67	39 22 03.2	18.318 ± 0.051	18.644 ± 0.036	0.326 ± 0.062
05 17 04.19	39 22 03.8	18.085 ± 0.029	18.421 ± 0.030	0.336 ± 0.042
05 17 22.49	39 22 04.3	17.236 ± 0.016	17.532 ± 0.016	0.296 ± 0.023
05 17 14.59	39 22 04.7	14.605 ± 0.004	15.179 ± 0.005	0.574 ± 0.006
05 17 09.03	39 22 04.8	17.654 ± 0.019	18.053 ± 0.015	0.399 ± 0.024
05 17 10.95	39 22 04.9	17.396 ± 0.014	17.777 ± 0.015	0.381 ± 0.021
05 17 13.84	39 22 05.2	17.162 ± 0.012	17.413 ± 0.010	0.251 ± 0.016
05 17 10.63	39 22 05.3	18.177 ± 0.024	18.498 ± 0.021	0.321 ± 0.032
05 17 17.21	39 22 05.6	17.371 ± 0.012	17.837 ± 0.015	0.466 ± 0.019
05 17 22.87	39 22 05.7	16.971 ± 0.011	17.245 ± 0.015	0.274 ± 0.019
05 17 23.84	39 22 05.8	18.591 ± 0.051	18.861 ± 0.052	0.270 ± 0.073
05 17 15.55	39 22 05.8	17.924 ± 0.022	19.533 ± 0.053	1.609 ± 0.057
05 17 16.51	39 22 06.2	15.543 ± 0.006	15.777 ± 0.006	0.234 ± 0.008
05 17 14.92	39 22 06.2	18.570 ± 0.036	19.277 ± 0.043	0.707 ± 0.056
05 17 10.93	39 22 06.5	18.356 ± 0.026	18.826 ± 0.032	0.470 ± 0.041
05 17 18.20	39 22 07.0	17.138 ± 0.014	17.603 ± 0.012	0.465 ± 0.018
05 17 23.46	39 22 07.2	18.399 ± 0.032	18.805 ± 0.040	0.406 ± 0.051
05 17 17.99	39 22 07.2	19.393 ± 0.071	19.523 ± 0.057	0.130 ± 0.091
05 17 09.74	39 22 07.1	18.471 ± 0.032	19.103 ± 0.040	0.632 ± 0.051
05 16 57.60	39 22 07.0	14.569 ± 0.022	14.746 ± 0.012	0.177 ± 0.025
05 17 23.08	39 22 07.4	17.522 ± 0.024	17.818 ± 0.020	0.296 ± 0.031

Table A.1. continued.

RA (hh mm ss)	Dec (dd mm ss)	H (mag)	K_s (mag)	H–K_s (mag)
05 17 19.41	39 22 07.8	13.137 ± 0.006	13.287 ± 0.008	0.150 ± 0.010
05 17 16.60	39 22 07.9	18.839 ± 0.038	19.312 ± 0.050	0.473 ± 0.063
05 17 00.77	39 22 08.1	18.048 ± 0.046	18.363 ± 0.033	0.315 ± 0.057
05 17 15.04	39 22 08.8	18.128 ± 0.027	18.976 ± 0.036	0.848 ± 0.045
05 17 10.86	39 22 09.5	18.390 ± 0.026	19.080 ± 0.042	0.690 ± 0.049
05 17 14.90	39 22 09.5	19.067 ± 0.047	19.708 ± 0.044	0.641 ± 0.064
05 17 13.28	39 22 09.6	19.310 ± 0.072	19.753 ± 0.055	0.443 ± 0.091
05 17 14.15	39 22 09.8	18.441 ± 0.029	18.976 ± 0.032	0.535 ± 0.043
05 17 12.67	39 22 10.6	18.946 ± 0.040	19.469 ± 0.045	0.523 ± 0.060
05 17 12.53	39 22 10.7	18.530 ± 0.028	19.150 ± 0.042	0.620 ± 0.050
05 17 16.97	39 22 10.9	18.820 ± 0.044	19.219 ± 0.040	0.399 ± 0.059
05 17 16.00	39 22 11.3	15.831 ± 0.006	16.255 ± 0.006	0.424 ± 0.008
05 17 16.36	39 22 12.2	16.663 ± 0.008	17.476 ± 0.011	0.813 ± 0.014
05 17 27.81	39 22 12.6	17.687 ± 0.046	18.143 ± 0.037	0.456 ± 0.059
05 17 14.25	39 22 12.8	17.828 ± 0.022	18.969 ± 0.036	1.141 ± 0.042
05 17 12.33	39 22 12.9	17.770 ± 0.017	18.261 ± 0.022	0.491 ± 0.028
05 17 06.56	39 22 12.9	18.909 ± 0.051	19.324 ± 0.060	0.415 ± 0.079
05 17 10.51	39 22 13.4	18.543 ± 0.031	18.957 ± 0.032	0.414 ± 0.045
05 17 23.09	39 22 13.7	19.194 ± 0.078	19.642 ± 0.078	0.448 ± 0.110
05 16 59.56	39 22 13.5	15.565 ± 0.013	15.723 ± 0.010	0.158 ± 0.016
05 16 58.87	39 22 13.5	18.854 ± 0.065	19.405 ± 0.096	0.551 ± 0.116
05 17 14.13	39 22 13.8	17.148 ± 0.050	17.925 ± 0.031	0.777 ± 0.059
05 17 11.25	39 22 13.9	18.641 ± 0.035	19.076 ± 0.037	0.435 ± 0.051
05 17 16.11	39 22 14.0	15.086 ± 0.005	15.272 ± 0.006	0.186 ± 0.008
05 17 09.14	39 22 14.3	13.144 ± 0.004	13.241 ± 0.003	0.097 ± 0.005
05 17 10.34	39 22 14.4	19.272 ± 0.069	19.606 ± 0.061	0.334 ± 0.092
05 17 16.15	39 22 15.5	18.087 ± 0.027	19.068 ± 0.043	0.981 ± 0.051
05 17 07.72	39 22 15.6	15.245 ± 0.007	15.443 ± 0.005	0.198 ± 0.009
05 17 12.62	39 22 15.8	18.720 ± 0.046	19.365 ± 0.045	0.645 ± 0.064
05 16 59.59	39 22 15.8	19.330 ± 0.124	19.536 ± 0.132	0.206 ± 0.181
05 17 15.84	39 22 16.3	15.401 ± 0.005	16.065 ± 0.007	0.664 ± 0.009
05 17 00.04	39 22 16.1	16.867 ± 0.017	17.088 ± 0.017	0.221 ± 0.024
05 17 23.49	39 22 16.8	18.333 ± 0.039	18.733 ± 0.031	0.400 ± 0.050
05 17 03.00	39 22 16.7	19.227 ± 0.084	19.778 ± 0.106	0.551 ± 0.135
05 17 24.83	39 22 17.1	18.978 ± 0.072	19.070 ± 0.066	0.092 ± 0.098
05 17 14.00	39 22 17.6	15.303 ± 0.018	17.549 ± 0.021	2.246 ± 0.028
05 17 14.62	39 22 17.1	18.018 ± 0.021	18.553 ± 0.023	0.535 ± 0.031
05 17 15.99	39 22 17.1	17.421 ± 0.014	18.184 ± 0.018	0.763 ± 0.023
05 17 06.01	39 22 17.4	19.153 ± 0.060	19.494 ± 0.058	0.341 ± 0.083
05 17 22.58	39 22 17.7	16.818 ± 0.014	17.074 ± 0.013	0.256 ± 0.019
05 17 15.26	39 22 17.9	17.912 ± 0.031	18.468 ± 0.022	0.556 ± 0.038
05 17 07.90	39 22 17.8	17.215 ± 0.016	17.625 ± 0.015	0.410 ± 0.022
05 17 29.15	39 22 18.3	17.662 ± 0.080	18.333 ± 0.069	0.671 ± 0.106
05 17 17.03	39 22 18.3	18.922 ± 0.049	19.454 ± 0.047	0.532 ± 0.068
05 17 13.08	39 22 18.3	16.901 ± 0.012	17.817 ± 0.075	0.916 ± 0.076
05 17 22.78	39 22 18.8	19.579 ± 0.108	19.777 ± 0.084	0.198 ± 0.137
05 17 09.71	39 22 18.7	16.623 ± 0.009	16.981 ± 0.008	0.358 ± 0.012
05 17 14.08	39 22 18.8	17.095 ± 0.013	18.689 ± 0.032	1.594 ± 0.035
05 17 17.27	39 22 19.1	16.856 ± 0.009	17.102 ± 0.010	0.246 ± 0.013
05 17 28.26	39 22 19.2	15.142 ± 0.015	15.445 ± 0.015	0.303 ± 0.021
05 17 10.14	39 22 19.3	17.735 ± 0.020	17.968 ± 0.016	0.233 ± 0.026
05 17 09.57	39 22 19.5	19.365 ± 0.074	19.864 ± 0.075	0.499 ± 0.105
05 17 05.36	39 22 19.5	18.787 ± 0.038	19.382 ± 0.059	0.595 ± 0.070
05 17 15.53	39 22 19.7	16.093 ± 0.008	16.430 ± 0.007	0.337 ± 0.011
05 17 07.61	39 22 19.6	14.306 ± 0.007	14.475 ± 0.005	0.169 ± 0.009
05 17 21.64	39 22 19.8	17.222 ± 0.016	17.565 ± 0.014	0.343 ± 0.021
05 17 14.90	39 22 19.9	16.733 ± 0.010	17.549 ± 0.009	0.816 ± 0.013
05 17 02.14	39 22 19.7	16.747 ± 0.019	16.989 ± 0.015	0.242 ± 0.024
05 17 11.99	39 22 19.9	17.878 ± 0.022	18.403 ± 0.023	0.525 ± 0.032
05 17 11.61	39 22 20.1	16.930 ± 0.013	17.363 ± 0.011	0.433 ± 0.017
05 17 29.43	39 22 20.3	17.520 ± 0.030	17.709 ± 0.027	0.189 ± 0.040
05 17 13.31	39 22 20.4	18.488 ± 0.041	19.176 ± 0.039	0.688 ± 0.057
05 17 26.06	39 22 21.2	18.296 ± 0.070	18.661 ± 0.062	0.365 ± 0.094
05 17 11.13	39 22 21.3	18.733 ± 0.037	19.311 ± 0.047	0.578 ± 0.060
05 17 14.52	39 22 21.4	18.725 ± 0.053	19.816 ± 0.090	1.091 ± 0.104

Table A.1. continued.

RA (hh mm ss)	Dec (dd mm ss)	H (mag)	K_s (mag)	H–K_s (mag)
05 17 22.65	39 22 21.7	15.800 ± 0.010	16.112 ± 0.009	0.312 ± 0.013
05 17 13.17	39 22 21.7	16.601 ± 0.010	17.614 ± 0.010	1.013 ± 0.014
05 17 21.87	39 22 21.7	19.410 ± 0.093	19.825 ± 0.083	0.415 ± 0.125
05 17 06.60	39 22 22.0	16.047 ± 0.008	16.334 ± 0.007	0.287 ± 0.011
05 17 22.44	39 22 22.1	19.749 ± 0.128	19.864 ± 0.096	0.115 ± 0.160
05 17 13.24	39 22 22.9	16.161 ± 0.007	17.573 ± 0.011	1.412 ± 0.013
05 17 13.29	39 22 23.4	17.805 ± 0.018	19.096 ± 0.037	1.291 ± 0.041
05 17 06.74	39 22 22.8	19.204 ± 0.065	19.894 ± 0.087	0.690 ± 0.109
05 17 11.50	39 22 22.9	17.113 ± 0.010	17.509 ± 0.012	0.396 ± 0.016
05 17 28.23	39 22 23.1	18.059 ± 0.055	18.294 ± 0.051	0.235 ± 0.075
05 16 59.71	39 22 23.2	16.543 ± 0.019	16.683 ± 0.012	0.140 ± 0.022
05 17 13.48	39 22 23.8	15.439 ± 0.045	16.190 ± 0.029	0.751 ± 0.054
05 17 11.10	39 22 24.0	19.298 ± 0.075	19.789 ± 0.061	0.491 ± 0.097
05 17 12.96	39 22 24.1	17.648 ± 0.016	19.710 ± 0.059	2.062 ± 0.061
05 17 13.64	39 22 24.2	17.060 ± 0.019	17.624 ± 0.015	0.564 ± 0.024
05 17 10.73	39 22 24.3	15.922 ± 0.006	16.128 ± 0.005	0.206 ± 0.008
05 17 01.52	39 22 24.2	17.610 ± 0.034	17.862 ± 0.027	0.252 ± 0.043
05 16 59.53	39 22 24.2	14.716 ± 0.012	14.818 ± 0.007	0.102 ± 0.014
05 17 16.74	39 22 24.5	18.836 ± 0.031	19.275 ± 0.051	0.439 ± 0.060
05 17 22.56	39 22 24.6	18.684 ± 0.053	19.051 ± 0.043	0.367 ± 0.068
05 17 11.97	39 22 24.9	17.737 ± 0.019	18.173 ± 0.019	0.436 ± 0.027
05 17 14.85	39 22 26.1	18.322 ± 0.028	18.943 ± 0.031	0.621 ± 0.042
05 17 13.94	39 22 26.2	17.939 ± 0.020	18.674 ± 0.032	0.735 ± 0.038
05 17 13.84	39 22 26.4	18.324 ± 0.030	18.949 ± 0.036	0.625 ± 0.047
05 17 27.34	39 22 26.6	14.314 ± 0.015	14.497 ± 0.011	0.183 ± 0.019
05 17 14.96	39 22 26.7	17.853 ± 0.022	18.499 ± 0.021	0.646 ± 0.030
05 17 21.76	39 22 27.3	16.239 ± 0.012	16.448 ± 0.010	0.209 ± 0.016
05 17 14.08	39 22 27.3	18.278 ± 0.033	19.100 ± 0.043	0.822 ± 0.054
05 17 13.67	39 22 27.4	17.200 ± 0.015	17.799 ± 0.013	0.599 ± 0.020
05 17 12.53	39 22 27.5	18.629 ± 0.041	19.068 ± 0.035	0.439 ± 0.054
05 17 09.30	39 22 27.8	19.151 ± 0.070	19.852 ± 0.073	0.701 ± 0.101
05 16 59.57	39 22 27.8	17.564 ± 0.028	17.784 ± 0.022	0.220 ± 0.036
05 17 13.40	39 22 28.0	17.864 ± 0.063	19.136 ± 0.043	1.272 ± 0.076
05 17 10.21	39 22 28.3	18.628 ± 0.034	19.368 ± 0.043	0.740 ± 0.055
05 17 12.44	39 22 28.9	18.085 ± 0.027	18.764 ± 0.022	0.679 ± 0.035
05 17 15.05	39 22 29.3	18.682 ± 0.056	19.195 ± 0.047	0.513 ± 0.073
05 17 12.73	39 22 29.3	18.509 ± 0.025	18.868 ± 0.032	0.359 ± 0.041
05 17 05.16	39 22 29.3	15.085 ± 0.010	15.257 ± 0.009	0.172 ± 0.013
05 17 21.61	39 22 29.6	18.831 ± 0.059	19.129 ± 0.049	0.298 ± 0.077
05 17 15.57	39 22 29.6	13.088 ± 0.005	13.253 ± 0.005	0.165 ± 0.007
05 17 08.52	39 22 29.8	18.752 ± 0.041	19.291 ± 0.057	0.539 ± 0.070
05 17 13.30	39 22 29.9	17.957 ± 0.019	18.369 ± 0.021	0.412 ± 0.028
05 17 13.73	39 22 30.0	15.769 ± 0.007	16.064 ± 0.006	0.295 ± 0.009
05 17 14.40	39 22 30.1	18.140 ± 0.024	18.951 ± 0.042	0.811 ± 0.048
05 17 10.62	39 22 30.1	18.273 ± 0.027	18.595 ± 0.026	0.322 ± 0.037
05 17 14.05	39 22 30.3	17.219 ± 0.018	17.484 ± 0.013	0.265 ± 0.022
05 17 14.32	39 22 30.9	19.235 ± 0.056	19.667 ± 0.063	0.432 ± 0.084
05 17 17.64	39 22 31.1	18.299 ± 0.031	18.537 ± 0.023	0.238 ± 0.039
05 17 08.97	39 22 31.4	19.149 ± 0.064	19.616 ± 0.069	0.467 ± 0.094
05 17 12.62	39 22 31.5	18.587 ± 0.031	18.919 ± 0.027	0.332 ± 0.041
05 17 13.80	39 22 31.6	16.662 ± 0.011	17.250 ± 0.010	0.588 ± 0.015
05 17 13.62	39 22 31.8	15.435 ± 0.007	15.672 ± 0.006	0.237 ± 0.009
05 17 16.71	39 22 32.1	19.182 ± 0.060	19.778 ± 0.058	0.596 ± 0.083
05 17 14.74	39 22 32.3	18.804 ± 0.047	19.269 ± 0.041	0.465 ± 0.062
05 17 11.28	39 22 32.6	19.583 ± 0.084	20.242 ± 0.104	0.659 ± 0.134
05 17 12.84	39 22 32.9	18.114 ± 0.025	18.668 ± 0.029	0.554 ± 0.038
05 17 07.55	39 22 33.6	19.007 ± 0.059	19.534 ± 0.051	0.527 ± 0.078
05 16 58.80	39 22 33.6	14.840 ± 0.011	15.016 ± 0.007	0.176 ± 0.013
05 17 09.70	39 22 33.8	18.214 ± 0.028	18.504 ± 0.019	0.290 ± 0.034
05 17 04.80	39 22 33.8	16.325 ± 0.008	16.653 ± 0.009	0.328 ± 0.012
05 17 13.79	39 22 34.3	17.549 ± 0.017	17.999 ± 0.014	0.450 ± 0.022
05 17 21.74	39 22 34.4	19.080 ± 0.056	19.514 ± 0.062	0.434 ± 0.084
05 17 19.45	39 22 34.7	14.955 ± 0.006	15.159 ± 0.007	0.204 ± 0.009
05 17 12.89	39 22 35.0	16.119 ± 0.008	16.343 ± 0.005	0.224 ± 0.009
05 16 58.57	39 22 35.0	18.239 ± 0.056	18.559 ± 0.046	0.320 ± 0.072

Table A.1. continued.

RA (hh mm ss)	Dec (dd mm ss)	H (mag)	K_s (mag)	H–K_s (mag)
05 17 02.85	39 22 35.2	17.437 ± 0.023	17.822 ± 0.019	0.385 ± 0.030
05 17 14.22	39 22 35.6	16.868 ± 0.010	17.486 ± 0.010	0.618 ± 0.014
05 17 28.28	39 22 36.2	18.913 ± 0.106	19.102 ± 0.085	0.189 ± 0.136
05 17 13.66	39 22 36.4	15.705 ± 0.006	15.919 ± 0.005	0.214 ± 0.008
05 17 08.20	39 22 36.5	17.023 ± 0.016	18.402 ± 0.028	1.379 ± 0.032
05 17 12.31	39 22 36.8	16.519 ± 0.007	16.848 ± 0.008	0.329 ± 0.011
05 17 11.91	39 22 36.9	19.161 ± 0.058	19.551 ± 0.059	0.390 ± 0.083
05 17 12.87	39 22 37.8	17.502 ± 0.016	18.069 ± 0.018	0.567 ± 0.024
05 17 16.44	39 22 38.0	19.772 ± 0.108	20.238 ± 0.091	0.466 ± 0.141
05 17 08.98	39 22 38.6	16.266 ± 0.008	16.906 ± 0.007	0.640 ± 0.011
05 17 02.08	39 22 38.6	18.148 ± 0.042	18.569 ± 0.045	0.421 ± 0.062
05 17 19.81	39 22 38.8	17.671 ± 0.021	17.961 ± 0.021	0.290 ± 0.030
05 17 25.00	39 22 38.9	18.248 ± 0.052	18.481 ± 0.050	0.233 ± 0.072
05 17 10.13	39 22 39.2	18.995 ± 0.053	19.272 ± 0.042	0.277 ± 0.068
05 16 59.96	39 22 39.0	16.214 ± 0.015	16.495 ± 0.012	0.281 ± 0.019
05 17 13.83	39 22 39.3	17.427 ± 0.017	18.028 ± 0.021	0.601 ± 0.027
05 17 15.75	39 22 39.3	17.493 ± 0.012	17.818 ± 0.018	0.325 ± 0.022
05 17 06.91	39 22 39.2	15.994 ± 0.008	16.195 ± 0.007	0.201 ± 0.011
05 17 22.21	39 22 39.7	19.607 ± 0.081	19.783 ± 0.085	0.176 ± 0.117
05 17 08.45	39 22 39.7	18.883 ± 0.051	19.445 ± 0.061	0.562 ± 0.080
05 17 11.61	39 22 39.8	16.833 ± 0.011	17.102 ± 0.009	0.269 ± 0.014
05 17 08.20	39 22 40.2	17.944 ± 0.017	18.366 ± 0.021	0.422 ± 0.027
05 17 02.97	39 22 40.3	18.342 ± 0.048	18.736 ± 0.040	0.394 ± 0.062
05 17 12.60	39 22 40.5	18.409 ± 0.028	18.829 ± 0.026	0.420 ± 0.038
05 16 58.32	39 22 40.4	14.998 ± 0.010	15.113 ± 0.008	0.115 ± 0.013
05 17 12.92	39 22 40.9	18.008 ± 0.020	18.372 ± 0.019	0.364 ± 0.028
05 17 09.38	39 22 41.8	17.161 ± 0.011	17.396 ± 0.011	0.235 ± 0.016
05 17 29.12	39 22 42.9	17.293 ± 0.036	17.685 ± 0.032	0.392 ± 0.048
05 16 58.04	39 22 43.0	18.292 ± 0.068	18.491 ± 0.052	0.199 ± 0.086
05 17 09.90	39 22 43.9	19.457 ± 0.077	19.968 ± 0.081	0.511 ± 0.112
05 17 09.04	39 22 43.9	16.663 ± 0.010	17.176 ± 0.009	0.513 ± 0.013
05 17 29.78	39 22 44.4	13.304 ± 0.040	13.505 ± 0.028	0.201 ± 0.049
05 17 18.43	39 22 44.8	19.084 ± 0.048	19.411 ± 0.048	0.327 ± 0.068
05 17 16.57	39 22 44.8	19.266 ± 0.056	19.544 ± 0.050	0.278 ± 0.075
05 17 11.68	39 22 45.4	18.439 ± 0.030	18.800 ± 0.035	0.361 ± 0.046
05 17 13.34	39 22 45.8	19.150 ± 0.045	19.664 ± 0.059	0.514 ± 0.074
05 17 09.93	39 22 46.0	17.102 ± 0.010	17.481 ± 0.010	0.379 ± 0.014
05 17 15.84	39 22 46.5	17.777 ± 0.018	18.144 ± 0.016	0.367 ± 0.024
05 17 12.56	39 22 46.8	16.504 ± 0.012	16.796 ± 0.005	0.292 ± 0.013
05 17 07.18	39 22 47.1	18.094 ± 0.026	18.547 ± 0.024	0.453 ± 0.035
05 17 13.57	39 22 47.6	17.664 ± 0.022	18.151 ± 0.017	0.487 ± 0.028
05 17 08.72	39 22 47.7	19.057 ± 0.054	19.393 ± 0.053	0.336 ± 0.076
05 17 03.06	39 22 47.8	18.621 ± 0.051	19.027 ± 0.055	0.406 ± 0.075
05 17 13.69	39 22 48.2	18.321 ± 0.031	18.748 ± 0.028	0.427 ± 0.042
05 16 58.14	39 22 48.4	16.740 ± 0.025	16.912 ± 0.021	0.172 ± 0.033
05 17 16.63	39 22 48.6	17.585 ± 0.017	17.873 ± 0.015	0.288 ± 0.023
05 17 13.60	39 22 48.7	18.046 ± 0.024	18.338 ± 0.017	0.292 ± 0.029
05 17 24.85	39 22 49.1	18.504 ± 0.067	18.734 ± 0.052	0.230 ± 0.085
05 17 22.65	39 22 49.1	19.510 ± 0.093	19.745 ± 0.080	0.235 ± 0.123
05 17 10.78	39 22 49.7	17.253 ± 0.014	17.551 ± 0.012	0.298 ± 0.018
05 17 17.69	39 22 50.0	19.237 ± 0.070	19.569 ± 0.062	0.332 ± 0.094
05 17 16.91	39 22 51.2	17.200 ± 0.012	17.503 ± 0.010	0.303 ± 0.016
05 17 10.16	39 22 51.4	18.608 ± 0.031	19.024 ± 0.032	0.416 ± 0.045
05 17 17.58	39 22 51.6	19.435 ± 0.072	19.640 ± 0.069	0.205 ± 0.100
05 17 14.35	39 22 51.9	17.898 ± 0.021	18.271 ± 0.017	0.373 ± 0.027
05 17 09.35	39 22 52.2	15.950 ± 0.009	16.279 ± 0.004	0.329 ± 0.010
05 17 12.00	39 22 52.4	19.104 ± 0.079	19.945 ± 0.098	0.841 ± 0.126
05 17 13.33	39 22 52.4	18.425 ± 0.031	19.146 ± 0.032	0.721 ± 0.045
05 17 03.61	39 22 52.5	16.961 ± 0.015	17.265 ± 0.012	0.304 ± 0.019
05 17 01.60	39 22 52.7	14.512 ± 0.011	14.738 ± 0.006	0.226 ± 0.013
05 17 21.60	39 22 53.1	17.704 ± 0.025	17.980 ± 0.020	0.276 ± 0.032
05 17 02.10	39 22 53.2	15.753 ± 0.012	15.909 ± 0.009	0.156 ± 0.015
05 17 12.84	39 22 53.4	19.160 ± 0.057	19.543 ± 0.051	0.383 ± 0.076
05 17 03.12	39 22 54.0	19.002 ± 0.076	19.221 ± 0.053	0.219 ± 0.093
05 17 17.00	39 22 54.4	17.986 ± 0.025	18.297 ± 0.017	0.311 ± 0.030

Table A.1. continued.

RA (hh mm ss)	Dec (dd mm ss)	H (mag)	K_s (mag)	H–K_s (mag)
05 17 22.73	39 22 54.5	17.025 ± 0.019	17.355 ± 0.012	0.330 ± 0.022
05 17 18.51	39 22 55.0	18.191 ± 0.050	18.276 ± 0.059	0.085 ± 0.077
05 17 16.75	39 22 55.1	17.139 ± 0.013	17.384 ± 0.012	0.245 ± 0.018
05 17 13.45	39 22 55.7	17.864 ± 0.019	18.221 ± 0.018	0.357 ± 0.026
05 16 59.74	39 22 56.2	17.888 ± 0.032	18.069 ± 0.030	0.181 ± 0.044
05 17 00.74	39 22 56.6	15.359 ± 0.011	15.535 ± 0.008	0.176 ± 0.014
05 17 11.29	39 22 56.8	17.162 ± 0.012	17.619 ± 0.013	0.457 ± 0.018
05 17 29.37	39 22 57.7	18.533 ± 0.073	18.608 ± 0.055	0.075 ± 0.091
05 17 02.09	39 22 57.7	16.699 ± 0.019	17.476 ± 0.019	0.777 ± 0.027
05 17 01.56	39 22 58.3	17.075 ± 0.021	17.432 ± 0.017	0.357 ± 0.027
05 17 12.49	39 22 58.8	16.730 ± 0.009	17.033 ± 0.009	0.303 ± 0.013
05 17 13.90	39 22 59.5	18.697 ± 0.038	19.166 ± 0.041	0.469 ± 0.056
05 17 26.13	39 23 00.2	16.856 ± 0.030	17.096 ± 0.020	0.240 ± 0.036
05 16 58.02	39 23 00.6	18.618 ± 0.084	19.447 ± 0.098	0.829 ± 0.129
05 17 17.17	39 23 01.5	18.000 ± 0.020	18.283 ± 0.023	0.283 ± 0.030
05 17 15.53	39 23 01.5	18.827 ± 0.037	19.246 ± 0.045	0.419 ± 0.058
05 17 29.76	39 23 01.6	17.890 ± 0.077	17.940 ± 0.042	0.050 ± 0.088
05 17 06.62	39 23 01.7	17.614 ± 0.020	17.986 ± 0.019	0.372 ± 0.028
05 17 19.26	39 23 02.6	16.677 ± 0.012	16.928 ± 0.011	0.251 ± 0.016
05 17 16.69	39 23 02.7	19.165 ± 0.061	19.525 ± 0.063	0.360 ± 0.088
05 17 04.33	39 23 02.9	16.740 ± 0.012	16.939 ± 0.006	0.199 ± 0.013
05 17 00.76	39 23 03.4	17.953 ± 0.035	18.669 ± 0.055	0.716 ± 0.065
05 17 04.77	39 23 03.9	11.104 ± 0.006	11.334 ± 0.003	0.230 ± 0.007
05 17 14.02	39 23 04.4	16.511 ± 0.009	16.706 ± 0.006	0.195 ± 0.011
05 17 21.63	39 23 04.7	17.772 ± 0.021	18.086 ± 0.020	0.314 ± 0.029
05 17 00.79	39 23 04.8	14.344 ± 0.010	14.452 ± 0.007	0.108 ± 0.012
05 16 59.74	39 23 05.0	18.538 ± 0.061	18.894 ± 0.056	0.356 ± 0.083
05 17 14.42	39 23 05.4	17.900 ± 0.018	18.144 ± 0.020	0.244 ± 0.027
05 17 17.51	39 23 05.6	16.139 ± 0.014	16.400 ± 0.011	0.261 ± 0.018
05 17 11.84	39 23 06.0	19.521 ± 0.079	19.986 ± 0.066	0.465 ± 0.103
05 17 20.35	39 23 06.7	16.973 ± 0.011	17.286 ± 0.012	0.313 ± 0.016
05 17 05.83	39 23 06.9	19.225 ± 0.053	19.414 ± 0.058	0.189 ± 0.079
05 17 21.15	39 23 07.7	18.024 ± 0.031	18.189 ± 0.021	0.165 ± 0.037
05 17 23.90	39 23 07.8	18.083 ± 0.038	18.317 ± 0.028	0.234 ± 0.047
05 16 59.32	39 23 08.1	17.716 ± 0.032	17.963 ± 0.028	0.247 ± 0.043
05 17 27.57	39 23 08.8	17.919 ± 0.045	18.135 ± 0.038	0.216 ± 0.059
05 17 01.18	39 23 09.1	17.162 ± 0.023	17.404 ± 0.018	0.242 ± 0.029
05 17 11.51	39 23 09.3	15.942 ± 0.007	16.179 ± 0.005	0.237 ± 0.009
05 16 59.55	39 23 09.2	17.912 ± 0.042	18.186 ± 0.031	0.274 ± 0.052
05 17 13.47	39 23 09.6	15.647 ± 0.006	15.810 ± 0.005	0.163 ± 0.008
05 17 06.63	39 23 09.5	19.502 ± 0.088	19.855 ± 0.084	0.353 ± 0.122
05 17 15.83	39 23 09.7	14.866 ± 0.004	15.063 ± 0.005	0.197 ± 0.006
05 17 12.69	39 23 09.7	17.563 ± 0.013	17.959 ± 0.013	0.396 ± 0.018
05 17 10.20	39 23 10.0	18.731 ± 0.032	19.105 ± 0.041	0.374 ± 0.052
05 17 02.33	39 23 10.3	18.042 ± 0.045	18.361 ± 0.036	0.319 ± 0.058
05 17 25.61	39 23 10.9	17.956 ± 0.050	18.298 ± 0.047	0.342 ± 0.069
05 17 22.77	39 23 10.9	17.713 ± 0.036	17.948 ± 0.021	0.235 ± 0.042
05 17 10.41	39 23 11.3	14.549 ± 0.005	14.672 ± 0.003	0.123 ± 0.006
05 17 29.24	39 23 11.6	14.079 ± 0.025	14.260 ± 0.016	0.181 ± 0.030
05 17 07.40	39 23 12.0	17.809 ± 0.023	18.014 ± 0.014	0.205 ± 0.027
05 17 00.56	39 23 12.4	18.197 ± 0.055	18.485 ± 0.047	0.288 ± 0.072
05 17 09.51	39 23 12.6	17.224 ± 0.013	17.452 ± 0.010	0.228 ± 0.016
05 17 09.96	39 23 13.4	18.326 ± 0.029	18.647 ± 0.020	0.321 ± 0.035
05 17 29.38	39 23 14.1	17.003 ± 0.028	17.117 ± 0.023	0.114 ± 0.036
05 17 09.19	39 23 14.3	19.081 ± 0.053	19.363 ± 0.050	0.282 ± 0.073
05 17 08.10	39 23 14.6	17.941 ± 0.021	18.211 ± 0.020	0.270 ± 0.029
05 17 07.21	39 23 14.9	16.595 ± 0.010	16.758 ± 0.009	0.163 ± 0.013
05 17 19.07	39 23 15.5	16.406 ± 0.013	16.709 ± 0.008	0.303 ± 0.015
05 16 58.98	39 23 16.2	17.185 ± 0.021	17.409 ± 0.017	0.224 ± 0.027
05 17 12.30	39 23 17.2	19.701 ± 0.095	19.979 ± 0.091	0.278 ± 0.132
05 17 05.53	39 23 17.2	16.643 ± 0.010	16.842 ± 0.009	0.199 ± 0.013
05 17 21.71	39 23 17.4	18.957 ± 0.067	20.082 ± 0.099	1.125 ± 0.120
05 16 57.48	39 23 18.6	18.708 ± 0.134	18.944 ± 0.114	0.236 ± 0.176
05 16 58.53	39 23 18.9	14.785 ± 0.015	14.958 ± 0.006	0.173 ± 0.016
05 17 21.32	39 23 19.7	18.921 ± 0.071	19.911 ± 0.112	0.990 ± 0.133

Table A.1. continued.

RA (hh mm ss)	Dec (dd mm ss)	H (mag)	K_s (mag)	H–K_s (mag)
05 17 14.49	39 23 21.6	16.025 ± 0.005	16.352 ± 0.004	0.327 ± 0.006
05 17 11.14	39 23 21.9	15.075 ± 0.005	15.229 ± 0.004	0.154 ± 0.006
05 17 20.35	39 23 22.7	18.596 ± 0.038	18.959 ± 0.043	0.363 ± 0.057
05 17 22.28	39 23 22.8	16.909 ± 0.025	17.109 ± 0.013	0.200 ± 0.028
05 17 23.25	39 23 22.9	18.975 ± 0.069	18.506 ± 0.106	–0.469 ± 0.126
05 17 03.87	39 23 22.8	19.419 ± 0.075	20.116 ± 0.121	0.697 ± 0.142
05 17 17.53	39 23 23.3	17.964 ± 0.027	18.176 ± 0.023	0.212 ± 0.035
05 16 58.40	39 23 23.2	18.493 ± 0.067	18.731 ± 0.053	0.238 ± 0.085
05 17 27.46	39 23 24.0	16.921 ± 0.030	17.068 ± 0.021	0.147 ± 0.037
05 17 08.82	39 23 24.0	18.218 ± 0.024	18.580 ± 0.027	0.362 ± 0.036
05 17 15.79	39 23 24.3	17.028 ± 0.015	17.253 ± 0.008	0.225 ± 0.017
05 17 23.21	39 23 24.5	18.828 ± 0.053	19.081 ± 0.049	0.253 ± 0.072
05 17 14.93	39 23 25.5	18.656 ± 0.037	18.989 ± 0.036	0.333 ± 0.052
05 17 02.59	39 23 25.6	18.201 ± 0.045	18.434 ± 0.037	0.233 ± 0.058
05 17 10.33	39 23 26.1	19.139 ± 0.053	19.372 ± 0.052	0.233 ± 0.074
05 17 22.20	39 23 27.0	16.669 ± 0.024	16.948 ± 0.013	0.279 ± 0.027
05 17 28.07	39 23 28.0	18.846 ± 0.118	19.258 ± 0.083	0.412 ± 0.144
05 17 13.57	39 23 28.0	17.731 ± 0.014	17.925 ± 0.015	0.194 ± 0.021
05 16 57.60	39 23 28.2	17.593 ± 0.053	17.802 ± 0.049	0.209 ± 0.072
05 17 08.04	39 23 28.5	16.675 ± 0.013	16.932 ± 0.009	0.257 ± 0.016
05 17 27.09	39 23 28.7	16.140 ± 0.022	16.395 ± 0.014	0.255 ± 0.026
05 17 20.15	39 23 28.9	19.481 ± 0.096	19.825 ± 0.093	0.344 ± 0.134
05 17 20.01	39 23 29.2	19.037 ± 0.072	19.392 ± 0.059	0.355 ± 0.093
05 17 12.87	39 23 29.9	15.766 ± 0.005	15.922 ± 0.004	0.156 ± 0.006
05 17 11.71	39 23 31.1	19.545 ± 0.102	20.047 ± 0.089	0.502 ± 0.135
05 17 07.11	39 23 32.5	18.816 ± 0.043	19.214 ± 0.038	0.398 ± 0.057
05 17 14.97	39 23 32.8	17.582 ± 0.017	17.831 ± 0.015	0.249 ± 0.023
05 17 21.74	39 23 33.0	18.626 ± 0.051	18.926 ± 0.043	0.300 ± 0.067
05 17 27.97	39 23 33.4	15.866 ± 0.025	16.106 ± 0.013	0.240 ± 0.028
05 17 19.52	39 23 33.7	18.171 ± 0.032	18.411 ± 0.033	0.240 ± 0.046
05 17 11.38	39 23 33.9	15.877 ± 0.009	16.054 ± 0.004	0.177 ± 0.010
05 17 21.41	39 23 34.1	19.209 ± 0.067	19.643 ± 0.078	0.434 ± 0.103
05 17 00.30	39 23 34.6	17.682 ± 0.030	17.974 ± 0.032	0.292 ± 0.044
05 17 20.96	39 23 34.9	18.571 ± 0.049	18.853 ± 0.041	0.282 ± 0.064
05 17 07.94	39 23 35.1	19.663 ± 0.096	19.997 ± 0.120	0.334 ± 0.154
05 17 14.48	39 23 35.2	19.690 ± 0.094	20.050 ± 0.076	0.360 ± 0.121
05 17 12.76	39 23 35.8	18.856 ± 0.042	19.157 ± 0.034	0.301 ± 0.054
05 17 02.69	39 23 36.5	17.997 ± 0.048	18.130 ± 0.028	0.133 ± 0.056
05 17 24.25	39 23 36.9	18.521 ± 0.077	18.539 ± 0.054	0.018 ± 0.094
05 17 06.27	39 23 36.7	18.415 ± 0.036	18.798 ± 0.035	0.383 ± 0.050
05 17 14.20	39 23 36.9	18.462 ± 0.032	18.690 ± 0.025	0.228 ± 0.041
05 16 58.44	39 23 36.7	17.934 ± 0.038	18.214 ± 0.031	0.280 ± 0.049
05 17 10.09	39 23 38.3	18.067 ± 0.027	18.278 ± 0.018	0.211 ± 0.032
05 17 04.67	39 23 38.9	16.502 ± 0.036	16.709 ± 0.027	0.207 ± 0.045
05 17 00.11	39 23 39.0	16.200 ± 0.020	16.348 ± 0.010	0.148 ± 0.022
05 17 05.87	39 23 39.3	16.777 ± 0.017	17.063 ± 0.011	0.286 ± 0.020
05 17 13.70	39 23 40.0	18.059 ± 0.025	18.283 ± 0.016	0.224 ± 0.030
05 17 24.96	39 23 40.2	15.836 ± 0.018	16.084 ± 0.012	0.248 ± 0.022
05 17 01.45	39 23 40.4	18.706 ± 0.070	19.258 ± 0.080	0.552 ± 0.106
05 17 01.78	39 23 40.5	13.913 ± 0.012	14.048 ± 0.007	0.135 ± 0.014
05 17 05.10	39 23 40.9	18.198 ± 0.033	18.484 ± 0.030	0.286 ± 0.045
05 17 11.65	39 23 42.7	18.042 ± 0.020	18.351 ± 0.021	0.309 ± 0.029
05 17 12.57	39 23 42.9	18.898 ± 0.044	19.229 ± 0.051	0.331 ± 0.067
05 16 58.82	39 23 43.1	16.473 ± 0.030	16.728 ± 0.018	0.255 ± 0.035
05 17 13.32	39 23 43.9	17.315 ± 0.013	17.543 ± 0.012	0.228 ± 0.018
05 17 01.46	39 23 44.4	17.593 ± 0.035	17.748 ± 0.030	0.155 ± 0.046
05 17 10.66	39 23 46.0	18.841 ± 0.045	19.126 ± 0.043	0.285 ± 0.062
05 17 10.08	39 23 46.5	18.389 ± 0.035	18.717 ± 0.031	0.328 ± 0.047
05 17 09.23	39 23 47.1	18.673 ± 0.046	19.036 ± 0.033	0.363 ± 0.057
05 16 59.08	39 23 47.4	17.749 ± 0.042	17.991 ± 0.029	0.242 ± 0.051
05 17 26.74	39 23 48.4	16.975 ± 0.027	17.203 ± 0.022	0.228 ± 0.035
05 17 20.44	39 23 48.5	16.880 ± 0.024	17.242 ± 0.012	0.362 ± 0.027
05 17 04.04	39 23 48.9	16.847 ± 0.064	17.066 ± 0.045	0.219 ± 0.078
05 16 57.95	39 23 48.8	17.241 ± 0.033	17.349 ± 0.025	0.108 ± 0.041
05 17 06.71	39 23 49.5	17.263 ± 0.017	17.470 ± 0.014	0.207 ± 0.022

Table A.1. continued.

RA (hh mm ss)	Dec (dd mm ss)	H (mag)	K_s (mag)	H–K_s (mag)
05 17 24.01	39 23 50.1	17.588 ± 0.033	17.402 ± 0.032	–0.186 ± 0.046
05 17 00.93	39 23 50.6	19.117 ± 0.087	19.540 ± 0.090	0.423 ± 0.125
05 17 05.43	39 23 51.0	15.041 ± 0.041	15.199 ± 0.028	0.158 ± 0.050
05 17 01.47	39 23 51.2	16.404 ± 0.017	16.575 ± 0.012	0.171 ± 0.021
05 16 59.26	39 23 51.3	15.157 ± 0.035	15.281 ± 0.021	0.124 ± 0.041
05 17 01.91	39 23 51.7	18.178 ± 0.046	18.342 ± 0.031	0.164 ± 0.055
05 17 05.95	39 23 51.9	19.145 ± 0.064	19.451 ± 0.058	0.306 ± 0.086
05 17 10.92	39 23 52.1	18.247 ± 0.029	18.584 ± 0.023	0.337 ± 0.037
05 17 19.64	39 23 52.4	18.819 ± 0.073	19.127 ± 0.051	0.308 ± 0.089
05 17 08.76	39 23 52.8	18.489 ± 0.034	18.778 ± 0.047	0.289 ± 0.058
05 17 08.66	39 23 53.8	18.691 ± 0.052	18.886 ± 0.039	0.195 ± 0.065
05 17 27.66	39 23 54.8	17.643 ± 0.061	17.761 ± 0.036	0.118 ± 0.071
05 17 26.31	39 23 55.4	16.050 ± 0.027	16.289 ± 0.016	0.239 ± 0.031
05 17 13.19	39 23 55.3	16.163 ± 0.009	16.423 ± 0.008	0.260 ± 0.012
05 17 16.10	39 23 55.7	19.178 ± 0.064	19.327 ± 0.055	0.149 ± 0.084
05 17 17.49	39 23 56.4	19.575 ± 0.095	19.918 ± 0.087	0.343 ± 0.129
05 17 01.66	39 23 57.0	17.435 ± 0.029	17.695 ± 0.025	0.260 ± 0.038
05 17 13.95	39 23 58.7	19.316 ± 0.066	19.806 ± 0.077	0.490 ± 0.101
05 17 06.72	39 23 59.4	15.404 ± 0.030	15.586 ± 0.021	0.182 ± 0.037
05 17 01.79	39 24 00.5	18.560 ± 0.067	18.880 ± 0.062	0.320 ± 0.091
05 16 59.86	39 24 00.9	17.945 ± 0.054	18.226 ± 0.035	0.281 ± 0.064
05 16 58.12	39 24 01.1	16.954 ± 0.035	17.169 ± 0.032	0.215 ± 0.047
05 16 58.72	39 24 01.2	17.884 ± 0.051	18.173 ± 0.038	0.289 ± 0.064
05 17 21.92	39 24 02.4	19.092 ± 0.080	19.413 ± 0.070	0.321 ± 0.106
05 17 12.72	39 24 02.9	17.765 ± 0.018	18.013 ± 0.018	0.248 ± 0.025
05 17 26.09	39 24 03.1	18.773 ± 0.116	19.627 ± 0.130	0.854 ± 0.174
05 17 07.40	39 24 05.1	16.118 ± 0.027	16.275 ± 0.015	0.157 ± 0.031
05 17 26.91	39 24 05.8	18.195 ± 0.067	18.428 ± 0.055	0.233 ± 0.087
05 17 12.47	39 24 06.0	15.610 ± 0.017	15.755 ± 0.013	0.145 ± 0.021
05 17 08.27	39 24 07.4	18.218 ± 0.038	18.448 ± 0.031	0.230 ± 0.049
05 17 00.45	39 24 08.7	17.285 ± 0.034	17.380 ± 0.025	0.095 ± 0.042
05 17 13.94	39 24 08.9	18.136 ± 0.033	18.471 ± 0.027	0.335 ± 0.043
05 17 12.28	39 24 10.3	18.219 ± 0.046	18.552 ± 0.032	0.333 ± 0.056
05 17 06.33	39 24 10.4	17.126 ± 0.060	17.314 ± 0.041	0.188 ± 0.073
05 17 12.41	39 24 10.8	19.225 ± 0.093	19.390 ± 0.071	0.165 ± 0.117
05 17 14.26	39 24 11.5	19.451 ± 0.115	19.783 ± 0.111	0.332 ± 0.160
05 17 13.19	39 24 12.1	17.419 ± 0.023	17.578 ± 0.017	0.159 ± 0.029
05 17 12.85	39 24 13.3	19.455 ± 0.102	19.717 ± 0.099	0.262 ± 0.142
05 16 59.39	39 24 13.5	17.249 ± 0.047	17.342 ± 0.036	0.093 ± 0.059
05 17 05.27	39 24 14.5	18.051 ± 0.043	17.819 ± 0.042	–0.232 ± 0.060
05 17 08.97	39 24 15.2	18.091 ± 0.049	18.244 ± 0.030	0.153 ± 0.057
05 17 24.98	39 24 15.5	18.123 ± 0.072	18.274 ± 0.068	0.151 ± 0.099
05 17 04.67	39 24 16.3	18.869 ± 0.099	19.094 ± 0.102	0.225 ± 0.142
05 17 28.64	39 24 16.8	17.683 ± 0.058	18.047 ± 0.067	0.364 ± 0.089
05 17 23.32	39 24 17.7	18.610 ± 0.095	18.785 ± 0.080	0.175 ± 0.124
05 16 58.04	39 24 18.6	16.357 ± 0.030	16.573 ± 0.025	0.216 ± 0.039
05 16 57.60	39 24 19.3	17.807 ± 0.050	18.097 ± 0.063	0.290 ± 0.080
05 17 08.88	39 24 20.6	16.221 ± 0.021	16.322 ± 0.010	0.101 ± 0.023
05 17 05.41	39 24 21.5	16.429 ± 0.056	16.592 ± 0.027	0.163 ± 0.062
05 17 03.78	39 24 22.1	17.673 ± 0.058	18.246 ± 0.067	0.573 ± 0.089
05 17 10.82	39 24 22.4	17.347 ± 0.035	17.588 ± 0.040	0.241 ± 0.053
05 17 18.48	39 20 03.8	17.091 ± 0.048	18.276 ± 0.074	1.185 ± 0.088
05 17 20.24	39 20 04.2	18.329 ± 0.093	19.368 ± 0.111	1.039 ± 0.145
05 17 15.28	39 20 07.4	17.144 ± 0.038	17.541 ± 0.038	0.397 ± 0.054
05 17 03.64	39 20 08.1	18.088 ± 0.077	18.651 ± 0.071	0.563 ± 0.105
05 17 13.33	39 20 08.3	18.154 ± 0.046	18.706 ± 0.053	0.552 ± 0.070
05 17 01.45	39 20 09.0	19.906 ± 0.351	20.424 ± 0.402	0.518 ± 0.534
05 17 18.14	39 20 10.7	18.970 ± 0.079	19.756 ± 0.111	0.786 ± 0.136
05 17 10.57	39 20 11.2	17.583 ± 0.035	17.918 ± 0.028	0.335 ± 0.045
05 17 18.76	39 20 12.1	18.450 ± 0.045	18.854 ± 0.052	0.404 ± 0.069
05 17 00.77	39 20 11.9	14.229 ± 0.023	14.371 ± 0.017	0.142 ± 0.029
05 17 20.66	39 20 14.4	16.388 ± 0.022	16.789 ± 0.027	0.401 ± 0.035
05 17 08.00	39 20 18.0	14.911 ± 0.019	15.127 ± 0.013	0.216 ± 0.023
05 17 27.33	39 20 19.2	16.032 ± 0.016	16.439 ± 0.027	0.407 ± 0.031
05 17 19.12	39 20 19.5	18.766 ± 0.039	19.100 ± 0.041	0.334 ± 0.057

Table A.1. continued.

RA (hh mm ss)	Dec (dd mm ss)	H (mag)	K_s (mag)	H–K_s (mag)
05 17 08.63	39 20 19.5	17.107 ± 0.018	17.683 ± 0.019	0.576 ± 0.026
05 17 21.45	39 20 20.3	17.639 ± 0.037	17.943 ± 0.028	0.304 ± 0.046
05 17 16.82	39 20 21.0	18.651 ± 0.048	19.009 ± 0.046	0.358 ± 0.066
05 17 11.83	39 20 21.3	16.062 ± 0.023	16.289 ± 0.019	0.227 ± 0.030
05 17 15.19	39 20 22.0	14.149 ± 0.023	14.385 ± 0.024	0.236 ± 0.033
05 17 09.61	39 20 23.8	17.480 ± 0.029	17.851 ± 0.020	0.371 ± 0.035
05 17 29.02	39 20 26.0	16.909 ± 0.035	17.169 ± 0.027	0.260 ± 0.044
05 17 25.30	39 20 27.4	16.854 ± 0.027	17.117 ± 0.019	0.263 ± 0.033
05 17 11.86	39 20 27.8	16.649 ± 0.016	16.892 ± 0.021	0.243 ± 0.026
05 17 25.29	39 20 29.5	15.685 ± 0.022	15.929 ± 0.016	0.244 ± 0.027
05 17 27.65	39 20 31.3	18.790 ± 0.109	19.232 ± 0.084	0.442 ± 0.138
05 17 19.76	39 20 31.5	18.880 ± 0.049	19.308 ± 0.054	0.428 ± 0.073
05 17 19.72	39 20 32.9	17.683 ± 0.030	18.044 ± 0.028	0.361 ± 0.041
05 17 16.35	39 20 33.4	19.445 ± 0.072	19.914 ± 0.066	0.469 ± 0.098
05 17 10.70	39 20 36.1	15.245 ± 0.022	15.501 ± 0.019	0.256 ± 0.029
05 17 04.64	39 20 38.5	12.639 ± 0.038	12.791 ± 0.024	0.152 ± 0.045
05 17 26.76	39 20 41.7	18.883 ± 0.103	19.079 ± 0.088	0.196 ± 0.135
05 17 07.59	39 20 41.8	13.003 ± 0.011	13.134 ± 0.011	0.131 ± 0.016
05 17 06.72	39 20 41.9	14.715 ± 0.013	14.905 ± 0.011	0.190 ± 0.017
05 17 08.94	39 20 42.2	16.696 ± 0.022	16.946 ± 0.017	0.250 ± 0.028
05 17 22.06	39 20 43.7	18.969 ± 0.056	19.425 ± 0.063	0.456 ± 0.084
05 17 27.06	39 20 44.1	15.611 ± 0.022	15.898 ± 0.014	0.287 ± 0.026
05 17 23.81	39 20 44.9	17.750 ± 0.043	18.025 ± 0.034	0.275 ± 0.055
05 17 20.80	39 20 46.2	18.069 ± 0.036	18.409 ± 0.034	0.340 ± 0.050
05 17 03.66	39 20 46.4	17.466 ± 0.045	17.773 ± 0.036	0.307 ± 0.058
05 17 28.32	39 20 48.2	14.230 ± 0.020	14.423 ± 0.014	0.193 ± 0.024
05 17 00.26	39 20 49.4	17.638 ± 0.034	17.946 ± 0.029	0.308 ± 0.045
05 17 13.06	39 20 50.5	17.714 ± 0.030	18.125 ± 0.025	0.411 ± 0.039
05 17 12.31	39 20 52.2	16.920 ± 0.013	17.186 ± 0.014	0.266 ± 0.019
05 17 04.38	39 20 52.3	18.955 ± 0.064	19.303 ± 0.059	0.348 ± 0.087
05 17 10.73	39 20 53.2	18.595 ± 0.046	19.027 ± 0.049	0.432 ± 0.067
05 17 06.65	39 20 53.1	18.274 ± 0.047	19.321 ± 0.061	1.047 ± 0.077
05 17 00.14	39 20 54.4	17.855 ± 0.034	18.156 ± 0.031	0.301 ± 0.046
05 17 21.85	39 20 54.7	17.360 ± 0.024	17.675 ± 0.018	0.315 ± 0.030
05 16 57.82	39 20 56.8	15.253 ± 0.015	15.370 ± 0.012	0.117 ± 0.019
05 17 18.79	39 20 58.0	18.621 ± 0.047	18.991 ± 0.039	0.370 ± 0.061
05 17 11.57	39 20 58.5	18.197 ± 0.022	18.696 ± 0.023	0.499 ± 0.032
05 17 10.73	39 20 58.8	19.950 ± 0.131	20.282 ± 0.121	0.332 ± 0.178
05 17 18.79	39 21 02.5	18.445 ± 0.032	18.842 ± 0.036	0.397 ± 0.048
05 17 10.45	39 21 02.4	17.293 ± 0.013	17.637 ± 0.015	0.344 ± 0.020
05 17 27.83	39 21 04.6	16.773 ± 0.025	17.016 ± 0.022	0.243 ± 0.033
05 17 20.18	39 21 07.3	18.908 ± 0.057	19.327 ± 0.050	0.419 ± 0.076
05 17 10.60	39 21 07.6	19.221 ± 0.065	19.683 ± 0.061	0.462 ± 0.089
05 17 10.15	39 21 08.2	15.612 ± 0.010	15.854 ± 0.011	0.242 ± 0.015
05 17 01.70	39 21 09.3	16.298 ± 0.028	16.552 ± 0.017	0.254 ± 0.033
05 17 11.16	39 21 10.4	18.787 ± 0.039	19.268 ± 0.034	0.481 ± 0.052
05 17 18.92	39 21 10.5	17.430 ± 0.026	17.790 ± 0.013	0.360 ± 0.029
05 17 21.79	39 21 11.6	19.201 ± 0.066	19.740 ± 0.077	0.539 ± 0.101
05 16 57.62	39 21 13.1	16.596 ± 0.028	16.770 ± 0.020	0.174 ± 0.034
05 17 23.64	39 21 14.5	12.762 ± 0.024	12.960 ± 0.020	0.198 ± 0.031
05 17 03.69	39 21 14.4	15.875 ± 0.018	16.150 ± 0.016	0.275 ± 0.024
05 17 25.64	39 21 16.2	17.265 ± 0.034	17.474 ± 0.025	0.209 ± 0.042
05 17 03.44	39 21 15.9	18.274 ± 0.031	18.795 ± 0.044	0.521 ± 0.054
05 17 26.37	39 21 16.8	17.269 ± 0.030	17.544 ± 0.027	0.275 ± 0.040
05 17 13.36	39 21 18.1	17.689 ± 0.021	18.077 ± 0.016	0.388 ± 0.026
05 17 28.46	39 21 20.5	18.289 ± 0.052	18.789 ± 0.074	0.500 ± 0.090
05 17 13.81	39 21 20.4	19.882 ± 0.094	20.174 ± 0.082	0.292 ± 0.125
05 17 14.56	39 21 20.5	19.354 ± 0.045	19.876 ± 0.088	0.522 ± 0.099
05 17 29.97	39 21 22.1	17.525 ± 0.053	17.791 ± 0.041	0.266 ± 0.067
05 17 12.17	39 21 23.0	18.724 ± 0.033	19.279 ± 0.044	0.555 ± 0.055
05 17 25.40	39 21 23.8	16.612 ± 0.025	16.909 ± 0.019	0.297 ± 0.031
05 17 14.12	39 21 24.3	19.053 ± 0.054	19.487 ± 0.058	0.434 ± 0.079
05 17 13.30	39 21 24.5	18.022 ± 0.020	18.359 ± 0.038	0.337 ± 0.043
05 17 08.02	39 21 27.4	18.459 ± 0.032	18.965 ± 0.036	0.506 ± 0.048
05 17 08.47	39 21 30.2	16.805 ± 0.013	17.084 ± 0.010	0.279 ± 0.016

Table A.1. continued.

RA (hh mm ss)	Dec (dd mm ss)	H (mag)	K_s (mag)	H–K_s (mag)
05 16 59.74	39 21 31.6	18.774 ± 0.067	19.030 ± 0.062	0.256 ± 0.091
05 17 25.88	39 21 32.0	17.321 ± 0.036	17.599 ± 0.032	0.278 ± 0.048
05 17 13.79	39 21 33.5	17.756 ± 0.016	18.070 ± 0.017	0.314 ± 0.023
05 17 13.26	39 21 33.5	15.728 ± 0.006	15.979 ± 0.006	0.251 ± 0.008
05 17 21.55	39 21 33.9	19.060 ± 0.060	19.329 ± 0.059	0.269 ± 0.084
05 17 28.94	39 21 34.9	15.455 ± 0.017	15.698 ± 0.015	0.243 ± 0.023
05 17 21.15	39 21 37.0	19.571 ± 0.081	20.090 ± 0.120	0.519 ± 0.145
05 16 57.89	39 21 36.8	18.026 ± 0.041	18.230 ± 0.042	0.204 ± 0.059
05 17 00.54	39 21 37.3	17.857 ± 0.038	18.092 ± 0.030	0.235 ± 0.048
05 17 14.37	39 21 37.9	18.033 ± 0.030	18.369 ± 0.024	0.336 ± 0.038
05 17 07.52	39 21 38.0	19.446 ± 0.083	19.671 ± 0.075	0.225 ± 0.112
05 17 17.87	39 21 38.8	17.698 ± 0.017	18.158 ± 0.018	0.460 ± 0.025
05 17 05.82	39 21 38.8	19.729 ± 0.096	20.164 ± 0.120	0.435 ± 0.154
05 17 10.24	39 21 38.9	18.507 ± 0.032	19.058 ± 0.028	0.551 ± 0.043
05 17 12.37	39 21 40.9	16.198 ± 0.007	17.500 ± 0.012	1.302 ± 0.014
05 17 14.47	39 21 41.3	18.174 ± 0.027	18.815 ± 0.038	0.641 ± 0.047
05 17 02.92	39 21 41.7	17.216 ± 0.019	17.471 ± 0.015	0.255 ± 0.024
05 17 21.37	39 21 42.7	18.955 ± 0.057	19.338 ± 0.070	0.383 ± 0.090
05 17 12.90	39 21 43.9	17.174 ± 0.017	18.179 ± 0.020	1.005 ± 0.026
05 17 11.93	39 21 44.8	14.402 ± 0.006	15.903 ± 0.007	1.501 ± 0.009
05 17 24.54	39 21 45.0	16.469 ± 0.017	16.677 ± 0.019	0.208 ± 0.025
05 17 15.69	39 21 46.2	19.698 ± 0.091	20.216 ± 0.106	0.518 ± 0.140
05 17 12.68	39 21 48.4	17.325 ± 0.017	17.738 ± 0.013	0.413 ± 0.021
05 17 26.09	39 21 48.6	15.982 ± 0.021	16.194 ± 0.015	0.212 ± 0.026
05 17 14.35	39 21 49.5	19.224 ± 0.052	19.767 ± 0.073	0.543 ± 0.090
05 17 13.82	39 21 49.8	18.084 ± 0.026	18.785 ± 0.025	0.701 ± 0.036
05 17 13.09	39 21 49.9	18.758 ± 0.048	19.351 ± 0.047	0.593 ± 0.067
05 17 15.86	39 21 51.2	18.501 ± 0.032	19.002 ± 0.029	0.501 ± 0.043
05 17 27.29	39 21 51.9	17.888 ± 0.043	18.200 ± 0.046	0.312 ± 0.063
05 17 12.02	39 21 52.4	15.065 ± 0.017	16.051 ± 0.011	0.986 ± 0.020
05 17 15.23	39 21 52.5	18.840 ± 0.046	19.451 ± 0.049	0.611 ± 0.067
05 17 19.60	39 21 53.2	15.960 ± 0.009	16.302 ± 0.006	0.342 ± 0.011
05 16 57.94	39 21 53.9	16.768 ± 0.027	16.892 ± 0.016	0.124 ± 0.031
05 17 07.11	39 21 54.9	18.614 ± 0.041	18.983 ± 0.045	0.369 ± 0.061
05 17 12.53	39 21 55.3	18.593 ± 0.029	19.029 ± 0.036	0.436 ± 0.046
05 17 15.05	39 21 55.7	18.982 ± 0.044	19.361 ± 0.056	0.379 ± 0.071
05 16 58.48	39 21 56.2	17.027 ± 0.023	17.262 ± 0.017	0.235 ± 0.029
05 17 19.43	39 21 57.6	16.531 ± 0.010	16.922 ± 0.010	0.391 ± 0.014
05 17 11.02	39 21 57.9	19.164 ± 0.078	19.749 ± 0.075	0.585 ± 0.108
05 17 16.60	39 21 59.8	16.861 ± 0.011	17.350 ± 0.010	0.489 ± 0.015
05 17 29.00	39 22 03.7	13.640 ± 0.018	13.900 ± 0.016	0.260 ± 0.024
05 17 15.82	39 22 04.0	19.580 ± 0.068	19.890 ± 0.103	0.310 ± 0.123
05 17 07.05	39 22 04.1	16.602 ± 0.011	17.058 ± 0.010	0.456 ± 0.015
05 17 11.73	39 22 04.4	17.307 ± 0.013	17.820 ± 0.014	0.513 ± 0.019
05 17 10.09	39 22 05.8	15.724 ± 0.006	15.931 ± 0.005	0.207 ± 0.008
05 17 11.55	39 22 07.0	19.356 ± 0.075	19.537 ± 0.059	0.181 ± 0.095
05 17 13.83	39 22 07.3	16.870 ± 0.013	17.372 ± 0.010	0.502 ± 0.016
05 17 16.42	39 22 07.7	19.392 ± 0.056	19.824 ± 0.092	0.432 ± 0.108
05 17 18.13	39 22 08.3	15.233 ± 0.023	15.448 ± 0.024	0.215 ± 0.033
05 17 13.99	39 22 08.5	18.142 ± 0.059	18.957 ± 0.033	0.815 ± 0.068
05 17 14.25	39 22 11.2	18.382 ± 0.026	19.121 ± 0.038	0.739 ± 0.046
05 17 14.96	39 22 12.8	18.109 ± 0.026	18.438 ± 0.020	0.329 ± 0.033
05 17 08.60	39 22 12.8	19.292 ± 0.076	19.778 ± 0.066	0.486 ± 0.101
05 17 12.59	39 22 14.8	18.253 ± 0.031	19.230 ± 0.042	0.977 ± 0.052
05 16 59.68	39 22 15.0	19.137 ± 0.097	19.956 ± 0.167	0.819 ± 0.193
05 17 13.91	39 22 18.3	15.720 ± 0.009	18.408 ± 0.032	2.688 ± 0.033
05 17 06.00	39 22 18.9	19.630 ± 0.080	20.128 ± 0.110	0.498 ± 0.136
05 17 13.68	39 22 19.5	11.007 ± 0.020	12.409 ± 0.012	1.402 ± 0.023
05 17 13.73	39 22 20.1	11.366 ± 0.020	14.548 ± 0.031	3.182 ± 0.037
05 17 29.27	39 22 19.6	16.978 ± 0.029	17.184 ± 0.020	0.206 ± 0.035
05 17 12.43	39 22 20.2	15.920 ± 0.008	16.739 ± 0.010	0.819 ± 0.013
05 17 07.26	39 22 20.6	19.008 ± 0.054	19.380 ± 0.056	0.372 ± 0.078
05 17 18.55	39 22 21.0	17.370 ± 0.038	17.605 ± 0.036	0.235 ± 0.052
05 17 19.71	39 22 21.5	15.811 ± 0.008	16.064 ± 0.008	0.253 ± 0.011
05 17 19.56	39 22 22.8	18.019 ± 0.032	18.430 ± 0.033	0.411 ± 0.046

Table A.1. continued.

RA (hh mm ss)	Dec (dd mm ss)	H (mag)	K_s (mag)	H–K_s (mag)
05 17 17.15	39 22 23.5	19.001 ± 0.053	19.468 ± 0.050	0.467 ± 0.073
05 17 18.32	39 22 25.1	18.829 ± 0.050	19.197 ± 0.052	0.368 ± 0.072
05 17 12.72	39 22 25.5	18.676 ± 0.044	19.660 ± 0.053	0.984 ± 0.069
05 17 03.13	39 22 25.5	17.411 ± 0.022	17.781 ± 0.020	0.370 ± 0.030
05 17 12.82	39 22 26.6	16.936 ± 0.010	17.233 ± 0.010	0.297 ± 0.014
05 17 13.98	39 22 27.1	17.574 ± 0.017	18.177 ± 0.018	0.603 ± 0.025
05 17 11.01	39 22 28.9	19.209 ± 0.056	19.969 ± 0.087	0.760 ± 0.103
05 17 12.00	39 22 30.1	19.225 ± 0.060	19.638 ± 0.050	0.413 ± 0.078
05 17 11.06	39 22 30.4	19.288 ± 0.067	19.717 ± 0.076	0.429 ± 0.101
05 17 07.33	39 22 30.5	17.611 ± 0.021	17.877 ± 0.016	0.266 ± 0.026
05 17 27.87	39 22 30.9	17.979 ± 0.052	18.248 ± 0.041	0.269 ± 0.066
05 17 22.36	39 22 32.6	19.246 ± 0.070	19.578 ± 0.069	0.332 ± 0.098
05 17 01.19	39 22 32.6	18.700 ± 0.059	18.998 ± 0.060	0.298 ± 0.084
05 17 14.79	39 22 33.5	18.690 ± 0.042	19.143 ± 0.040	0.453 ± 0.058
05 17 02.28	39 22 33.4	18.623 ± 0.050	18.891 ± 0.056	0.268 ± 0.075
05 16 57.83	39 22 34.1	12.488 ± 0.014	12.740 ± 0.008	0.252 ± 0.016
05 17 15.98	39 22 34.9	16.788 ± 0.020	17.198 ± 0.012	0.410 ± 0.023
05 17 02.49	39 22 39.3	15.969 ± 0.017	16.168 ± 0.009	0.199 ± 0.019
05 17 08.93	39 22 43.0	18.840 ± 0.040	19.476 ± 0.056	0.636 ± 0.069
05 17 04.30	39 22 43.3	18.428 ± 0.036	18.836 ± 0.028	0.408 ± 0.046
05 17 07.03	39 22 46.0	18.937 ± 0.051	19.366 ± 0.045	0.429 ± 0.068
05 17 10.93	39 22 47.7	16.898 ± 0.011	17.264 ± 0.010	0.366 ± 0.015
05 16 59.03	39 22 48.1	18.810 ± 0.076	19.114 ± 0.065	0.304 ± 0.100
05 16 58.24	39 22 48.4	16.044 ± 0.013	16.189 ± 0.007	0.145 ± 0.015
05 17 26.06	39 22 49.9	18.588 ± 0.074	18.745 ± 0.084	0.157 ± 0.112
05 17 25.40	39 22 52.6	19.172 ± 0.127	19.253 ± 0.084	0.081 ± 0.152
05 17 14.90	39 22 53.5	19.041 ± 0.053	19.490 ± 0.063	0.449 ± 0.082
05 17 25.89	39 22 55.0	18.677 ± 0.073	19.156 ± 0.097	0.479 ± 0.121
05 17 18.03	39 22 55.3	16.666 ± 0.015	16.921 ± 0.014	0.255 ± 0.021
05 17 25.96	39 22 56.7	17.517 ± 0.040	17.727 ± 0.029	0.210 ± 0.049
05 17 24.76	39 22 58.1	19.258 ± 0.097	19.683 ± 0.106	0.425 ± 0.144
05 17 12.10	39 22 58.4	17.270 ± 0.013	17.639 ± 0.013	0.369 ± 0.018
05 16 57.76	39 22 58.4	14.951 ± 0.016	15.064 ± 0.008	0.113 ± 0.018
05 17 06.69	39 22 59.1	19.699 ± 0.096	19.861 ± 0.086	0.162 ± 0.129
05 17 16.95	39 23 00.2	16.823 ± 0.013	17.035 ± 0.010	0.212 ± 0.016
05 17 26.82	39 23 00.8	18.999 ± 0.105	19.436 ± 0.138	0.437 ± 0.173
05 17 15.80	39 23 01.0	19.599 ± 0.077	19.907 ± 0.092	0.308 ± 0.120
05 17 05.88	39 23 01.2	17.784 ± 0.019	18.094 ± 0.020	0.310 ± 0.028
05 17 20.78	39 23 02.2	15.847 ± 0.008	16.048 ± 0.009	0.201 ± 0.012
05 17 14.97	39 23 02.7	17.999 ± 0.026	18.330 ± 0.026	0.331 ± 0.037
05 17 24.14	39 23 02.9	16.112 ± 0.033	16.277 ± 0.015	0.165 ± 0.036
05 17 06.77	39 23 08.9	19.490 ± 0.085	20.009 ± 0.095	0.519 ± 0.127
05 17 27.56	39 23 10.2	18.775 ± 0.091	19.144 ± 0.082	0.369 ± 0.122
05 17 14.30	39 23 12.4	18.798 ± 0.048	19.216 ± 0.047	0.418 ± 0.067
05 17 04.89	39 23 14.0	18.039 ± 0.028	18.369 ± 0.028	0.330 ± 0.040
05 17 01.02	39 23 14.1	14.027 ± 0.012	14.141 ± 0.005	0.114 ± 0.013
05 17 20.80	39 23 16.2	18.848 ± 0.064	19.733 ± 0.074	0.885 ± 0.098
05 17 19.46	39 23 17.7	17.522 ± 0.019	17.843 ± 0.020	0.321 ± 0.028
05 16 57.82	39 23 19.7	18.227 ± 0.057	18.578 ± 0.054	0.351 ± 0.079
05 16 57.80	39 23 20.3	17.715 ± 0.038	17.912 ± 0.042	0.197 ± 0.057
05 17 11.89	39 23 20.7	18.420 ± 0.031	18.670 ± 0.029	0.250 ± 0.042
05 16 59.55	39 23 22.1	15.908 ± 0.014	16.057 ± 0.008	0.149 ± 0.016
05 16 57.91	39 23 22.9	18.035 ± 0.050	18.283 ± 0.042	0.248 ± 0.065
05 17 22.74	39 23 24.0	15.609 ± 0.031	15.928 ± 0.014	0.319 ± 0.034
05 17 02.21	39 23 27.7	18.930 ± 0.073	19.545 ± 0.113	0.615 ± 0.135
05 17 23.90	39 23 29.5	18.750 ± 0.061	19.102 ± 0.059	0.352 ± 0.085
05 17 13.41	39 23 31.1	19.368 ± 0.065	19.711 ± 0.052	0.343 ± 0.083
05 17 10.76	39 23 33.0	15.559 ± 0.010	15.725 ± 0.007	0.166 ± 0.012
05 17 01.03	39 23 34.6	17.917 ± 0.038	18.328 ± 0.036	0.411 ± 0.052
05 17 19.44	39 23 35.8	16.673 ± 0.025	16.847 ± 0.021	0.174 ± 0.033
05 17 21.13	39 23 35.8	19.816 ± 0.103	20.143 ± 0.139	0.327 ± 0.173
05 17 03.13	39 23 35.6	18.029 ± 0.040	18.319 ± 0.026	0.290 ± 0.048
05 17 22.67	39 23 36.6	18.840 ± 0.062	18.990 ± 0.050	0.150 ± 0.080
05 17 28.10	39 23 37.3	15.843 ± 0.024	16.041 ± 0.016	0.198 ± 0.029
05 17 12.84	39 23 38.9	19.311 ± 0.068	19.747 ± 0.069	0.436 ± 0.097

Table A.1. continued.

RA (hh mm ss)	Dec (dd mm ss)	H (mag)	K_s (mag)	H–K_s (mag)
05 16 58.12	39 23 38.9	18.154 ± 0.039	18.516 ± 0.059	0.362 ± 0.071
05 17 03.97	39 23 39.5	16.367 ± 0.051	16.565 ± 0.031	0.198 ± 0.060
05 17 27.29	39 23 40.5	17.007 ± 0.034	17.252 ± 0.024	0.245 ± 0.042
05 17 22.56	39 23 42.8	19.211 ± 0.077	19.553 ± 0.066	0.342 ± 0.101
05 17 12.61	39 23 44.0	17.331 ± 0.014	17.617 ± 0.009	0.286 ± 0.017
05 17 15.30	39 23 46.0	18.981 ± 0.056	19.398 ± 0.057	0.417 ± 0.080
05 17 00.31	39 23 46.2	18.632 ± 0.073	18.828 ± 0.058	0.196 ± 0.093
05 17 27.30	39 23 47.6	16.968 ± 0.038	17.191 ± 0.020	0.223 ± 0.043
05 17 25.36	39 23 48.2	15.398 ± 0.018	15.525 ± 0.012	0.127 ± 0.022
05 17 26.75	39 23 50.7	18.994 ± 0.105	19.193 ± 0.095	0.199 ± 0.142
05 17 01.63	39 23 51.2	19.207 ± 0.101	19.363 ± 0.089	0.156 ± 0.135
05 17 18.97	39 23 52.7	15.944 ± 0.016	16.103 ± 0.012	0.159 ± 0.020
05 17 01.27	39 23 52.8	17.258 ± 0.029	17.451 ± 0.024	0.193 ± 0.038
05 17 04.30	39 23 53.0	17.471 ± 0.065	17.618 ± 0.054	0.147 ± 0.085
05 17 20.53	39 23 53.9	17.674 ± 0.026	17.908 ± 0.016	0.234 ± 0.031
05 17 27.41	39 23 54.0	16.475 ± 0.031	16.635 ± 0.020	0.160 ± 0.037
05 17 07.94	39 23 54.1	17.315 ± 0.013	17.568 ± 0.013	0.253 ± 0.018
05 17 19.93	39 23 54.6	16.660 ± 0.024	16.840 ± 0.011	0.180 ± 0.026
05 17 20.49	39 23 54.9	19.112 ± 0.074	19.192 ± 0.049	0.080 ± 0.089
05 17 18.43	39 23 55.5	19.005 ± 0.050	19.312 ± 0.050	0.307 ± 0.071
05 17 09.69	39 23 56.2	17.283 ± 0.016	17.444 ± 0.020	0.161 ± 0.026
05 17 09.22	39 23 56.7	19.168 ± 0.053	19.533 ± 0.063	0.365 ± 0.082
05 17 18.24	39 23 57.3	17.282 ± 0.018	17.584 ± 0.011	0.302 ± 0.021
05 17 15.46	39 23 57.5	17.931 ± 0.028	18.117 ± 0.022	0.186 ± 0.036
05 17 25.49	39 23 59.2	18.331 ± 0.065	18.501 ± 0.053	0.170 ± 0.084
05 17 04.11	39 23 59.8	16.151 ± 0.022	16.190 ± 0.019	0.039 ± 0.029
05 17 04.08	39 24 00.1	16.074 ± 0.025	16.332 ± 0.024	0.258 ± 0.035
05 17 02.52	39 23 59.9	16.037 ± 0.069	16.828 ± 0.049	0.791 ± 0.085
05 17 16.45	39 24 01.9	18.785 ± 0.068	19.089 ± 0.047	0.304 ± 0.083
05 17 25.31	39 24 02.3	15.944 ± 0.023	16.178 ± 0.021	0.234 ± 0.031
05 17 05.30	39 24 03.8	18.625 ± 0.073	18.744 ± 0.052	0.119 ± 0.090
05 17 12.80	39 24 05.4	18.944 ± 0.072	19.634 ± 0.076	0.690 ± 0.105
05 17 18.51	39 24 05.5	18.511 ± 0.055	18.785 ± 0.040	0.274 ± 0.068
05 17 18.82	39 24 08.3	18.643 ± 0.043	18.783 ± 0.038	0.140 ± 0.057
05 17 19.37	39 24 09.1	15.365 ± 0.027	15.536 ± 0.006	0.171 ± 0.028
05 17 27.02	39 24 09.8	17.566 ± 0.056	17.854 ± 0.063	0.288 ± 0.084
05 17 29.84	39 24 10.5	17.025 ± 0.047	17.237 ± 0.029	0.212 ± 0.055
05 17 22.72	39 24 11.8	18.067 ± 0.044	18.109 ± 0.040	0.042 ± 0.059
05 17 22.39	39 24 12.5	17.337 ± 0.042	17.453 ± 0.029	0.116 ± 0.051
05 17 01.22	39 24 12.4	16.106 ± 0.022	16.273 ± 0.021	0.167 ± 0.030
05 17 14.33	39 24 14.3	15.659 ± 0.025	15.818 ± 0.023	0.159 ± 0.034
05 17 26.40	39 24 16.6	19.534 ± 0.332	19.691 ± 0.234	0.157 ± 0.406
05 17 29.74	39 24 16.7	17.987 ± 0.085	18.293 ± 0.055	0.306 ± 0.101
05 17 10.88	39 24 17.1	16.749 ± 0.016	16.678 ± 0.019	–0.071 ± 0.025
05 17 06.16	39 24 18.6	16.275 ± 0.036	16.483 ± 0.020	0.208 ± 0.041
05 17 19.40	39 24 21.1	17.334 ± 0.056	17.484 ± 0.034	0.150 ± 0.066
05 17 17.76	39 24 25.4	14.197 ± 0.013	14.273 ± 0.014	0.076 ± 0.019
05 17 21.72	39 24 25.6	16.992 ± 0.040	17.231 ± 0.032	0.239 ± 0.051
05 17 14.10	39 24 27.0	16.229 ± 0.021	16.431 ± 0.014	0.202 ± 0.025
05 17 09.85	39 20 08.6	18.009 ± 0.047	18.387 ± 0.042	0.378 ± 0.063
05 17 06.80	39 20 11.6	13.114 ± 0.039	13.386 ± 0.021	0.272 ± 0.044
05 17 17.42	39 20 16.5	16.658 ± 0.023	16.852 ± 0.043	0.194 ± 0.049
05 17 12.44	39 20 20.5	15.804 ± 0.023	16.044 ± 0.019	0.240 ± 0.030
05 17 17.06	39 20 21.2	17.995 ± 0.045	18.334 ± 0.035	0.339 ± 0.057
05 17 17.54	39 20 23.2	17.324 ± 0.034	17.584 ± 0.034	0.260 ± 0.048
05 17 03.06	39 20 26.0	16.667 ± 0.044	16.930 ± 0.021	0.263 ± 0.049
05 17 24.76	39 20 27.1	17.369 ± 0.044	17.547 ± 0.049	0.178 ± 0.066
05 17 22.00	39 20 29.6	15.364 ± 0.036	15.776 ± 0.037	0.412 ± 0.052
05 17 18.79	39 20 33.1	15.929 ± 0.024	16.163 ± 0.024	0.234 ± 0.034
05 17 12.02	39 20 40.6	12.847 ± 0.030	13.004 ± 0.022	0.157 ± 0.037
05 17 24.68	39 20 40.8	14.683 ± 0.048	14.873 ± 0.035	0.190 ± 0.059
05 17 24.18	39 20 41.1	17.723 ± 0.062	18.063 ± 0.045	0.340 ± 0.077
05 17 28.95	39 20 44.1	13.613 ± 0.020	13.760 ± 0.015	0.147 ± 0.025
05 17 27.05	39 20 52.7	13.362 ± 0.019	13.529 ± 0.013	0.167 ± 0.023
05 17 02.85	39 20 58.5	11.371 ± 0.037	11.682 ± 0.025	0.311 ± 0.045

Table A.1. continued.

RA (hh mm ss)	Dec (dd mm ss)	H (mag)	K_s (mag)	H–K_s (mag)
05 17 07.35	39 20 58.8	15.297 ± 0.009	15.492 ± 0.010	0.195 ± 0.013
05 17 10.35	39 21 07.0	15.179 ± 0.010	15.374 ± 0.010	0.195 ± 0.014
05 17 14.18	39 21 12.1	14.967 ± 0.008	15.258 ± 0.007	0.291 ± 0.011
05 17 09.45	39 21 13.3	15.877 ± 0.014	16.096 ± 0.011	0.219 ± 0.018
05 17 20.29	39 21 13.8	19.526 ± 0.089	19.792 ± 0.072	0.266 ± 0.114
05 17 28.03	39 21 13.9	14.268 ± 0.019	14.476 ± 0.014	0.208 ± 0.024
05 17 16.08	39 21 22.2	18.533 ± 0.027	19.060 ± 0.040	0.527 ± 0.048
05 17 24.18	39 21 23.6	17.822 ± 0.036	18.454 ± 0.030	0.632 ± 0.047
05 17 13.55	39 21 29.7	19.594 ± 0.077	20.213 ± 0.113	0.619 ± 0.137
05 16 58.57	39 21 30.3	17.738 ± 0.035	18.041 ± 0.042	0.303 ± 0.055
05 17 09.54	39 21 32.2	17.598 ± 0.016	18.065 ± 0.018	0.467 ± 0.024
05 17 05.73	39 21 33.0	18.795 ± 0.047	19.181 ± 0.049	0.386 ± 0.068
05 17 22.32	39 21 36.8	18.753 ± 0.058	19.240 ± 0.049	0.487 ± 0.076
05 17 04.22	39 21 39.9	18.454 ± 0.042	19.505 ± 0.076	1.051 ± 0.087
05 17 03.62	39 21 40.2	19.709 ± 0.103	20.037 ± 0.107	0.328 ± 0.149
05 17 01.81	39 21 49.1	16.057 ± 0.016	16.219 ± 0.011	0.162 ± 0.019
05 17 17.68	39 21 49.9	16.530 ± 0.010	16.843 ± 0.010	0.313 ± 0.014
05 17 18.15	39 21 55.7	15.978 ± 0.022	16.277 ± 0.012	0.299 ± 0.025
05 17 12.20	39 21 55.6	13.754 ± 0.008	14.836 ± 0.007	1.082 ± 0.011
05 17 12.74	39 21 56.3	15.548 ± 0.006	16.194 ± 0.006	0.646 ± 0.008
05 17 14.38	39 22 00.6	18.022 ± 0.025	18.662 ± 0.027	0.640 ± 0.037
05 17 23.07	39 22 01.4	15.952 ± 0.010	16.226 ± 0.010	0.274 ± 0.014
05 17 12.67	39 22 04.7	14.668 ± 0.033	15.208 ± 0.020	0.540 ± 0.039
05 16 57.90	39 22 04.9	17.168 ± 0.024	17.377 ± 0.019	0.209 ± 0.031
05 17 14.55	39 22 14.7	17.868 ± 0.018	18.514 ± 0.016	0.646 ± 0.024
05 17 12.85	39 22 18.9	11.294 ± 0.005	11.390 ± 0.005	0.096 ± 0.007
05 17 14.38	39 22 21.9	15.101 ± 0.006	16.227 ± 0.006	1.126 ± 0.008
05 17 13.74	39 22 23.5	15.487 ± 0.011	16.776 ± 0.009	1.289 ± 0.014
05 17 12.61	39 22 26.1	17.371 ± 0.012	18.271 ± 0.021	0.900 ± 0.024
05 17 13.02	39 22 26.5	16.797 ± 0.015	17.576 ± 0.011	0.779 ± 0.019
05 17 15.40	39 22 30.3	16.543 ± 0.016	16.724 ± 0.009	0.181 ± 0.018
05 17 13.09	39 22 30.7	16.758 ± 0.014	17.541 ± 0.013	0.783 ± 0.019
05 17 14.12	39 22 32.3	18.739 ± 0.036	19.332 ± 0.042	0.593 ± 0.055
05 17 28.10	39 22 36.8	18.272 ± 0.061	18.416 ± 0.054	0.144 ± 0.081
05 17 09.35	39 22 44.6	19.771 ± 0.111	20.123 ± 0.113	0.352 ± 0.158
05 17 14.53	39 22 48.7	18.308 ± 0.031	18.670 ± 0.022	0.362 ± 0.038
05 16 58.15	39 22 54.2	18.620 ± 0.063	19.017 ± 0.055	0.397 ± 0.084
05 17 07.28	39 22 58.2	15.031 ± 0.006	15.196 ± 0.005	0.165 ± 0.008
05 17 18.55	39 23 07.0	12.584 ± 0.017	12.724 ± 0.009	0.140 ± 0.019
05 17 28.62	39 23 17.0	15.407 ± 0.024	15.579 ± 0.014	0.172 ± 0.028
05 17 00.79	39 23 21.5	18.872 ± 0.085	19.571 ± 0.110	0.699 ± 0.139
05 17 02.84	39 23 24.2	13.946 ± 0.042	14.127 ± 0.015	0.181 ± 0.045
05 17 13.62	39 23 28.8	18.783 ± 0.041	19.280 ± 0.054	0.497 ± 0.068
05 17 29.49	39 23 29.4	15.288 ± 0.029	15.445 ± 0.017	0.157 ± 0.034
05 17 23.43	39 23 31.8	17.577 ± 0.050	17.744 ± 0.025	0.167 ± 0.056
05 17 17.05	39 23 39.0	17.458 ± 0.029	17.713 ± 0.023	0.255 ± 0.037
05 17 09.69	39 23 42.5	19.322 ± 0.066	19.717 ± 0.064	0.395 ± 0.092
05 17 22.48	39 23 46.0	19.018 ± 0.075	19.351 ± 0.057	0.333 ± 0.094
05 17 29.17	39 23 54.8	18.258 ± 0.069	18.455 ± 0.063	0.197 ± 0.093
05 17 25.86	39 23 54.8	18.810 ± 0.111	18.840 ± 0.081	0.030 ± 0.137
05 16 59.19	39 23 59.6	15.632 ± 0.043	15.743 ± 0.029	0.111 ± 0.052
05 17 09.21	39 24 01.1	16.130 ± 0.010	16.332 ± 0.008	0.202 ± 0.013
05 17 00.76	39 24 01.7	14.127 ± 0.032	14.255 ± 0.020	0.128 ± 0.038
05 17 25.09	39 24 05.1	18.847 ± 0.097	19.367 ± 0.124	0.520 ± 0.157
05 17 08.36	39 24 06.2	18.997 ± 0.055	19.534 ± 0.059	0.537 ± 0.081
05 17 09.61	39 24 09.7	16.556 ± 0.015	16.618 ± 0.015	0.062 ± 0.021
05 17 16.17	39 24 11.1	18.095 ± 0.050	18.201 ± 0.039	0.106 ± 0.063
05 17 01.92	39 24 13.2	16.446 ± 0.026	16.534 ± 0.018	0.088 ± 0.032
05 16 58.22	39 24 15.4	14.121 ± 0.021	14.236 ± 0.019	0.115 ± 0.028
05 17 17.16	39 24 16.1	15.392 ± 0.018	15.492 ± 0.010	0.100 ± 0.021
05 17 28.67	39 24 20.7	19.743 ± 0.271	18.771 ± 0.120	–0.972 ± 0.296
05 17 00.71	39 24 20.8	18.146 ± 0.075	18.259 ± 0.054	0.113 ± 0.092
05 17 22.42	39 24 25.5	20.239 ± 0.453	20.230 ± 0.380	–0.009 ± 0.591
05 17 10.32	39 20 14.9	16.397 ± 0.039	16.648 ± 0.028	0.251 ± 0.048
05 17 08.96	39 20 17.0	17.194 ± 0.027	17.411 ± 0.022	0.217 ± 0.035

Table A.1. continued.

RA (hh mm ss)	Dec (dd mm ss)	H (mag)	K_s (mag)	H–K_s (mag)
05 17 17.21	39 20 19.8	16.507 ± 0.028	16.810 ± 0.028	0.303 ± 0.040
05 17 09.67	39 20 21.4	16.464 ± 0.029	16.720 ± 0.021	0.256 ± 0.036
05 17 16.77	39 20 25.4	15.236 ± 0.034	15.462 ± 0.034	0.226 ± 0.048
05 17 24.09	39 20 27.0	17.442 ± 0.062	17.606 ± 0.049	0.164 ± 0.079
05 17 23.48	39 20 33.6	15.660 ± 0.049	15.945 ± 0.039	0.285 ± 0.063
05 17 08.79	39 20 35.4	14.743 ± 0.024	14.937 ± 0.016	0.194 ± 0.029
05 17 18.91	39 20 39.5	16.538 ± 0.024	16.851 ± 0.019	0.313 ± 0.031
05 17 09.83	39 20 44.2	17.529 ± 0.047	17.793 ± 0.044	0.264 ± 0.064
05 17 28.08	39 20 46.5	13.433 ± 0.019	13.571 ± 0.014	0.138 ± 0.024
05 17 23.26	39 21 28.5	18.842 ± 0.067	18.481 ± 0.104	–0.361 ± 0.124
05 17 14.40	39 21 33.8	19.154 ± 0.053	20.107 ± 0.097	0.953 ± 0.111
05 17 25.42	39 21 48.8	17.490 ± 0.039	17.683 ± 0.032	0.193 ± 0.050
05 17 24.90	39 21 49.9	17.548 ± 0.116	18.167 ± 0.058	0.619 ± 0.130
05 17 14.32	39 22 02.1	16.896 ± 0.024	17.923 ± 0.027	1.027 ± 0.036
05 17 21.41	39 22 02.2	17.096 ± 0.015	17.490 ± 0.015	0.394 ± 0.021
05 17 23.24	39 22 04.4	14.978 ± 0.030	15.213 ± 0.030	0.235 ± 0.042
05 17 14.13	39 22 18.0	16.961 ± 0.017	17.904 ± 0.019	0.943 ± 0.025
05 17 17.22	39 22 19.2	18.535 ± 0.043	18.959 ± 0.031	0.424 ± 0.053
05 17 13.27	39 22 22.3	18.714 ± 0.041	19.271 ± 0.042	0.557 ± 0.059
05 17 12.52	39 22 35.7	17.961 ± 0.064	18.140 ± 0.051	0.179 ± 0.082
05 17 30.03	39 23 02.6	14.630 ± 0.047	14.926 ± 0.038	0.296 ± 0.060
05 17 03.07	39 23 32.2	18.852 ± 0.061	19.255 ± 0.058	0.403 ± 0.084
05 17 10.42	39 23 42.0	15.392 ± 0.018	15.638 ± 0.013	0.246 ± 0.022
05 17 24.05	39 23 47.3	18.057 ± 0.063	18.147 ± 0.039	0.090 ± 0.074
05 17 17.24	39 23 48.1	16.730 ± 0.035	17.303 ± 0.023	0.573 ± 0.042
05 17 23.22	39 23 56.9	19.167 ± 0.077	19.546 ± 0.062	0.379 ± 0.099
05 17 02.51	39 24 07.0	16.912 ± 0.050	16.968 ± 0.034	0.056 ± 0.060
05 16 59.24	39 24 07.4	16.544 ± 0.055	16.676 ± 0.037	0.132 ± 0.066
05 17 11.90	39 24 15.4	15.953 ± 0.034	16.061 ± 0.017	0.108 ± 0.038
05 16 59.51	39 24 15.6	16.844 ± 0.032	17.005 ± 0.028	0.161 ± 0.043
05 17 10.82	39 24 27.5	13.966 ± 0.019	14.046 ± 0.011	0.080 ± 0.022
05 17 24.12	39 20 09.9	17.644 ± 0.072	18.063 ± 0.036	0.419 ± 0.080
05 17 03.03	39 20 39.8	16.655 ± 0.049	16.989 ± 0.032	0.334 ± 0.059
05 17 12.57	39 21 48.0	18.215 ± 0.073	18.617 ± 0.057	0.402 ± 0.093
05 17 12.36	39 22 19.4	17.989 ± 0.026	18.528 ± 0.029	0.539 ± 0.039
05 17 12.84	39 22 35.0	17.357 ± 0.020	17.739 ± 0.013	0.382 ± 0.024
05 16 58.37	39 22 40.6	15.719 ± 0.021	15.947 ± 0.009	0.228 ± 0.023
05 17 18.43	39 23 29.5	13.688 ± 0.028	13.845 ± 0.023	0.157 ± 0.036
05 17 10.42	39 23 44.9	14.488 ± 0.021	14.616 ± 0.014	0.128 ± 0.025
05 17 03.86	39 23 57.6	18.353 ± 0.080	18.645 ± 0.052	0.292 ± 0.095
05 17 02.68	39 23 59.3	16.006 ± 0.048	16.104 ± 0.027	0.098 ± 0.055
05 17 29.62	39 23 59.6	16.675 ± 0.041	16.788 ± 0.029	0.113 ± 0.050
05 17 15.57	39 24 04.1	14.552 ± 0.029	14.681 ± 0.021	0.129 ± 0.036
05 17 10.52	39 24 09.5	13.900 ± 0.025	13.980 ± 0.017	0.080 ± 0.030
05 17 23.70	39 24 12.6	17.866 ± 0.067	17.841 ± 0.038	–0.025 ± 0.077
05 17 10.55	39 24 18.0	11.901 ± 0.015	11.881 ± 0.007	–0.020 ± 0.017
05 17 04.66	39 24 22.4	12.802 ± 0.027	12.965 ± 0.025	0.163 ± 0.037
05 17 11.74	39 21 55.8	17.485 ± 0.049	17.801 ± 0.032	0.316 ± 0.059
05 17 13.64	39 22 25.6	17.316 ± 0.046	18.002 ± 0.042	0.686 ± 0.062
05 17 24.79	39 23 45.2	14.813 ± 0.045	15.093 ± 0.033	0.280 ± 0.056
05 17 23.26	39 23 46.3	15.357 ± 0.053	15.478 ± 0.032	0.121 ± 0.062
05 17 21.85	39 23 59.3	13.687 ± 0.048	13.804 ± 0.021	0.117 ± 0.052
05 17 27.40	39 24 03.4	14.908 ± 0.036	15.060 ± 0.019	0.152 ± 0.041
05 17 10.24	39 24 08.0	13.874 ± 0.031	13.955 ± 0.020	0.081 ± 0.037
05 17 09.96	39 20 21.8	15.094 ± 0.029	15.253 ± 0.025	0.159 ± 0.038
05 17 14.64	39 22 08.1	19.294 ± 0.071	20.040 ± 0.086	0.746 ± 0.112
05 17 13.62	39 22 21.9	16.016 ± 0.058	16.682 ± 0.021	0.666 ± 0.062
05 17 13.75	39 22 22.6	16.084 ± 0.058	16.606 ± 0.014	0.522 ± 0.060
05 17 24.63	39 23 30.5	17.521 ± 0.055	16.832 ± 0.052	–0.689 ± 0.076
05 17 04.21	39 20 24.6	18.124 ± 0.069	18.420 ± 0.039	0.296 ± 0.079
05 17 22.89	39 21 22.4	18.159 ± 0.029	18.618 ± 0.031	0.459 ± 0.042
05 17 24.40	39 20 22.8	17.896 ± 0.080	18.503 ± 0.043	0.607 ± 0.091
05 17 23.41	39 20 19.7	19.444 ± 0.106	19.878 ± 0.100	0.434 ± 0.146
05 17 03.42	39 24 00.9	18.565 ± 0.076	18.480 ± 0.042	–0.085 ± 0.087
05 17 13.75	39 22 21.2	14.992 ± 0.114	15.845 ± 0.053	0.853 ± 0.126

Table A.1. continued.

RA (hh mm ss)	Dec (dd mm ss)	H (mag)	K_s (mag)	H–K_s (mag)
05 17 04.28	39 23 59.8	17.960 ± 0.066	18.666 ± 0.041	0.706 ± 0.078
05 17 12.85	39 22 18.2	14.121 ± 0.009	14.238 ± 0.010	0.117 ± 0.013
05 17 10.51	39 24 18.4	13.124 ± 0.041	13.255 ± 0.025	0.131 ± 0.048
05 17 17.47	39 20 44.7	9.265 ± 0.018	9.310 ± 0.026	0.045 ± 0.032
05 17 18.96	39 23 06.7	14.313 ± 0.067	14.499 ± 0.056	0.186 ± 0.087
05 17 20.78	39 20 03.6	17.285 ± 0.044	–	–
05 17 17.46	39 20 16.3	17.528 ± 0.037	–	–
05 17 08.33	39 20 47.1	19.494 ± 0.104	–	–
05 17 06.96	39 20 57.0	19.953 ± 0.130	–	–
05 17 23.20	39 21 06.9	18.935 ± 0.062	–	–
05 17 02.68	39 21 21.0	19.529 ± 0.106	–	–
05 17 10.36	39 21 36.7	19.623 ± 0.081	–	–
05 17 13.70	39 22 12.4	18.698 ± 0.036	–	–
05 17 14.96	39 22 13.4	19.429 ± 0.075	–	–
05 17 01.02	39 22 13.4	19.591 ± 0.133	–	–
05 17 13.90	39 22 16.1	17.378 ± 0.023	–	–
05 17 18.88	39 22 19.6	19.176 ± 0.049	–	–
05 17 08.68	39 22 25.4	19.931 ± 0.121	–	–
05 17 13.82	39 22 33.2	19.432 ± 0.060	–	–
05 17 14.20	39 22 37.4	18.639 ± 0.041	–	–
05 17 12.38	39 22 51.1	19.832 ± 0.089	–	–
05 17 19.95	39 23 10.2	19.686 ± 0.123	–	–
05 17 04.81	39 23 14.8	17.584 ± 0.049	–	–
05 17 02.10	39 23 36.7	19.561 ± 0.161	–	–
05 17 09.17	39 24 01.6	18.341 ± 0.043	–	–
05 17 05.42	39 20 05.5	18.607 ± 0.128	–	–
05 17 04.91	39 20 15.2	17.851 ± 0.044	–	–
05 17 16.98	39 20 20.4	19.626 ± 0.084	–	–
05 17 09.72	39 20 22.9	19.384 ± 0.066	–	–
05 17 21.91	39 20 27.1	19.279 ± 0.077	–	–
05 16 59.33	39 20 40.9	19.307 ± 0.102	–	–
05 17 01.14	39 20 46.0	19.244 ± 0.120	–	–
05 17 22.20	39 20 50.2	19.686 ± 0.095	–	–
05 17 16.27	39 20 54.1	19.852 ± 0.094	–	–
05 17 15.77	39 21 13.5	19.658 ± 0.092	–	–
05 17 10.92	39 21 14.7	19.975 ± 0.122	–	–
05 17 15.81	39 21 19.5	20.107 ± 0.135	–	–
05 17 11.62	39 21 19.8	19.650 ± 0.089	–	–
05 17 14.12	39 21 22.1	17.936 ± 0.027	–	–
05 17 10.39	39 21 26.1	19.626 ± 0.081	–	–
05 16 59.28	39 21 36.9	18.437 ± 0.066	–	–
05 17 12.11	39 21 45.4	17.925 ± 0.046	–	–
05 17 11.40	39 21 47.9	19.469 ± 0.078	–	–
05 17 26.07	39 21 50.1	18.662 ± 0.090	–	–
05 17 24.16	39 21 51.1	18.804 ± 0.066	–	–
05 17 11.53	39 21 53.2	19.244 ± 0.052	–	–
05 17 12.17	39 21 57.7	18.110 ± 0.034	–	–
05 17 06.13	39 22 00.0	19.834 ± 0.100	–	–
05 17 13.94	39 22 02.6	19.242 ± 0.053	–	–
05 17 15.75	39 22 05.2	19.331 ± 0.072	–	–
05 17 13.55	39 22 05.8	19.599 ± 0.079	–	–
05 17 02.83	39 22 06.2	19.273 ± 0.115	–	–
05 17 16.82	39 22 07.0	19.297 ± 0.079	–	–
05 17 27.22	39 22 08.5	18.895 ± 0.113	–	–
05 17 14.61	39 22 10.4	19.737 ± 0.093	–	–
05 17 14.52	39 22 11.3	18.898 ± 0.052	–	–
05 17 07.52	39 22 12.2	19.433 ± 0.075	–	–
05 17 27.95	39 22 12.9	18.683 ± 0.088	–	–
05 17 14.71	39 22 14.6	18.160 ± 0.026	–	–
05 17 14.66	39 22 15.3	18.834 ± 0.044	–	–
05 17 24.54	39 22 15.1	18.960 ± 0.082	–	–
05 17 13.69	39 22 15.6	17.559 ± 0.021	–	–
05 17 12.74	39 22 16.5	17.700 ± 0.021	–	–
05 17 14.91	39 22 17.0	19.451 ± 0.064	–	–
05 17 14.36	39 22 17.1	18.600 ± 0.036	–	–

Table A.1. continued.

RA (hh mm ss)	Dec (dd mm ss)	H (mag)	K_s (mag)	H–K_s (mag)
05 17 20.47	39 22 17.4	19.659 ± 0.090	–	–
05 17 08.21	39 22 20.2	19.519 ± 0.103	–	–
05 17 15.28	39 22 21.9	19.619 ± 0.083	–	–
05 16 59.40	39 22 21.8	19.224 ± 0.108	–	–
05 17 13.07	39 22 26.0	18.833 ± 0.043	–	–
05 17 00.84	39 22 26.6	19.690 ± 0.153	–	–
05 17 21.32	39 22 27.0	19.698 ± 0.096	–	–
05 17 15.47	39 22 28.9	18.025 ± 0.036	–	–
05 17 14.41	39 22 35.9	19.192 ± 0.068	–	–
05 17 15.20	39 22 36.2	19.500 ± 0.054	–	–
05 17 10.89	39 22 37.4	19.366 ± 0.072	–	–
05 17 17.89	39 22 40.9	19.613 ± 0.101	–	–
05 17 12.85	39 22 55.8	19.922 ± 0.095	–	–
05 17 07.23	39 23 05.8	19.881 ± 0.149	–	–
05 17 17.02	39 23 12.8	19.759 ± 0.076	–	–
05 17 17.40	39 23 14.5	19.814 ± 0.080	–	–
05 17 10.23	39 23 15.4	19.578 ± 0.074	–	–
05 17 10.14	39 23 16.3	19.974 ± 0.090	–	–
05 17 03.55	39 23 17.2	19.598 ± 0.092	–	–
05 17 14.67	39 23 32.8	19.875 ± 0.099	–	–
05 17 16.64	39 23 32.9	19.332 ± 0.075	–	–
05 17 00.59	39 23 34.3	19.204 ± 0.104	–	–
05 17 14.21	39 23 35.9	19.591 ± 0.089	–	–
05 17 12.34	39 23 39.4	20.134 ± 0.158	–	–
05 17 24.99	39 23 41.0	18.853 ± 0.094	–	–
05 17 00.62	39 23 47.3	19.124 ± 0.124	–	–
05 17 23.97	39 23 49.8	17.937 ± 0.036	–	–
05 17 07.84	39 23 51.0	19.829 ± 0.102	–	–
05 17 18.32	39 24 07.2	19.766 ± 0.119	–	–
05 17 09.00	39 20 16.1	18.650 ± 0.039	–	–
05 17 13.22	39 21 15.2	19.755 ± 0.100	–	–
05 16 58.29	39 21 30.4	18.846 ± 0.076	–	–
05 17 13.58	39 22 00.9	18.961 ± 0.055	–	–
05 17 28.99	39 22 06.8	19.073 ± 0.136	–	–
05 17 10.78	39 22 13.6	20.068 ± 0.134	–	–
05 17 10.79	39 22 16.1	19.286 ± 0.068	–	–
05 17 12.78	39 22 22.5	19.682 ± 0.093	–	–
05 16 57.93	39 22 44.8	18.933 ± 0.125	–	–
05 17 18.17	39 22 45.6	19.084 ± 0.068	–	–
05 16 57.49	39 22 49.4	18.581 ± 0.106	–	–
05 17 00.08	39 23 00.2	18.923 ± 0.078	–	–
05 17 20.04	39 23 12.6	19.785 ± 0.128	–	–
05 17 13.91	39 23 15.8	19.659 ± 0.077	–	–
05 17 23.23	39 23 40.1	19.422 ± 0.096	–	–
05 17 03.42	39 23 41.7	19.243 ± 0.097	–	–
05 17 10.72	39 23 43.2	19.659 ± 0.082	–	–
05 17 24.94	39 24 06.4	18.857 ± 0.108	–	–
05 17 04.34	39 24 14.4	18.975 ± 0.092	–	–
05 17 08.93	39 20 15.9	18.952 ± 0.068	–	–
05 17 01.06	39 20 47.9	18.862 ± 0.079	–	–
05 17 14.87	39 21 04.7	20.221 ± 0.158	–	–
05 17 15.25	39 21 15.0	20.031 ± 0.125	–	–
05 17 11.89	39 21 50.0	19.184 ± 0.090	–	–
05 17 14.90	39 22 06.9	19.267 ± 0.060	–	–
05 17 12.99	39 22 12.7	19.434 ± 0.069	–	–
05 17 13.72	39 22 17.0	17.004 ± 0.056	–	–
05 17 17.82	39 23 20.7	19.683 ± 0.068	–	–
05 17 25.58	39 23 22.1	20.161 ± 0.312	–	–
05 17 24.60	39 23 30.2	17.220 ± 0.041	–	–
05 17 09.70	39 23 32.8	19.838 ± 0.085	–	–
05 17 03.33	39 23 42.5	19.529 ± 0.126	–	–
05 17 17.15	39 20 08.7	19.472 ± 0.103	–	–
05 17 15.83	39 21 13.9	19.785 ± 0.079	–	–
05 17 20.02	39 21 18.4	19.588 ± 0.115	–	–
05 17 23.27	39 21 42.6	17.954 ± 0.052	–	–

Table A.1. continued.

RA (hh mm ss)	Dec (dd mm ss)	H (mag)	K_s (mag)	H–K_s (mag)
05 17 10.87	39 21 50.4	18.667 ± 0.041	–	–
05 17 28.18	39 21 51.0	19.205 ± 0.151	–	–
05 17 28.81	39 23 40.7	18.911 ± 0.109	–	–
05 17 13.25	39 21 24.6	18.515 ± 0.046	–	–
05 17 23.45	39 21 26.8	18.925 ± 0.075	–	–
05 16 58.72	39 23 25.5	19.354 ± 0.112	–	–
05 17 19.39	39 23 35.5	18.095 ± 0.045	–	–
05 17 09.66	39 23 56.5	18.828 ± 0.057	–	–
05 17 27.93	39 24 10.8	19.621 ± 0.310	–	–
05 17 14.06	39 22 17.0	17.691 ± 0.042	–	–
05 17 21.01	39 23 16.5	19.188 ± 0.058	–	–
05 17 10.84	39 24 17.4	17.947 ± 0.054	–	–
05 17 00.03	39 21 55.8	20.428 ± 0.415	–	–
05 17 13.80	39 22 20.9	15.052 ± 0.044	–	–
05 17 29.06	39 22 18.0	18.936 ± 0.141	–	–
05 17 00.87	39 23 59.0	19.315 ± 0.122	–	–
05 17 09.57	39 24 10.2	18.451 ± 0.087	–	–
05 17 25.63	39 21 15.4	18.638 ± 0.115	–	–
05 17 03.79	39 20 27.9	–	20.231 ± 0.136	–
05 17 10.22	39 22 44.7	–	20.519 ± 0.150	–
05 17 29.33	39 22 56.0	–	19.543 ± 0.174	–
05 17 28.68	39 23 53.9	–	19.266 ± 0.117	–
05 17 02.13	39 23 58.2	–	19.411 ± 0.086	–
05 17 25.01	39 20 25.1	–	20.678 ± 0.394	–
05 17 17.46	39 20 35.4	–	19.869 ± 0.093	–
05 17 04.92	39 20 47.3	–	19.876 ± 0.086	–
05 17 03.99	39 20 50.6	–	20.080 ± 0.095	–
05 17 05.63	39 20 55.5	–	20.081 ± 0.117	–
05 17 25.77	39 21 01.1	–	19.351 ± 0.120	–
05 17 10.98	39 21 03.3	–	20.499 ± 0.112	–
05 17 24.24	39 21 04.0	–	16.441 ± 0.035	–
05 17 13.66	39 21 50.8	–	20.123 ± 0.107	–
05 17 17.19	39 21 54.0	–	20.221 ± 0.092	–
05 17 27.96	39 22 22.2	–	19.537 ± 0.153	–
05 17 13.55	39 22 29.1	–	19.908 ± 0.082	–
05 17 14.21	39 22 41.4	–	18.648 ± 0.061	–
05 17 04.65	39 22 55.4	–	19.555 ± 0.058	–
05 17 10.50	39 23 00.9	–	20.287 ± 0.110	–
05 17 16.24	39 23 12.8	–	19.870 ± 0.070	–
05 17 09.42	39 23 13.6	–	20.331 ± 0.096	–
05 17 29.53	39 23 20.5	–	18.936 ± 0.098	–
05 17 10.62	39 23 27.8	–	20.330 ± 0.117	–
05 17 29.33	39 23 41.4	–	18.360 ± 0.056	–
05 17 16.57	39 23 41.4	–	19.469 ± 0.075	–
05 17 28.19	39 23 43.3	–	19.809 ± 0.175	–
05 17 28.90	39 23 52.6	–	19.223 ± 0.106	–
05 17 28.99	39 23 55.9	–	19.389 ± 0.130	–
05 17 08.43	39 23 59.6	–	19.868 ± 0.075	–
05 17 29.07	39 24 05.0	–	19.093 ± 0.118	–
05 17 07.34	39 24 18.2	–	19.358 ± 0.107	–
05 17 03.81	39 24 21.6	–	18.426 ± 0.070	–
05 17 05.89	39 24 22.4	–	18.591 ± 0.086	–
05 17 23.65	39 20 25.0	–	19.987 ± 0.129	–
05 17 00.35	39 20 32.2	–	19.810 ± 0.129	–
05 17 25.66	39 20 58.4	–	19.623 ± 0.141	–
05 17 26.86	39 23 16.1	–	20.326 ± 0.257	–
05 17 04.25	39 23 21.9	–	20.076 ± 0.107	–
05 17 25.49	39 24 04.1	–	20.372 ± 0.362	–
05 17 28.45	39 24 05.8	–	20.867 ± 0.492	–
05 17 23.28	39 24 17.1	–	18.939 ± 0.092	–
05 17 03.42	39 20 23.5	–	19.738 ± 0.082	–
05 17 23.10	39 20 34.2	–	19.803 ± 0.083	–
05 17 29.93	39 21 03.6	–	19.193 ± 0.134	–
05 17 20.00	39 21 23.1	–	20.183 ± 0.137	–
05 17 28.70	39 23 24.0	–	19.434 ± 0.130	–

Table A.1. continued.

RA (hh mm ss)	Dec (dd mm ss)	H (mag)	K_s (mag)	H–K_s (mag)
05 17 04.30	39 23 59.5	–	18.369 ± 0.029	–
05 17 07.63	39 24 18.3	–	19.156 ± 0.081	–
05 17 24.08	39 20 10.2	–	18.194 ± 0.051	–
05 17 07.76	39 22 59.6	–	20.031 ± 0.097	–
05 16 58.51	39 23 20.0	–	18.371 ± 0.040	–
05 17 24.37	39 20 23.0	–	18.607 ± 0.064	–
05 17 23.11	39 20 26.3	–	20.235 ± 0.161	–
05 17 23.31	39 23 49.1	–	17.802 ± 0.031	–
05 17 02.68	39 20 38.6	–	19.693 ± 0.106	–
05 17 18.51	39 20 03.8	–	18.620 ± 0.133	–
05 17 17.26	39 23 48.4	–	18.091 ± 0.025	–
05 17 06.94	39 24 17.8	–	18.707 ± 0.054	–
05 17 13.20	39 21 25.1	–	19.276 ± 0.050	–

Table A.2. Coordinates and fluxes of the H_2 knots belonging to Jet 1.

α(J2000) (hh mm ss)	δ(J2000) (dd mm ss)	Flux (10^{-16} erg cm^{-2} s^{-1})
05 17 14.495	39 22 43.28	584.7 ± 0.6
05 17 14.488	39 22 45.27	527.2 ± 0.5
05 17 14.505	39 22 46.32	20.8 ± 0.2
05 17 14.595	39 22 43.51	85.0 ± 0.3
05 17 14.640	39 22 42.72	89.0 ± 0.4
05 17 14.539	39 22 41.90	66.9 ± 0.3
05 17 14.361	39 22 42.39	62.9 ± 0.3
05 17 14.232	39 22 41.31	351.1 ± 0.4
O5 17 14.133	39 22 39.21	80.7 ± 0.3
05 17 14.194	39 22 38.78	118.6 ± 0.4
05 17 14.248	39 22 39.37	45.9 ± 0.3
05 17 14.432	39 22 35.76	21.5 ± 0.3
05 17 14.579	39 22 39.30	22.4 ± 0.3
05 17 14.646	39 22 40.59	22.3 ± 0.3
05 17 13.463	39 22 11.80	2.6 ± 0.2
05 17 13.423	39 22 09.35	10.8 ± 0.5
05 17 13.847	39 21 49.04	92.3 ± 0.6
05 17 13.722	39 21 50.53	173.2 ± 0.7
05 17 13.510	39 21 51.96	163.4 ± 0.7
05 17 13.507	39 21 48.83	26.7 ± 0.5
05 17 12.896	39 21 46.80	65.3 ± 0.7
05 17 12.975	39 21 43.35	14.4 ± 0.4
05 17 13.160	39 21 45.05	18.2 ± 0.5
05 17 11.922	39 21 46.06	41.9 ± 0.4
05 17 11.807	39 21 47.71	21.7 ± 0.3
05 17 12.035	39 21 51.89	40.1 ± 0.4
05 17 12.113	39 21 45.85	13.6 ± 0.3

Table A.3. Coordinates and fluxes of the H_2 knots belonging to Jet 2.

α(J2000) (hh mm ss)	δ(J2000) (dd mm ss)	Flux (10^{-16} erg cm^{-2} s^{-1})
05:17:13.398	39:22:27.89	39.4 ± 0.4
05:17:13.493	39:22:26.33	115.1 ± 0.6
05:17:13.626	39:22:25.50	19.4 ± 0.3
05:17:13.563	39:22:23.34	27.4 ± 0.3
05:17:13.592	39:22:22.56	21.1 ± 0.3
05:17:13.746	39:22:18.50	18.3 ± 0.3
05:17:13.789	39:22:16.12	9.5 ± 0.3
05:17:13.836	39:22:14.67	11.3 ± 0.3
05:17:13.878	39:22:13.11	11.5 ± 0.3
05:17:13.956	39:22:10.97	16.9 ± 0.5
05:17:14.020	39:22:07.75	83.0 ± 0.4
05:17:13.973	39:22:06.39	156.0 ± 0.5
05:17:14.051	39:22:05.20	10.8 ± 0.2
05:17:13.897	39:22:07.08	37.6 ± 0.3

Table A.4. Coordinates and fluxes of the H_2 knots belonging to Jet 3.

α(J2000) (hh mm ss)	δ(J2000) (dd mm ss)	Flux (10^{-16} erg cm^{-2} s^{-1})
05 17 13.618	39 22 16.98	47.3 ± 0.4
05 17 13.391	39 22 15.94	38.5 ± 0.4
05 17 12.928	39 22 13.28	3.3 ± 0.2

Table A.5. Coordinates, magnitudes, and colour of the sources identified in the PISCES field. The symbol "–" indicates a non-detection.

RA (hh mm ss)	Dec (dd mm ss)	H (mag)	K_s (mag)	H–K_s (mag)
05 17 13.98	39 22 08.6	18.578 ± 0.014	19.241 ± 0.029	0.663 ± 0.032
05 17 13.28	39 22 09.6	19.101 ± 0.010	19.625 ± 0.037	0.524 ± 0.038
05 17 14.15	39 22 09.8	18.494 ± 0.008	19.227 ± 0.037	0.733 ± 0.038
05 17 14.25	39 22 11.2	18.443 ± 0.007	19.295 ± 0.038	0.852 ± 0.039
05 17 13.71	39 22 12.4	18.429 ± 0.005	20.119 ± 0.071	1.690 ± 0.071
05 17 12.99	39 22 12.6	19.705 ± 0.056	20.092 ± 0.054	0.387 ± 0.078
05 17 14.25	39 22 12.8	17.837 ± 0.004	18.901 ± 0.031	1.064 ± 0.031
05 17 14.14	39 22 13.6	17.793 ± 0.004	19.046 ± 0.038	1.253 ± 0.038
05 17 13.27	39 22 13.7	19.191 ± 0.011	20.032 ± 0.062	0.841 ± 0.063
05 17 14.13	39 22 13.9	17.694 ± 0.004	18.431 ± 0.020	0.737 ± 0.020
05 17 13.69	39 22 15.6	17.522 ± 0.003	20.137 ± 0.074	2.615 ± 0.074
05 17 13.82	39 22 15.7	18.777 ± 0.008	20.226 ± 0.067	1.449 ± 0.067
05 17 13.90	39 22 16.1	17.131 ± 0.002	19.856 ± 0.047	2.725 ± 0.047
05 17 13.72	39 22 16.9	17.691 ± 0.007	19.608 ± 0.052	1.917 ± 0.052
05 17 14.06	39 22 17.0	18.158 ± 0.005	20.072 ± 0.072	1.914 ± 0.072
05 17 13.73	39 22 17.0	18.007 ± 0.009	20.412 ± 0.099	2.405 ± 0.099
05 17 14.36	39 22 17.1	16.769 ± 0.002	18.779 ± 0.039	2.010 ± 0.039
05 17 13.98	39 22 17.4	17.763 ± 0.011	20.249 ± 0.083	2.486 ± 0.084
05 17 14.00	39 22 17.6	15.764 ± 0.002	18.229 ± 0.020	2.465 ± 0.020
05 17 13.55	39 22 17.7	17.325 ± 0.010	18.849 ± 0.026	1.524 ± 0.028
05 17 14.13	39 22 17.9	16.956 ± 0.003	18.107 ± 0.017	1.151 ± 0.017
05 17 13.57	39 22 18.1	18.172 ± 0.025	19.459 ± 0.063	1.287 ± 0.068
05 17 13.91	39 22 18.3	15.497 ± 0.001	17.930 ± 0.012	2.433 ± 0.012
05 17 13.08	39 22 18.3	16.675 ± 0.001	17.476 ± 0.009	0.801 ± 0.009
05 17 13.36	39 22 18.6	19.155 ± 0.011	19.812 ± 0.042	0.657 ± 0.043
05 17 13.65	39 22 18.7	16.762 ± 0.059	17.214 ± 0.036	0.452 ± 0.069
05 17 14.08	39 22 18.8	17.076 ± 0.003	18.901 ± 0.026	1.825 ± 0.026
05 17 13.21	39 22 19.2	18.485 ± 0.006	19.049 ± 0.022	0.564 ± 0.023
05 17 13.40	39 22 19.3	19.020 ± 0.009	19.597 ± 0.042	0.577 ± 0.043
05 17 13.67	39 22 19.5	11.273 ± 0.001	12.523 ± 0.003	1.250 ± 0.003
05 17 13.73	39 22 20.1	11.181 ± 0.002	14.933 ± 0.007	3.752 ± 0.007
05 17 13.74	39 22 20.3	13.359 ± 0.009	15.474 ± 0.008	2.115 ± 0.012
05 17 13.30	39 22 20.4	18.373 ± 0.005	19.131 ± 0.029	0.758 ± 0.029
05 17 13.61	39 22 20.5	17.899 ± 0.021	19.386 ± 0.060	1.487 ± 0.064
05 17 13.64	39 22 20.7	18.080 ± 0.049	18.464 ± 0.032	0.384 ± 0.059
05 17 13.81	39 22 20.9	15.467 ± 0.002	16.731 ± 0.008	1.264 ± 0.008
05 17 13.76	39 22 21.0	15.677 ± 0.006	16.339 ± 0.006	0.662 ± 0.008
05 17 14.28	39 22 21.3	18.729 ± 0.010	20.168 ± 0.076	1.439 ± 0.077
05 17 13.76	39 22 21.3	16.585 ± 0.006	17.512 ± 0.020	0.927 ± 0.021
05 17 13.99	39 22 21.7	18.924 ± 0.012	20.008 ± 0.061	1.084 ± 0.062
05 17 13.17	39 22 21.7	16.251 ± 0.001	17.232 ± 0.007	0.981 ± 0.007
05 17 12.93	39 22 21.7	19.246 ± 0.011	19.913 ± 0.049	0.667 ± 0.050
05 17 14.38	39 22 21.9	15.128 ± 0.002	16.452 ± 0.008	1.324 ± 0.008
05 17 13.62	39 22 22.0	16.174 ± 0.002	16.852 ± 0.007	0.678 ± 0.007
05 17 13.26	39 22 22.2	19.373 ± 0.016	19.984 ± 0.059	0.611 ± 0.061
05 17 13.27	39 22 22.3	18.928 ± 0.011	19.500 ± 0.033	0.572 ± 0.035
05 17 13.75	39 22 22.6	16.122 ± 0.002	16.470 ± 0.005	0.348 ± 0.005
05 17 13.24	39 22 22.9	15.813 ± 0.001	17.180 ± 0.008	1.367 ± 0.008
05 17 13.79	39 22 23.3	18.081 ± 0.007	18.996 ± 0.028	0.915 ± 0.029
05 17 13.29	39 22 23.4	17.441 ± 0.003	18.739 ± 0.022	1.298 ± 0.022
05 17 13.74	39 22 23.5	15.352 ± 0.001	16.594 ± 0.006	1.242 ± 0.006
05 17 13.46	39 22 23.7	15.961 ± 0.001	16.557 ± 0.006	0.596 ± 0.006
05 17 13.49	39 22 23.8	15.914 ± 0.001	16.719 ± 0.007	0.805 ± 0.007
05 17 12.96	39 22 24.1	18.064 ± 0.005	19.907 ± 0.046	1.843 ± 0.046
05 17 13.64	39 22 24.2	16.860 ± 0.002	17.408 ± 0.009	0.548 ± 0.009
05 17 13.29	39 22 25.4	18.034 ± 0.004	19.315 ± 0.033	1.281 ± 0.033

Table A.5. continued.

RA (hh mm ss)	Dec (dd mm ss)	H (mag)	K_s (mag)	H–K_s (mag)
05 17 13.65	39 22 25.6	17.250 ± 0.003	17.946 ± 0.013	0.696 ± 0.013
05 17 13.73	39 22 26.0	18.838 ± 0.009	19.759 ± 0.061	0.921 ± 0.062
05 17 14.30	39 22 26.2	18.260 ± 0.007	19.127 ± 0.030	0.867 ± 0.031
05 17 13.94	39 22 26.2	17.800 ± 0.004	18.645 ± 0.021	0.845 ± 0.021
05 17 13.62	39 22 26.2	18.332 ± 0.009	19.252 ± 0.033	0.920 ± 0.034
05 17 12.99	39 22 26.3	18.691 ± 0.017	20.393 ± 0.098	1.702 ± 0.099
05 17 13.84	39 22 26.4	18.075 ± 0.005	18.751 ± 0.024	0.676 ± 0.025
05 17 13.02	39 22 26.5	16.701 ± 0.003	17.448 ± 0.009	0.747 ± 0.009
05 17 13.97	39 22 27.1	17.494 ± 0.004	17.975 ± 0.016	0.481 ± 0.016
05 17 13.66	39 22 27.4	16.969 ± 0.003	17.338 ± 0.011	0.369 ± 0.011
05 17 13.77	39 22 09.2	19.618 ± 0.020	–	–
05 17 14.52	39 22 11.4	18.818 ± 0.009	–	–
05 17 14.55	39 22 14.7	18.372 ± 0.008	–	–
05 17 14.55	39 22 14.8	18.375 ± 0.008	–	–
05 17 13.95	39 22 15.0	20.158 ± 0.027	–	–
05 17 13.54	39 22 15.5	18.599 ± 0.026	–	–
05 17 13.39	39 22 16.3	20.077 ± 0.046	–	–
05 17 14.41	39 22 17.3	20.207 ± 0.037	–	–
05 17 13.66	39 22 17.5	19.286 ± 0.035	–	–
05 17 13.96	39 22 17.7	20.167 ± 0.048	–	–
05 17 13.89	39 22 17.9	18.872 ± 0.019	–	–
05 17 13.93	39 22 18.0	20.264 ± 0.062	–	–
05 17 13.70	39 22 18.3	18.758 ± 0.100	–	–
05 17 13.71	39 22 18.4	18.040 ± 0.057	–	–
05 17 13.76	39 22 19.9	16.632 ± 0.033	–	–
05 17 13.70	39 22 20.0	16.678 ± 0.179	–	–
05 17 13.65	39 22 20.0	16.960 ± 0.030	–	–
05 17 13.65	39 22 20.1	17.510 ± 0.107	–	–
05 17 13.77	39 22 20.1	16.031 ± 0.043	–	–
05 17 13.33	39 22 20.5	19.388 ± 0.011	–	–
05 17 13.61	39 22 20.5	18.870 ± 0.064	–	–
05 17 14.53	39 22 21.4	18.848 ± 0.012	–	–
05 17 13.45	39 22 21.4	19.304 ± 0.011	–	–
05 17 13.82	39 22 21.4	18.591 ± 0.025	–	–
05 17 13.42	39 22 21.5	19.654 ± 0.015	–	–
05 17 13.28	39 22 21.5	20.355 ± 0.032	–	–
05 17 14.09	39 22 21.6	18.881 ± 0.010	–	–
05 17 14.44	39 22 22.0	20.133 ± 0.047	–	–
05 17 14.15	39 22 22.0	20.083 ± 0.027	–	–
05 17 13.73	39 22 22.0	20.152 ± 0.109	–	–
05 17 13.69	39 22 22.1	17.890 ± 0.010	–	–
05 17 13.83	39 22 22.1	20.630 ± 0.081	–	–
05 17 13.89	39 22 22.9	19.482 ± 0.017	–	–
05 17 13.75	39 22 23.0	20.277 ± 0.041	–	–
05 17 13.47	39 22 23.1	19.875 ± 0.026	–	–
05 17 14.52	39 22 23.2	22.691 ± 0.630	–	–
05 17 13.51	39 22 23.1	19.878 ± 0.026	–	–
05 17 13.24	39 22 23.8	19.625 ± 0.020	–	–
05 17 13.25	39 22 25.7	20.467 ± 0.040	–	–
05 17 13.07	39 22 26.0	18.918 ± 0.015	–	–
05 17 13.08	39 22 26.5	22.006 ± 0.348	–	–
05 17 14.11	39 22 26.9	19.902 ± 0.024	–	–
05 17 14.08	39 22 27.3	18.252 ± 0.007	–	–
05 17 13.41	39 22 28.0	18.605 ± 0.029	–	–
05 17 14.01	39 22 28.2	20.145 ± 0.034	–	–
05 17 13.59	39 22 28.2	18.920 ± 0.030	–	–
05 17 13.93	39 22 28.5	19.688 ± 0.028	–	–
05 17 14.06	39 22 28.7	19.558 ± 0.025	–	–
05 17 13.49	39 22 21.1	20.754 ± 0.054	–	–
05 17 13.42	39 22 17.0	21.092 ± 0.065	–	–
05 17 13.38	39 22 16.2	20.656 ± 0.067	–	–
05 17 14.34	39 22 14.4	20.266 ± 0.031	–	–
05 17 14.20	39 22 17.6	20.519 ± 0.047	–	–
05 17 14.13	39 22 19.1	20.673 ± 0.057	–	–
05 17 13.54	39 22 23.3	19.322 ± 0.016	–	–

Table A.5. continued.

RA (hh mm ss)	Dec (dd mm ss)	H (mag)	K_s (mag)	H–K_s (mag)
05 17 13.10	39 22 17.5	21.237 ± 0.060	–	–
05 17 13.12	39 22 18.5	22.093 ± 0.177	–	–
05 17 14.35	39 22 28.5	20.113 ± 0.042	–	–
05 17 13.21	39 22 27.1	21.253 ± 0.249	–	–
05 17 13.93	39 22 27.5	21.653 ± 0.134	–	–
05 17 13.96	39 22 26.8	20.928 ± 0.058	–	–
05 17 14.52	39 22 20.9	20.888 ± 0.065	–	–
05 17 13.99	39 22 22.6	20.919 ± 0.069	–	–
05 17 14.02	39 22 22.3	21.444 ± 0.086	–	–
05 17 13.00	39 22 24.1	21.878 ± 0.117	–	–
05 17 13.17	39 22 20.1	22.059 ± 0.144	–	–
05 17 13.33	39 22 19.1	21.220 ± 0.072	–	–
05 17 13.49	39 22 21.1	20.721 ± 0.052	–	–
05 17 13.49	39 22 21.1	20.721 ± 0.052	–	–
05 17 13.53	39 22 21.4	20.957 ± 0.075	–	–
05 17 13.56	39 22 21.2	21.926 ± 0.326	–	–
05 17 14.32	39 22 20.6	21.398 ± 0.081	–	–
05 17 14.29	39 22 19.4	22.263 ± 0.215	–	–
05 17 14.16	39 22 16.1	20.754 ± 0.039	–	–
05 17 12.99	39 22 12.6	19.690 ± 0.055	–	–
05 17 13.76	39 22 11.7	21.560 ± 0.102	–	–
05 17 13.25	39 22 07.9	21.034 ± 0.059	–	–
05 17 13.39	39 22 08.8	21.513 ± 0.072	–	–
05 17 13.74	39 22 10.1	21.308 ± 0.066	–	–
05 17 13.74	39 22 07.8	20.720 ± 0.080	–	–
05 17 13.88	39 22 08.3	19.758 ± 0.047	–	–
05 17 14.04	39 22 08.4	19.750 ± 0.062	–	–
05 17 14.04	39 22 08.4	19.750 ± 0.062	–	–
05 17 12.67	39 22 10.6	–	19.074 ± 0.036	–
05 17 13.03	39 22 10.9	–	19.198 ± 0.030	–
05 17 14.01	39 22 13.6	–	21.852 ± 0.399	–
05 17 12.74	39 22 16.5	–	18.071 ± 0.012	–
05 17 14.01	39 22 17.3	–	20.888 ± 0.203	–
05 17 13.84	39 22 17.4	–	20.933 ± 0.129	–
05 17 13.98	39 22 20.8	–	20.872 ± 0.123	–
05 17 13.54	39 22 21.4	–	19.830 ± 0.062	–
05 17 13.37	39 22 21.6	–	18.964 ± 0.022	–
05 17 13.92	39 22 22.3	–	21.191 ± 0.186	–
05 17 14.04	39 22 22.5	–	20.784 ± 0.155	–
05 17 12.72	39 22 25.5	–	19.091 ± 0.042	–
05 17 12.87	39 22 25.5	–	20.637 ± 0.112	–
05 17 13.68	39 22 25.6	–	21.092 ± 0.163	–
05 17 12.82	39 22 26.6	–	16.906 ± 0.006	–
05 17 13.47	39 22 24.0	–	19.609 ± 0.098	–
05 17 13.28	39 22 09.0	–	20.577 ± 0.094	–
05 17 12.81	39 22 16.1	–	20.324 ± 0.098	–
05 17 12.77	39 22 27.3	–	19.882 ± 0.061	–
05 17 13.35	39 22 20.2	–	20.597 ± 0.089	–
05 17 13.90	39 22 16.1	–	19.848 ± 0.047	–
05 17 12.97	39 22 09.2	–	20.258 ± 0.066	–
05 17 13.77	39 22 09.1	–	20.566 ± 0.090	–
05 17 13.79	39 22 08.4	–	19.390 ± 0.042	–

Table A.6. Continuum flux densities, S_ν, of clumps C1 and C2 and corresponding solid angles, Ω, over which the integration was performed.

		C1		C2		
λ (μm)	ν (GHz)	Ω (arcmin^2)	S_ν (Jy)	Ω (arcmin^2)	S_ν (Jy)	Database
850	353	[a]	2.86	1.09	0.9	Di Francesco et al. (2008)
500	599	2.81	12	2.73	6.9	Hi-GAL
450	666	[a]	13.18	–	–	Di Francesco et al. (2008)
350	856	2.81	30	2.73	16	Hi-GAL
250	1199	2.81	77	2.73	38	Hi-GAL
160	1874	2.81	130	2.73	61	Hi-GAL
100	2998	[a]	175	–	–	IRAS
70	4283	2.81	142	2.73	39	Hi-GAL
60	4997	[a]	140	–	–	IRAS
25	11 992	[a]	30.3	–	–	IRAS
22	13 627	[a]	20.6	[a]	4.31	WISE
21	14 075	[a]	13.7	–	–	MSX
18.7	16 032	0.0035	10.7	–	–	this paper
15	20 394	[a]	6.40	–	–	MSX
12.7	23 606	0.0035	3.8	–	–	this paper
12	24 776	[a]	4.61	–	–	MSX
12	24 983	[a]	5.08	[a]	0.705	WISE
12	24 983	[a]	7.13	–	–	IRAS
9.9	30 282	0.0035	1.5	–	–	this paper
8.9	33 685	0.0035	1.2	–	–	this paper
8	36 119	[a]	2.81	[a]	–	MSX
4.6	65 172	[a]	1.71	[a]	0.0407	WISE
4.5	66 620	0.28	0.56	0.12	0.05	*Spitzer*
3.6	83 275	0.17	0.32	0.12	0.06	*Spitzer*
3.5	85 654	[a]	0.29	–	–	Ishii et al. (1998)
3.4	88 174	[a]	0.361	[a]	0.0378	WISE
2.15	136 269	[a]	0.0555	–	–	2MASS Ks
1.63	181 692	[a]	0.0148	–	–	2MASS H
1.24	239 834	[a]	0.0058	–	–	2MASS J

Notes. [(a)] From catalogue or literature.